Rodrigo Olival Lima

Bachelor Degree in Biomedical Engineering Sciences

Autonoumous Nervous System biosignal processing via EDA and HRV from a wearable device

Dissertation submitted in partial fulfillment
of the requirements for the degree of

Master of Science in
Biomedical Engineering

Adviser: Doutor Hugo Filipe Silveira Gamboa, Professor Auxiliar, Universidade Nova de Lisboa - Faculdade de Ciências e Tecnologia

Examination Committee

Chairperson: Professor Paulo António Martins Ferreira Ribeiro
Raporteur: Doutora Carla Maria Quintão Pereira
Member: Doutor Hugo Filipe Silveira Gamboa

FACULDADE DE CIÊNCIAS E TECNOLOGIA
UNIVERSIDADE NOVA DE LISBOA

September, 2018

Rodrigo Olival Lima
Bachelor Degree in Biomedical Engineering Sciences

Autonomous Nervous System biosignal processing via EDA and HRV from a wearable device

Dissertation submitted in partial fulfillment
of the requirements for the degree of

Master of Science in
Biomedical Engineering

Adviser: Prof. Dr. Hugo Gamboa, Auxiliar Professor,
NOVA University of Lisbon

September, 2018

Autonoumous Nervous System biosignal processing via EDA and HRV from a wearable device

This document was created using the (pdf)LaTeX processor, based in the "novathesis" template[1], developed at the Dep. Informática of FCT-NOVA [2].
[1] https://github.com/joaomlourenco/novathesis [2] http://www.di.fct.unl.pt

To my Mother and Family,
who made it all possible.

ACKNOWLEDGEMENTS

Com o desfecho do meu percurso a aproximar-se, é fundamental dirigir umas palavras de agradecimento a todos aqueles que me acompanharam durante estes 5 anos.

Começo por destacar o papel do Prof. Dr. Hugo Gamboa, que como meu orientador de dissertação, possibilitou-me a oportunidade de realizar a minha dissertação na empresa PLUX – Wireless Biosignals, e orientou-me em situações de dúvida, removendo obstáculos durante o processo científico.

Não menos importante, tenho de agradecer ao aluno de doutoramento e investigador do LIBPHYS-UNL, Daniel Osório, que ao longo de toda a minha dissertação acompanhou-me diariamente e sempre se disponibilizou para retirar dúvidas que apareciam, guiou-me pelo caminho correto em situações difíceis, e transmitiu-me uma quantia inestimável de conhecimento científico.

A realização da dissertação na empresa PLUX – Wireless Biosignals teve grande importância na minha evolução tanto a nível pessoal como profissional, pois permitiu-me conhecer o ambiente empresarial, bem como adaptar-me e ter acesso ao mercado de trabalho durante o meu percurso académico.

Um agradecimento a todo o pessoal da PLUX, pelo ambiente descontraído e divertido que encontrei desde o momento em que comecei a minha dissertação, e por me acolherem de uma forma magnífica na empresa.

Em especial, gostaria de agradecer ao CEO Manuel Pacheco, que durante a dissertação incutiu tarefas que desafiaram a dar o melhor de mim, e pela disponibilidade e amabilidade que sempre demonstrou.

Aos membros da equipa de desenvolvimento de software, Rui Freixo, Gonçalo Telo, Maria Magalhães, André Lemos e Miquel Alfaras, um obrigado por me acompanharem durante estes últimos meses.

A toda a equipa de produção de hardware, em especial ao Paulo Aires que possibilitou toda a aquisição de sinal fisiológico através do dispositivo wearable. Agradecimento também à equipa do projeto LISA (Learning Analytics for Sensor-Based Adaptive Learning) que contribuíram para o desenvolvimento do dispositivo wearable.

Finalmente, gostaria de agradecer ao pessoal de Operações e Recursos Humanos, à Joana

Lobo, ao José Lopes, à Maysa Gomes, e à fisioterapeuta Catarina Oliveira que também me acompanharam durante este percurso.

Um agradecimento também à Prof. Dr. Claúdia Quaresma que me disponibilizou o laboratório na Faculdade de Ciências e Tecnologia, para recolha de dados a voluntários.

Esta dissertação realizou-se apenas no 2º semestre do último ano de faculdade, no entanto, o resto do meu percurso académico foi realizado com o apoio de um grupo de amigos durante 5 anos. Só eles sabem o que me custou estar estes 5 anos longe da família, e sem eles não conseguiria encontrar a motivação e alegria para continuar focado no meu objetivo.

Um agradecimento do fundo do coração para a Beatriz Barata, o Bernardo Gonçalves, a Inês Marques, a Maria Afonso, a Mariana Carvalho, o Pedro Moura, o Rui Varandas e o Tomás Pinheiro, vocês são a minha segunda família.

A todos os meus amigos de infância, especialmente ao Gonçalo Nóbrega que me acompanhou durante os 5 anos na mesma faculdade, um agradecimento especial.

A toda a minha família, à minha mãe e aos meus avós que me apoiaram em todos os sentidos possíveis. Sem eles ao meu lado nada disto seria possível, e os meus objetivos nunca seriam cumpridos. Obrigado família!

This is how you do it: you sit down at the keyboard and you put one word after another until its done. It's that easy, and that hard.

Neil Gaiman

ABSTRACT

The assessment of changes in the autonomous nervous system (ANS) with certain diseases and pathologies conditions, has been demonstrated to have important prognostic and diagnostic value, so delineating the role of autonomous activity is important to prevent health diseases.

There are many approaches to directly measure the sympathetic and parasympathetic nervous system, although, most of them are invasive and unable to provide continuous monitoring, leading to inaccurate assessment of the autonomous nervous system.

Heart rate variability (HRV) and Electrodermal activity (EDA) are presented has noninvasive methods to assess the ANS, by computing the spectral analysis of both HRV and EDA biosignals. The combination of these signals is necessary to correctly measure the activity of the sympathetic and parasympathetic system, due to the fact that frequency analysis of HRV only provides the level of unbalance between these two systems, while EDA reflects only activity from the sympathetic system. ANS biosignal processing via HRV and EDA from a wearable device was studied in this thesis, in order to provide continuous monitoring. A wearable device is the ideal solution, as HRV can be calculated with photoplethysmography signals from the wrist and EDA from the fingers, providing wireless and continuous monitoring of the subjects.

The extraction of the HRV and EDA features, that describe the activity of the sympathetic and parasympathetic system, were obtained by submitting the subjects to a mental arithmetic stress test, and then compared to the baseline values, in order to verify changes in the autonomous nervous system between the two situations.

The distinct response to stress for the subjects was then predicted using machine-learning classification mechanisms, with the ability to predict how the subject will respond when submitted to a situation of stress, using only time-domain features, instead of frequency-domain features, which reduces the time needed to perform the classification.

Keywords: Heart Rate Variability; Electrodermal Activity; Photoplethysmography; Biosignals; Autonomous Nervous System; Wearable Device; Machine-learning; Classification;

RESUMO

A avaliação das alterações do sistema nervoso autónomo (SNA), associadas a determinadas doenças e patologias, têm vindo a ganhar um importante papel no prognóstico de doenças, daí a importância de delinear o papel da atividade do SNA na prevenção de doenças.

Atualmente, existem diversas técnicas para medir diretamente os sistemas nervosos simpático e parassimpático, no entanto, a maioria destas técnicas são invasivas e não permitem a monitorização de forma contínua, o que leva a uma incorreta conclusão acerca das alterações no SNA.

A Variabilidade Cardíaca (VC) e a Atividade Eletrodérmica (EDA) surgem como métodos não invasivos para avaliar o SNA, através da análise espectral destes mesmos bio-sinais. A combinação destes sinais é necessária para determinar de forma correta a atividade dos sistemas simpático e parassimpático, pois a análise espectral da VC apenas fornece informação sobre o balanço entre estes dois sistemas, enquanto que a EDA apenas reflete a atividade do sistema simpático. De forma a colmatar o problema da monitorização contínua, um dispositivo wearable foi utilizado, medindo a VC através da fotopletismografia no punho, e a EDA nos dedos da mão. A computação dos parâmetros de VC e EDA que descrevem a atividade do sistema nervoso, foram obtidos, submetendo os participantes a um teste de stress aritmético mental, comparando os valores em situação de repouso com os valores obtidos em situação de stress, de forma a verificar alterações no SNA.

As distintas respostas dos participantes, quando submetidos a uma situação de stress, foram previstas através de mecanismos de classificação, de forma a prever de que maneira os participantes respondem a uma situação de stress, utilizando apenas parâmetros calculados no domínio do tempo, o que reduz significativamente o tempo necessário para efetuar uma classificação do tipo de resposta de cada pessoa.

Palavras-chave: Variabilidade Cardíaca; Atividade Eletrodérmica; Fotopletismografia; Bio-sinais; Sistema Nervoso Autónomo; Dispositivo wearable; Machine-learning; Classificação;

CONTENTS

List of Figures **xxi**

List of Tables **xxiii**

Acronyms **xxv**

1 Introduction **1**
1.1 Context 1
1.2 Goals 3

2 Theoretical Concepts **5**
2.1 Autonomous Nervous System 5
2.2 Photoplethysmography (PPG) 7
2.3 Heart Rate Variability (HRV) 8
2.3.1 HRV Concepts 8
2.3.2 Time domain methods 8
2.3.3 Frequency domain methods 11
2.4 Electrodermal Activity (EDA) 12
2.4.1 EDA Concepts 12
2.4.2 EDA Measurement 13
2.4.3 EDA Models 14
2.4.4 EDA Processing 16
2.5 HRV and EDA relationship: Review 17
2.6 Paced Auditory Serial Addition Test (PASAT) 17
2.7 Statistical Analysis 19
2.7.1 Kruskal-Wallis test 19
2.7.2 Chi-square test for Goodness of Fit 20
2.8 Support Vector Machines (SVM) 21
2.9 Random Forest Classifier 23

3 Materials and Procedure **25**
3.1 Study Population . . . 25
3.2 Wearable Device . . . 25
3.3 Acquisition Protocol . . . 26
3.4 Software . . . 28

4 Data Processing **29**
4.1 HRV . . . 29
4.1.1 Peak Detection Algorithm for PPG . . . 30
4.1.2 Heart Rate Computation . . . 31
4.1.3 RR-interval series filtering . . . 32
4.1.4 Statistical Variables . . . 33
4.1.5 Non-linear Variables . . . 33
4.1.6 Frequency Components . . . 34
4.2 EDA . . . 35
4.2.1 EDA Pre-Processing . . . 35
4.2.2 SCL . . . 35
4.2.3 SCR Features . . . 36
4.2.4 Frequency Analysis . . . 37

5 Results **39**
5.1 EDA Features . . . 39
5.1.1 Time-domain Analysis . . . 39
5.1.2 Frequency-domain Analysis . . . 40
5.2 HRV Features . . . 45
5.2.1 Time-domain Analysis . . . 45
5.2.2 Frequency-domain Analysis . . . 48
5.3 HRV Non-linear Variables Boxplots . . . 51
5.4 Kruskal-Wallis test . . . 52
5.4.1 EDA Kruskal-Wallis test . . . 53
5.4.2 HRV Kruskal-Wallis test . . . 53
5.5 Group 1 Features . . . 54
5.5.1 HRV Features . . . 54
5.5.2 EDA Features . . . 54
5.6 Group 2 Features . . . 55
5.6.1 HRV Features . . . 55
5.6.2 EDA Features . . . 55
5.7 Groups Separation . . . 56
5.8 Classification . . . 58
5.8.1 HRV features Random Forest Classifier . . . 58
5.8.2 HRV-EDA features Random Forest Classifier . . . 62

6 Discussion **65**

7 Future Expectations **67**

Bibliography **69**

A Appendix A - HRV Features **77**

B Appendix B - EDA Features **81**

C Appendix C - Group 1 HRV Features **87**

D Appendix D - Group 2 HRV Features **91**

E Appendix E - Group 1 EDA Features **95**

F Appendix F - Group 2 EDA Features **101**

G Appendix G - EDA Features Kruskal-Wallis test **107**

H Appendix H - EDA Groups Kruskal-Wallis test **109**

I Appendix I - HRV Random Forest Classifier **113**

J Appendix J - HRV and EDA Random Forest Classifier **115**

I Annex 1 - Publication **117**

List of Figures

2.1 Schematic of the autonomous nervous system 6
2.2 Schematic of the synaptic transmitter substances 6
2.3 Photoplethysmogram pulse waveform 7
2.4 HRV triangular index 10
2.5 Poincaré Plot 11
2.6 Electrodermal activity 12
2.7 Skin Conductance Response 13
2.8 Skin Conductance Level 13
2.9 Proposed SCR event model. 15
2.10 SCR component derivatives 15
2.11 Synchronization in the increase of EDA and heart rate 17
2.12 Flow of the Paced Auditory Serial Addition Test (PASAT) 19
2.13 SVM Hyperplane 23
2.14 Structure of a Decision Tree 24
2.15 Structure of a Random Forest Classifier 24

3.1 Wearable Device 26
3.2 Visualization of the Recording Sites 27
3.3 Digit Presentation in PVSAT 27
3.4 Representation of the warning and start of the PVSAT 28

4.1 HRV data segmentation 29
4.2 Comparison between PPG raw signal and filtered 31
4.3 Peaks Detected in PPG 31
4.4 Normal Heart Cycle 32
4.5 RR series linear interpolation 33
4.6 HRV power spectrum 35
4.7 EDA data segmentation 36
4.8 SCR features 36

4.9 EDA power spectrum 37

5.1 EDA Time-domain Variables Boxplots 40
5.2 EDA Frequency-domain Variables Boxplots 43
5.3 HRV Time-domain Variables Boxplots. 46
5.4 HRV Frequency-domain Variables Boxplots. 49
5.5 HRV Non-linear Variables Boxplots 51
5.6 SVM Group Separation 57
5.7 Groups Linear Regression 58
5.8 HRV Decision Tree in Random Forest Classifier 59
5.9 Feature Importance for HRV features 60
5.10 3D Decision Surface 60
5.11 2D Decision Boundaries 61
5.12 HRV-EDA Decision Tree in Random Forest Classifier 62
5.13 Feature Importance for HRV and EDA 63

List of Tables

3.1 Study Population Statistics 25
3.2 Wearable wrist device specifications 26

A.1 HRV Features Baseline 78
A.2 HRV Features Stress 79
A.3 HRV Features Baseline-Stress 80

B.1 EDA Features Baseline 1 82
B.2 EDA Features Baseline 2 83
B.3 EDA Features Stress 1 84
B.4 EDA Features Stress 2 85
B.5 EDA Features Baseline-Stress 86

C.1 Group 1 - HRV Features Baseline 88
C.2 Group 1 - HRV Features Stress 89
C.3 Group 1 - HRV Features Baseline-Stress 90

D.1 Group 2 - HRV Features Baseline 92
D.2 Group 2 - HRV Features Stress 93
D.3 Group 2 - HRV Features Baseline-Stress 94

E.1 Group 1 - EDA Features Baseline 1 96
E.2 Group 1 - EDA Features Baseline 2 97
E.3 Group 1 - EDA Features Stress 1 98
E.4 Group 1 - EDA Features Stress 2 99
E.5 Group 1 - EDA Features Baseline - Stress 100

F.1 Group 2 - EDA Features Baseline 1 102
F.2 Group 2 - EDA Features Baseline 2 103
F.3 Group 2 - EDA Features Stress 1 104
F.4 Group 2 - EDA Features Stress 2 105

F.5 Group 2 - EDA Features Baseline-Stress 106

G.1 EDA Kruskal-Wallis test 108

H.1 EDA Group 1 Kruskal-Wallis test 110
H.2 EDA Group 2 Kruskal-Wallis test 111

ACRONYMS

ANOVA	Analysis of Variance.
ANS	Autonomous Nervous System.
B1	Baseline 1 (0-min to 2-min).
B2	Baseline 2 (2-min to 4-min).
Bpm	Beats-per-minute.
ECG	Electrocardiogram.
EDA	Electrodermal Activity.
EDASympn	Electrodermal Activity Sympathetic tone.
FFT	Fast Fourier Transform.
GSR	Galvanic skin response.
HF	High Frequency.
HRV	Heart Rate Variability.
Hz	Hertz.
IHR	Instantaneous Heart Rate.
ISI	Inter-stimuli interval.
LED	Light-Emitting Diode.
LF	Low Frequency.
ms	milliseconds.

n.u	normalized units.
NN	Normal-to-Normal.
NN50	Number of interval differences of successive NN intervals greater than 50 ms.
PASAT	Paced Auditory Serial Addition Test.
PGR	Psycho-galvanic reflex.
pNN50	Proportion of NN50.
PNS	Parasympathetic Nervous System.
PPG	Photoplethysmography.
PSD	Power spectral density.
PVSAT	Paced Visual Serial Addition Test.
RMSSD	Square root of the mean squared differences of successive NN intervals.
s	seconds.
S1	Stress 1 (6-min to 8-min).
S2	Stress 2 (8-min to 10-min).
SCL	Skin conductance level.
SCR	Skin conductance response.
SDANN	Standard deviation of the average NN interval.
SDNN	Standard deviation of the NN interval.
SDRR	Standard deviation of RR intervals.
SDSD	Standard deviation of the successive differences.
SE	Standard Error.
SNS	Sympathetic Nervous System.
SSR	Sympathetic skin response.
SVM	Support Vector Machine.
TBI	Traumatic brain injury.
TINN	Triangular interpolation of NN interval histogram.
TVOC	Total volatile organic compound.
ULF	Ultra-Low Frequency.
VLF	Very-Low Frequency.

CHAPTER 1

INTRODUCTION

1.1 Context

In the past years there has been a significant relationship between the autonomous nervous system (ANS) and cardiovascular research [1]. The assessment of the changes in the sympathetic and parasympathetic activity of the ANS with certain diseases and pathologies, such as myocardial infarction, cardiac transplantation, myocardial dysfunction, diabetic neuropathy and depression, has been demonstrated to have important prognostic and diagnostic value [1]. Given this relationship, delineating the role of autonomous cardiac reactivity is important to prevent these serious health conditions. The autonomous nervous system is regulated by the central autonomous network in the brain, comprised of multiple neuroanatomical structures which receives input regarding the internal and external environment. These brain related structures influence heart activity, responding and adapting to environmental challenges and self-regulate, each influencing the heart in a different manner, actuating mainly on the sinoatrial node of the heart [2]. The autonomous control is transmitted to the organs of the body through two divisions of the ANS: the sympathetic nervous system (SNS) and the parasympathetic nervous system (PNS). The two systems of the ANS influence the heart in different ways. The parasympathetic system influences the heart through the vagus nerve, which mainly decreases the heart rate. Stress usually withdraws vagal activity, decreasing control of the heart via the vagus nerve. This facilitates the activation of the sympathetic system. The sympathetic system is associated with excitatory influences on the heart, resulting in an acceleration of heart rate [2].

There are many approaches to directly measure the sympathetic and parasympathetic function, although, most of them have not been materialized due to high costs, the invasiveness of the technique, the inability to provide continuous monitoring or the inaccurate assessment of the sympathetic dynamics [3]. A common, simple and noninvasive method to assess the ANS is to analyze the power spectral analysis of the Heart Rate Variability (HRV) [1, 4–7]. HRV is the study of the differences between consecutive heart beat, obtained from the time series of beat-to-beat intervals from an electrocardiogram (ECG) between consecutive heart beats,

represented by the R peak in the QRS complex of the ECG [8]. HRV can also be computed by acquiring photoplethysmography (PPG) signals, which are an optical measurement technique with widespread clinical application, such as ambulatoy patient monitoring, used to detect blood volume changes in the microvascular bed of tissue. PPG signals are a source of heart rate information, since there is a correlation between heart beats and a blood volume change. These signals are already being applied in many different clinical settings, including clinical physiological monitoring, vascular assessment, and autonomic function, such as HRV [9].

The heart rate is influenced by the autonomous nervous system, thus making HRV one of the most promising markers of autonomous activity, that allows to monitor the propensity for lethal arrhythmia and signs of either increased sympathetic or reduced vagal activity. Spectral analysis of HRV has been used to understand the modulatory effects of neural mechanisms. The parasympathetic activity is a major contributor to the high frequency (HF) component while the low frequency (LF) component is considered to be a marker of the sympathetic modulation when expressed in normalized units, but it is also influenced by the PNS [10]. The ratio between the LF and HF gives us information about the sympathetic and parasympathetic balance [11], but there is some conflicting ideas in academia about its power to be an accurate measure of the ANS since the LF component also contains information about the parasympathetic system [1].

An alternative method to directly assess the sympathetic nervous system is to measure and process electrodermal activity (EDA) [12]. This activity has been studied from two distinct theories: the vascular theory and the excretory theory. The vascular theory is based on the relationship between skin conductance changes and an increase in blood flow, implying a direct relationship between EDA and the circulatory system. This thesis will focus on the excretory theory, due to the relationship between EDA and the sympathetic branch of the ANS, stating that EDA is directly related to the sympathetic system [13]. The human skin is innervated by numerous efferent fibers, including sympathetic fibers for innervation of the eccrine sweat gland's secretory segment. The eccrine glands in the skin produce sweat when the acetylcholine transmitter passes from sudomotor fibers to these glands, which means that sudomotor transmittion is cholinergic, increasing sweat concentration and thus changing the skin electrical characteristics [14]. Eccrine glands are mostly involved in emotional responses to external stimulus [15], and only reflect activity of the sympathetic nervous system, because there is no innervation of the PNS in these glands [16]. The magnitude of sweating depends on the density of sweat eccrine glands, which varies between individuals, thus the location where EDA is measured, is an important factor to take into account. Standard sites for EDA recording are palmar locations or finger phalanges [14], although several studies started to explore the measurement of EDA at other locations, such as feet, chest, neck, wrist and ankle [15].

In order to measure these changes in the skin electrical characteristics and in heart rate, the PPG and EDA data will be acquired simultaneously, using a wearable device developed by *PLUX - wireless biosignals S.A.*, measuring EDA in the middle phalanges of the left hand. The participants will be submitted to a mental arithmetic stress test, the Paced Visual Serial Addition Test (PVSAT). In this test, the participants are presented with a series of digits that

must be summed in a narrow time interval, triggering a state of anxiety and stress among the participants, changing sweat concentration and instantaneous heart rate, thus making it easier to detect impairments in the parasympathetic and sympathetic nervous systems, due to neuropsychological syndromes.

The objective of this thesis is to analyze HRV and EDA features that describe the ANS. This work will make it possible to detect disorders in the ANS, identifying potential opportunities for clinical intervention such as prognostic or diagnosis of the diseases and pathologies named previously in this section. Finally, classification mechanisms will be applied to establish the level of unbalance between the parasympathetic and sympathetic system, in response to stress situations, mechanisms that should be validated in real use case environments.

This thesis is divided in 5 chapters. In chapter 2, theoretical concepts are presented in order to understand the basis of the ANS, PPG, HRV, EDA, PASAT, Support Vector Machines (SVM), Statistical analysis and the Random forest classifier. In chapter 3, the characterization of the study population, the description of the wearable device used, and the acquisition protocol are presented. In chapter 4, processing methods to analyze HRV and EDA features are presented, both in time-domain and frequency-domain methods. The results obtained in this thesis are presented in chapter 5, in which HRV and EDA features are calculated and their significance is analyzed with statistical tests. Also in this chapter, the separation of the subjects into two different groups according to the response to stress, is performed. Finally, a discussion of the results obtained are presented in chapter 6.

1.2 Goals

The goals of this thesis are: try to monitor the autonomous nervous system with a wearable device by processing HRV and EDA, induce stress to the participants and classify the level of stress of the participants.

The step-by-step goals to achieve the thesis objective are discriminated in the next items:

1. HRV and EDA familiarization and state-of-the-art;
2. Methods for extracting HRV and EDA;
3. Design a data acquisition protocol;
4. Data collecting using a wearable device;
5. Processing HRV and EDA data;
6. Analyze features from HRV and EDA in baseline and stress;
7. Classification of the data;
8. Validation in real use case environments.

CHAPTER 2

THEORETICAL CONCEPTS

2.1 Autonomous Nervous System

The autonomous nervous system is responsible for controlling arterial pressure, sweating, body temperature, heart rate, among others activities. One of the most striking characteristics of the ANS is the quickness and intensity with which it can increase heart rate to twice the normal (in 3 to 5 seconds) or induce sweating within seconds. The ANS is activated mainly by centers located in the spinal cord, brain stem and hypothalamus [17].

The autonomous signals are transmitted to the body through two branches of the ANS: the sympathetic nervous system (SNS) and the parasympathetic nervous system (PNS) (Fig.2.1). The sympathetic and parasympathetic nerve fibers secrete two synaptic transmitter substances: acetylcholine and epinephrine. The fibers that secrete acetylcholine are called cholinergic while those that secrete epinephrine are called adrenergic (a term derived from adrenalin). The terminal nerve endings of the parasympathetic system all secrete acetylcholine, thus its influence on heart rate is mediated via release of acetylcholine by the vagus nerve, while the terminal nerve endings of the sympathetic system secrete epinephrine (Figure 2.2), thus its influence on heart rate is mediated via release of this neurotransmitter [13, 17].

An example of the effects of the ANS in the heart is the modulation of its beating. A sympathetic stimulati increases the overall activity of the heart by increasing its rythm and its force of contraction. On the other hand, a parasympathetic stimulati decreases the heart rate and strength of contraction [2]. During resting conditions, the activity of the vagus nerve is dominant and variations in heart rate are largely dependent on vagal modulation.

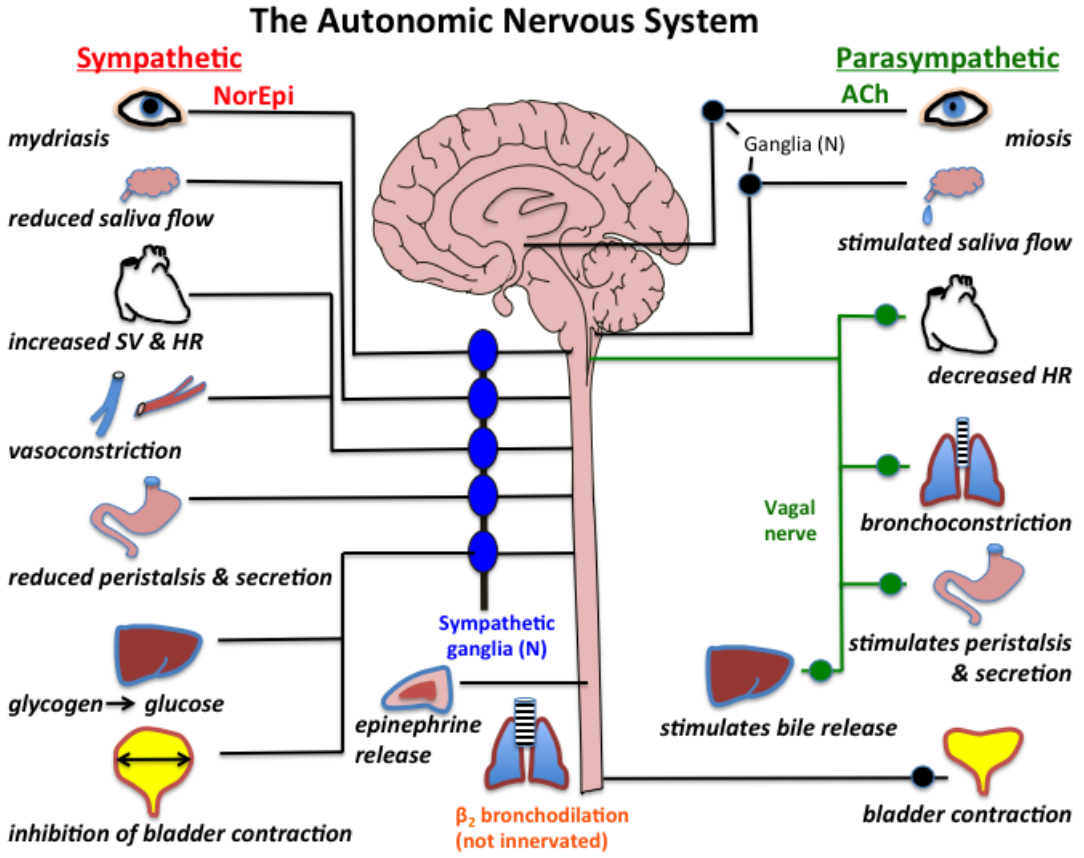

Figure 2.1: Schematic of the autonomous nervous system and its divisions into the parasympathetic and sympathetic systems. The release of the neurotransmitter acetylcholine by the parasympathetic system and epinephrine by the sympathetic system, affects the major organs shown in the schematic [18].

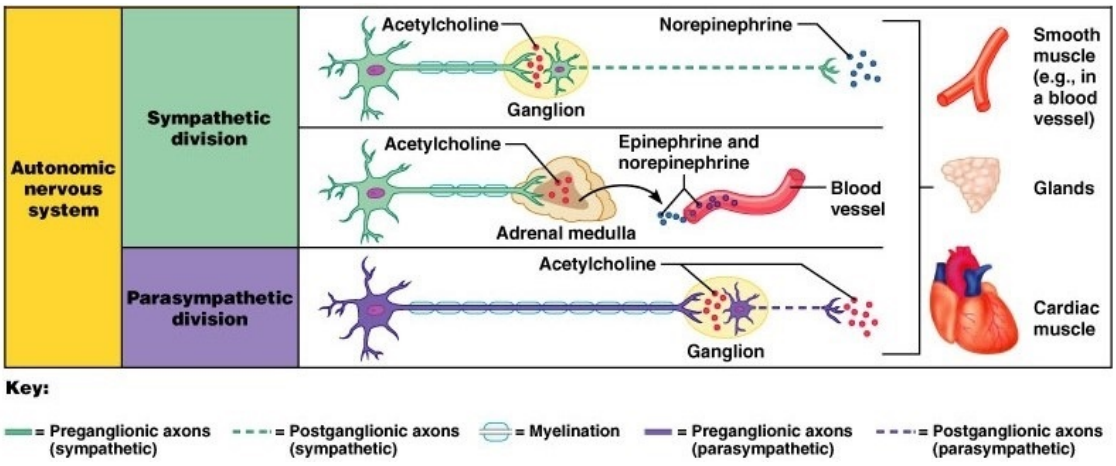

Figure 2.2: Schematic of the synaptic transmitter substances in the ANS. Adapted from [19].

2.2 Photoplethysmography (PPG)

Photoplethysmography (PPG) is an optical measurement technique with widespread clinical application, used to detect blood volume changes in the microvascular bed of tissue. PPG requires the usage of only two opto-electronic components in order to acquire a signal: a light source (light-emitting diode) to illuminate the skin, and a photodetector to measure variations in light intensity associated with changes in perfusion. The amount of light received is influenced by key factors, such as blood volume, blood vessel wall movement and the orientation of red blood cells [9, 20]. The interaction of light with the skin is complex and involves processes such as, scattering, absorption, reflection, transmission and fluorescence. In this thesis, the configuration used to detect PPG is the reflection mode, where the LED and detector are placed side-by-side in the skin, and the signal received is the amount of light reflected, emphasizing that a good contact with the skin is necessary to acquire a clean signal, without excessive pressure, to avoid blanching. The PPG waveform pulse (Fig.2.3) is defined by the appearance of two phases: the anacrotic phase and the catacrotic phase. The anacrotic phase refers to the rising edge of the pulse, related to the systole, and the catacrotic phase refers to the diastole and wave reflections from the periphery. Also, a dicrotic notch is usually seen in the catacrotic phase in patients with healthy arteries [9]. Heart rate can be estimated by the difference between two consecutive systolic peaks.

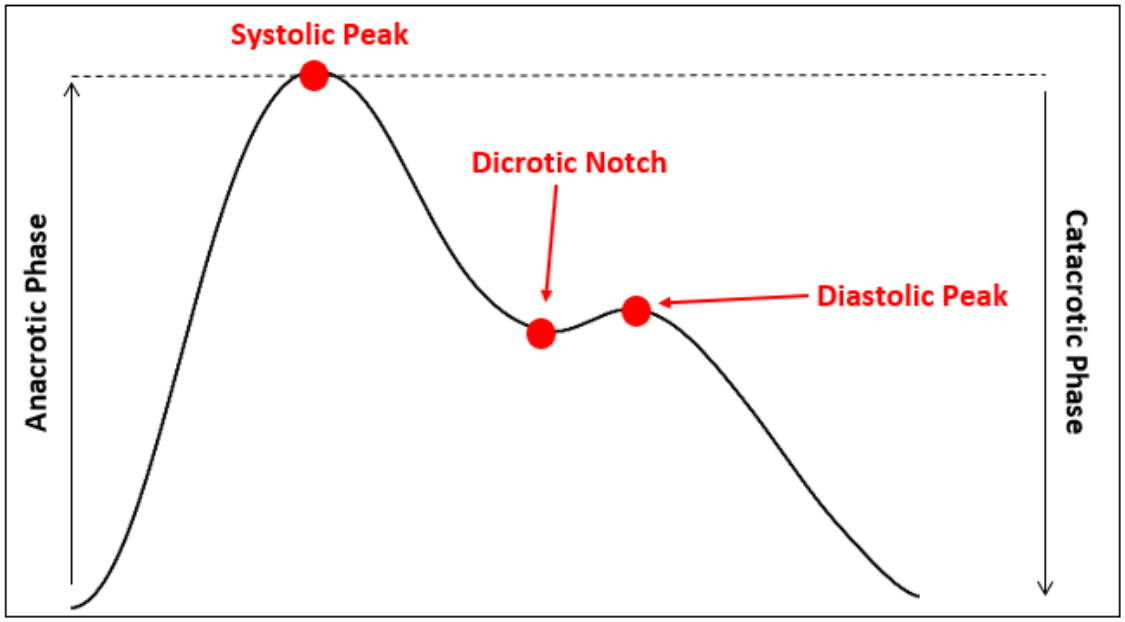

Figure 2.3: Photoplethysmogram pulse waveform. The PPG pulse is composed by the anacrotic Phase and the catacrotic phase. The systolic peak corresponds to the systole and the diastolic peak corresponds to the diastole.

2.3 Heart Rate Variability (HRV)

2.3.1 HRV Concepts

HRV is the study of the differences between consecutive heart beat, obtained from the time series of beat-to-beat intervals from an electrocardiogram (ECG) between consecutive heart beats, represented by the R peak in the QRS complex of the ECG [8]. An ECG is a time-series signal measured on skin surface which reflects the electrical activity of the heart [8]. It is obtained by recording the potential difference between two electrodes and a reference placed on the body surface, requiring a minimum of three electrodes connected with wires to the subject, to obtain an ECG recording.

The PPG signal reduces the number of contact surfaces to simply one wire, which is desirable for cardiac monitoring in ambulatory situations [20, 21]. Heart rate in a PPG signal is obtained by calculating the difference in time between two consecutive systolic peaks corresponding to the ventricular depolarization, and HRV can be infered from differences in heart rate [22–24]. There are several methods and features possible to extract from the information of HRV, as we will see in sections 2.3.2 and 2.3.3.

2.3.2 Time domain methods

Time domain methods are the simplest methods to perform. After removal of artifacts in RR intervals, these intervals are also called as normal-to-normal intervals (NN). From these two measurements, it is possible to calculate time variables, such as, the mean NN interval, the mean heart rate, the longest and the shortest NN interval, the standard deviaton of NN intervals and instantaneous heart rate (IHR), as well as statistical and geometrical features [10].

2.3.2.1 Statistical methods

From series of IHR or NN intervals, particularly those that are recorded over 5-min or 24h, more complex statistical time domain variables [8, 25–27] can be calculated such as:

- Standard deviation of the NN interval (SDNN)
- Standard deviation of the average NN interval (SDANN)
- SDNN index
- RMSSD
- NN50
- pNN50

These variables are derived from direct measurements of NN intervals. The simplest variable to calculate is the standard deviaton of the NN intervals (SDNN). SDNN is calculated over a 5-min or 24h period, and thus, including both short-term high frequency variations as well

as the lowest frequency components in the 24h period recording, being influenced by both the SNS and PNS activity. The RMSSD is the square root of the mean squared differences of sucessive NN intervals and is used to estimate the changes reflected in HRV by the PNS, the NN50 is the number of interval differences of successive NN intervals greater than 50 ms, and finally, the pNN50 is the proportion of dividing NN50 by the total number of NN intervals, and is closely correlated to the PNS [8, 10, 25, 28]. Another statistical variable is the standard deviation of the average NN interval (SDANN) calculated over periods of 5 min, which is an estimate of heart rate changes due to cycles longer than 5 min. The SDNN index is the mean of the 5 min SDNN calculated over 24h, measuring the variability due to cycles shorter than 5 min. These last two variables will no be included in this thesis, due to the length of the recordings chosen (5-min) [10].

2.3.2.2 Geometrical methods

The series of NN intervals can also be converted into a geometric pattern, such as the sample density distribution of NN intervals duration, the sample density distribution of differences between adjacent NN intervals and the Lorenz plot of NN intervals. There are three main approaches that are used in geometric methods:

1 - The geometric pattern is converted into the measure of HRV.

2 - The geometric pattern is interpolated by a mathematically defined shape.

3 - The geometric shape is classified into several pattern-based categories which represent different classes of HRV.

The HRV triangular index measurement is the integral of the density distribution (D in Fig.2.4), i.e., the number of all NN intervals divided by the maximum of the density distribution. The triangular interpolation of NN interval histogram (TINN) is the baseline width of the distribution measured as a base of a triangle, approximating the NN interval distribution. The details of computing the HRV triangular index and the triangular interpolation of NN interval are shown in figure 2.4 [10, 27].

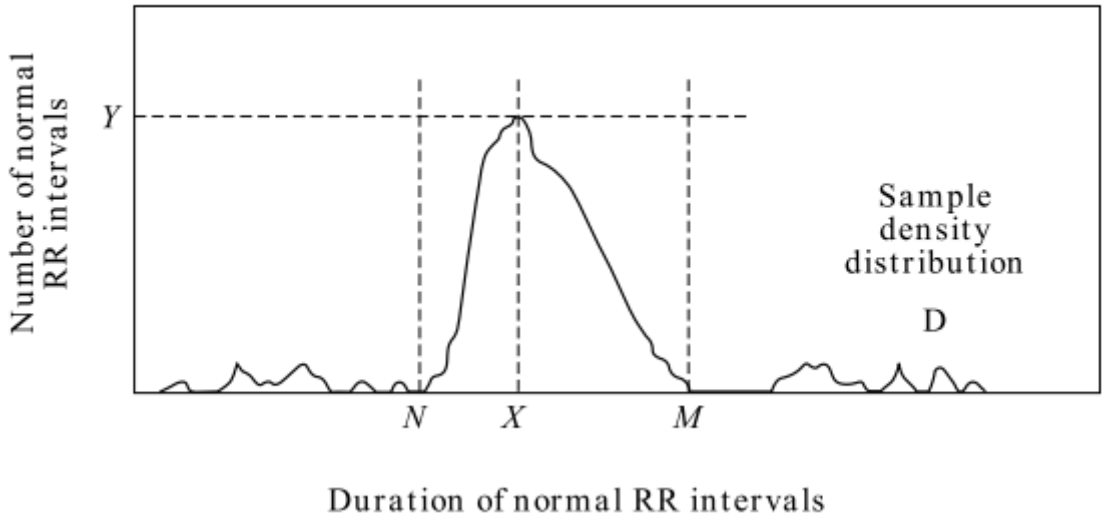

Figure 2.4: The HRV triangular index is calculated by dividing the number of all NN intervals by the maximum of the density distribution Y=D(X). The TINN is calculated by the difference between the values M and N (TINN=M-N)[10].

2.3.2.3 Nonlinear Geometrical Methods

HRV nonlinear geometric measures are derived from the 5-min Poincaré plot. This plot represents the diagram in which each RR interval is plotted against the previous RR interval [7, 28]. The markings of the Poincaré plot are gathered around a line of unitary slope (slope=1) passing through the origin. The center point of the markings represents the average length of the RR interval. An ellipse is then fitted to the plot with the center of the ellipse coinciding with the center point of the markings and comparing points, from two lines, a longitudinal and a transverse, through this center point. The length of the longitudinal line is defined as the SD2 of the plot data, while the transverse line is defined as the SD1 of the plot data (Fig.2.5). The SD2/SD1 ratio reflects the balance between the sympathetic and parasympathetic system, as the SD2 length refers to the sympathetic activity, and the SD1 length refers to the parasympathetic activity [7].

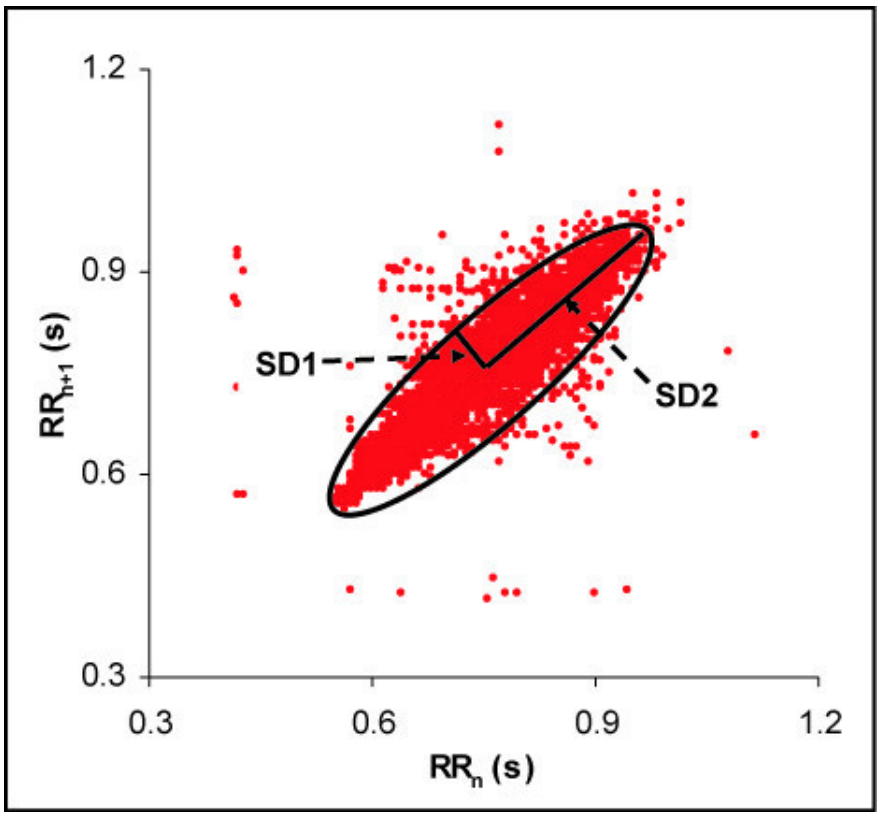

Figure 2.5: Poincaré Plot. SD1 - length of the transverse line. SD2 - length of the longitudinal line. The SD2/SD1 ratio reflects the nonlinear balance between the sympathetic and parasympathetic systems.

2.3.3 Frequency domain methods

In frequency-domain methods, power spectral density (PSD) analysis provides information on how the HRV is distributed in the frequency domain. These methods can be classified as non-parametric and parametric. The advantages of the non-parametric methods are: the simplicity of the algorithm employed (Fast Fourier Transform (FFT)) and the high processing speed.

In short-term recordings (5-min) it is possible to distinguish three main spectral components: very low frequency (VLF) band between 0.0033 and 0.04 Hz , low frequency (LF) band between 0.04 and 0.15 Hz and high frequency (HF) band between 0.15 and 0.4 Hz [8, 29, 30]. The measurement of these components is made in absolute values of power (ms^2), but LF and HF can also be measured in normalized units (n.u.), which represent the relative value of each power component in proportion to the total power minus the VLF component. The representation of LF and HF in normalized units emphasizes the control and balanced behaviour between the two branches of the autonomous nervous system, so that HF derives from vagal activity or the PNS, and LF derives from sympathetic activity [8]. In long-term recordings, such as a 24h period, the result of spectral analysis includes an ultra-low frequency (ULF) component [10].

2.4 Electrodermal Activity (EDA)

2.4.1 EDA Concepts

As mentioned in section 1.1, the human skin is innervated by numerous efferent fibers, including sympathetic fibers for innervation of the eccrine sweat gland's secretory segment. The eccrine glands in the skin produce sweat when the acetylcholine transmitter passes from sudomotor fibers to these glands, increasing sweat concentration that changes the skin electrical characteristics [14], making it possible to measure EDA.

EDA (Fig.2.6) can be divided into the following components: skin conductance response (SCR),skin conductance level (SCL), sympathetic skin response (SSR), galvanic skin response (GSR) and the psycho-galvanic reflex (PGR). In this thesis, the signal will be divided in the SCL (tonic component) and the SCR (phasic component). The phasic component (Fig.2.7) is the result of the activation of the sympathetic system, after a stimulus presentation, being usually overlapped by the tonic component (Fig.2.8), which is not directly related to the presentation of the stimulus [31]. The skin conductance response (SCR) is composed by two zones: a rise zone and a decay zone. The rise zone starts at the initial instant (t_0), and marks the moment the sudomotor system reacts to the ANS. The rise time is defined as the time that it takes from the moment t_0 to reach the maximum of the rise zone, t_2 (Fig.2.10) [13].

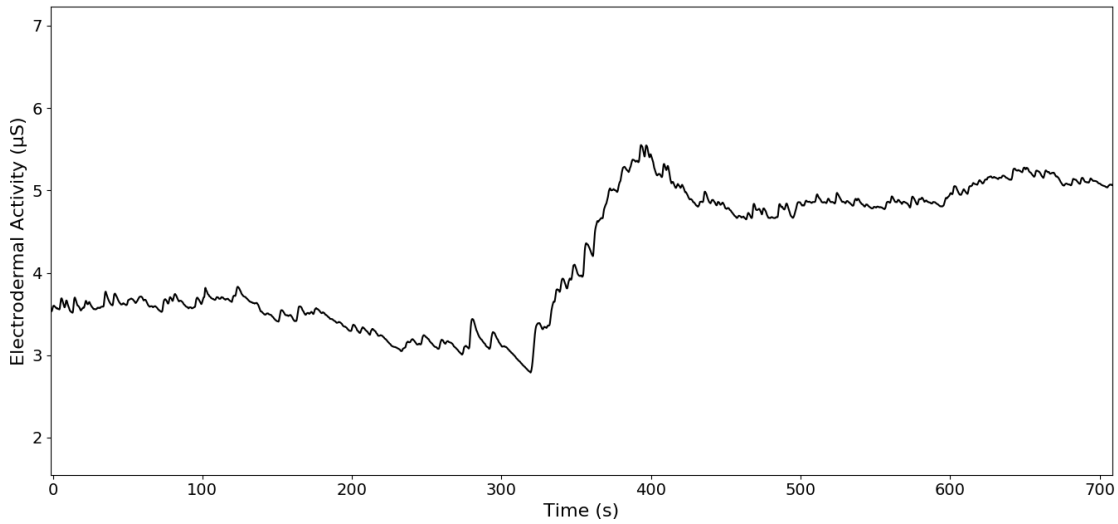

Figure 2.6: Electrodermal activity signal.

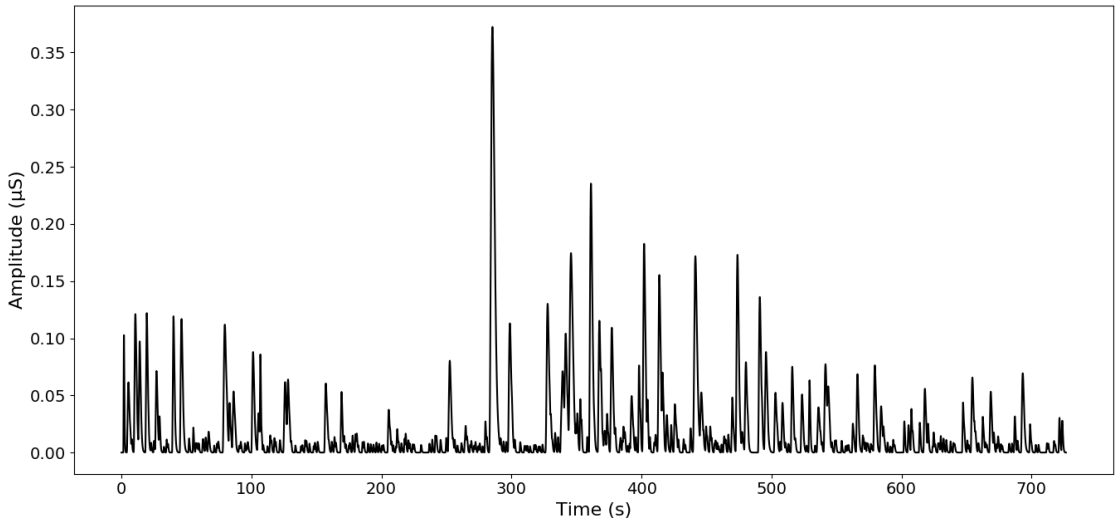

Figure 2.7: Skin Conductance Response (SCR) component of the EDA signal.

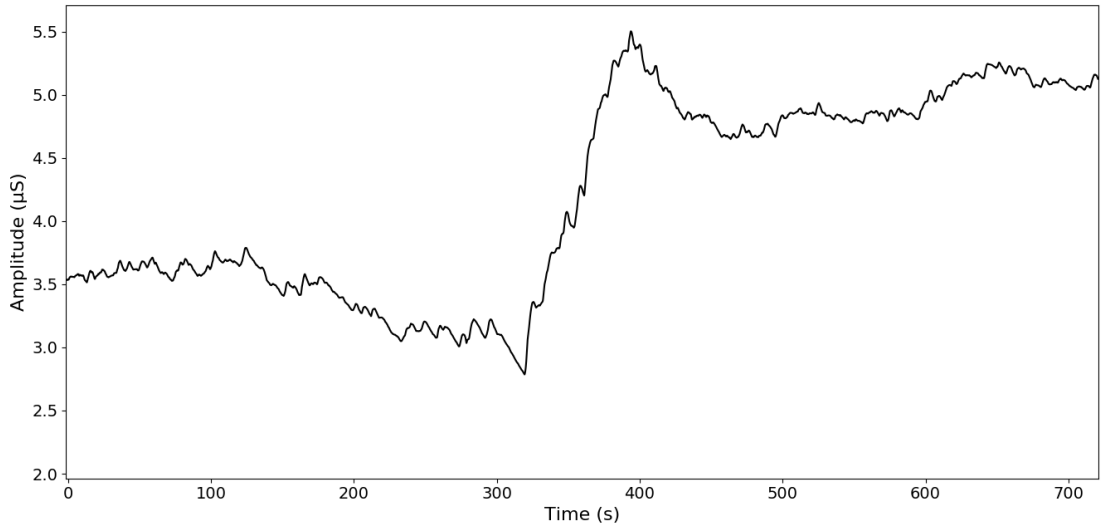

Figure 2.8: Skin Conductance Level (SCL) component of the EDA signal.

2.4.2 EDA Measurement

EDA measurement is usually performed in the hand palm, particularly in the anterior part of the finger tips. In order not to disturb people while performing some task using the hands, it is common to place the electrodes on the non-dominant hand, given that EDA presents a symmetrical characteristic. Using the endosomatic approach (constant current) to measure the electrical mechanism, the sympathetic skin response is the result of a distinct processing path where the low frequencies (SCL) are typically obtained by band passing the signal in the $0.1 - 2$ Hz frequency [13].

2.4.3 EDA Models

2.4.3.1 Modeling Difficulties

The two main difficulties encountered by EDA models in electrodermal events detection and quantification is the overlapping events and the occurrence of low amplitude events, leading to distorted values extracted for the events [32]. The problem of overlapping events in an SCR event occurs when an event ensues immediately after another SCR event, usually masking the real values of the event in the decay zone of the SCR peak. When an EDA event has low amplitude compared to the decreasing exponential of a previous SCR event, it will not be detected by either models based on visual detection or those that are based in the first derivative and zeros. In both these problems, the parameters of an SCR event will not be correctly extracted from the signal [13].

2.4.3.2 EDA Models

The modeling of the EDA has passed through several phases along its research history and technological evolution. The first models to interpretate EDA signal were based on visual detection of skin conductance responses, where the observer manually annotated the time instants of the start of the events. This approach is considered to be a qualitative approach. With the improvement of computational resources, the next models applied to the EDA were based on the identification of the valleys and peaks of the signal. These models assumed the existence of two zones in a SCR event, that were computed by the signal derivatives and corresponding zero crossings. As with the latter, these models were unable to retrieve correct parameters in a case of an event overlap or in case of an event so smooth that does not have a peak or a valley. The sigmoid-exponential model proposed a set of models of increasing complexity, solving the problem of the overlapping SCR events, but the intrinsic problems of the optimization were still a problem, as the success a good fit to the model depended on the parameter initialization [13].

2.4.3.3 Model Applied

The proposed model [13] is based on a morphological study of the EDA signal. In order to detect the SCR component, this model applies signal filtering and computation of signal derivatives, eliminating the constant components, such as the SCL. The first step of the algorithm is to filter the signal with a lowpass butterworth 4th order filter (1 Hz). For simplicity of the model, it is assumed that the SCR event is isolated, with null SCL. After filtering, it is necessary to detect the second order derivative zeros, corresponding to the instants t_1 and t_3 as shown in Figure 2.10. From this figure, it is possible to note that the SCR signal is continuously differentiable. Then, considering the SCR events as the impulsive response with transfer function H(s) from equation 2.1, the overlapping events were considered as a linear operation, as shown in figure 2.9. The impulsive response $h(t)$ is given by the inverse Laplace transform (Eq.2.2) with $u(t)$

being the unitary step function and $k = 4$.

$$H(s) = \frac{\alpha}{(s+b)^n} \tag{2.1}$$

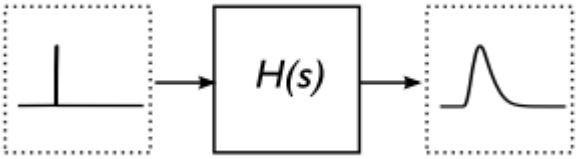

Figure 2.9: Proposed SCR event model.

$$h(t) = \mathscr{L}^{-1}(H(s)) = \alpha t^k e^{-bt} u(t) = f(t)u(t) \tag{2.2}$$

Next, for each pair of zeros (t_1, t_3), compute the parameters α, b, t_0 of the proposed model given by equations 2.3,2.4,2.5, and finally compute the SCL component (Fig.2.8) by subtracting the detected events from the total EDA signal. This model is then, able to detect and quantify normal events, overlapping events and small events [13].

$$\alpha = b^3 \frac{f'(t_1) - f'(t_3)}{16e^{-2} + 432e^{-6}} \tag{2.3}$$

$$b = \frac{4}{t_3 - t_1} \tag{2.4}$$

$$t_0 = \frac{3t_1 - t_3}{2} \tag{2.5}$$

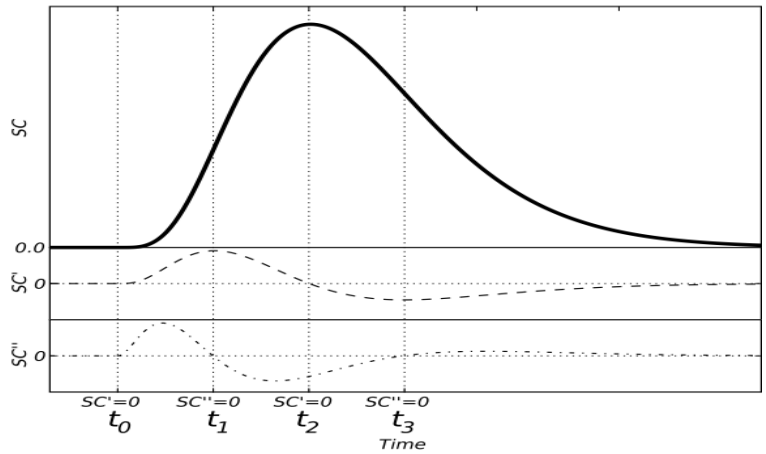

Figure 2.10: SCR component derivatives of the algorithm implemented [13].

2.4.4 EDA Processing

2.4.4.1 Time Domain methods

EDA recording is based on relatively slow-changing and high latency physiological processes, so the analysis of EDA is mainly performed in time-domain methods, using the SCR and the SCL components. These latencies are normally between 1 and 2 seconds, but may be delayed up to 5 seconds in cases of skin cooling [14]. A measure of the amplitude of the EDA event is the most frequently metric, measuring an increase or decrease of the amplitude of the components of the EDA, due to a presentation of a stimulus after a certain latency [14]. Although these time domain methods are the most used procedures to analyse EDA, several studies have reported a high variability between subjects and low consistency when using time domain methods and therefore, frequency domain methods have been reported as a tool of sympathetic tone (EDASympn) assessment [4].

2.4.4.2 Frequency Domain methods

Frequency domain methods have rarely been used to analyze EDA. Posada-Quintero et al. [1] performed PSD analysis of EDA using Welch's periodogram method to obtain the power spectra of the EDA.

2.5 HRV and EDA relationship: Review

In a situation of induced stress, the balance of the PNS and SNS changes. The control mechanisms of the ANS to this stimuli, is a reduction of the parasympathetic activity and increase of sympathetic activity, leading to an increase in heart rate. EDA is known to be directly related to the dynamics of the cardiac and peripheral sympathetic nervous systems [33], so its association with HRV as been studied for the last years. The low frequency component of HRV provides information about the sympathetic system, although it is also influenced by the parasympathetic system, so EDA gives us clear information about the sympathetic response to stress. Posada-Quintero et al.[1] showed that there was a considerable increase in the power spectra of the EDA in the same frequency range of the low frequency component of the HRV [1]. Kettunen et al. [34] showed that changes in EDA and heart rate, tend to exhibit interdependent changes in certain cognitive tests, as an acceleration in heart rate was synchronized with an increase in EDA level (although the increase in EDA was slightly later than the increase in heart rate, as shown in figure 2.11). This synchronization suggests that both EDA and heart rate are influenced by a common autonomic mechanism, such as the ANS [35]. Also, studies around specific pathologies, such as schizophrenia, showed that HRV and EDA are more interrelated than with control patients [36], so it is possible to monitor changes in the ANS through an EDA and HRV wearable device in patients with neural impairments.

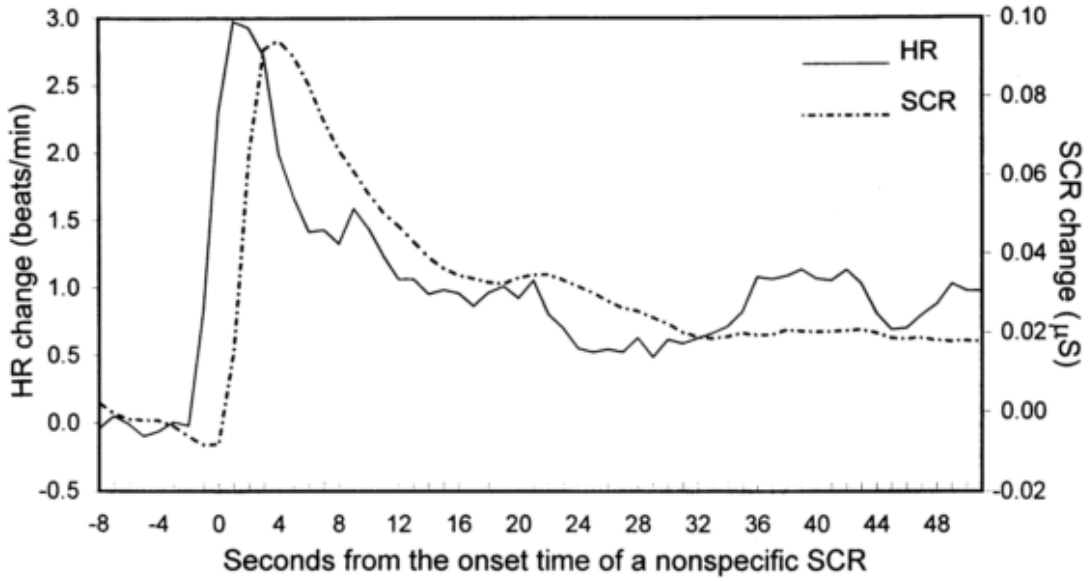

Figure 2.11: Synchronization in the increase of EDA and heart rate [34].

2.6 Paced Auditory Serial Addition Test (PASAT)

The Paced Auditory Serial Addition Test (PASAT) was developed to assess the effects of traumatic brain injury (TBI) on cognitive functioning, though subsequent research has shown that the

PASAT has clinical utility in also detecting impairments in cognitive processing in patients with neuropsychological syndromes [37–39]. The PASAT involves presenting a series of single digit numbers and ask the subject to sum the two most recent digits, for example, if the digits '3', '2' and '4' were presented, the participant would correctly respond, '5' and '6', as shown in Figure 2.12. The participant must respond prior to the presentation of the next digit for a response to be scored as correct. Usually four different rates (2.4s, 2.0s, 1.6s and 1.2s) are used to present the next digit [38, 40]. The scores reported for the PASAT are the number of correct responses for each trial and the total number of correct responses summed over all trials. An alternative score is the average time per correct response, giving a statistic that allows comparing results from studies that use different number of trials or different number of digits within a trial. Other PASAT scoring procedures include percent correct, latency of responding, and number of errors. There are two versions of the PASAT: the auditory and the visual test, named PVSAT. The performance on the PVSAT is superior to that on the PASAT, due to reduced input-output competition, so there is less interference between the articulated response and incoming visual stimuli, because each is processed in separate pathways, providing a better measure of speed of information processing [37]. Perhaps the most important weakness of the PASAT is that it does not determine precisely at what speed information is processed and any temporal threshold measure when an individual is no longer able to consistently process information [40]. To perform the PASAT, several cognitive functions are required to complete the test. These included sustained attention, working memory, and simultaneously performing several cognitive tasks under specific time constraints [37]. The repeated experience with the PASAT improves the performance, showing more pronounced practical effects at shorter inter-stimuli interval (ISI) values. After the second administration of the PASAT there is a great stability in the performance of the patient. The PASAT is considered to be a difficult and complex test, so it requires time and practice to develop an effective strategy to perform on this type of test, leading to states of anxiety and frustration among patients. One indication of the degree of difficulty is relatively low percent of correct responses that occur at the faster presentation rates. By measuring the skin conductance from EDA, it is possible to measure different levels of stress, due to anxiety, difficulty concentrating, irritability and physiological arousal, when administrating the PASAT [37].

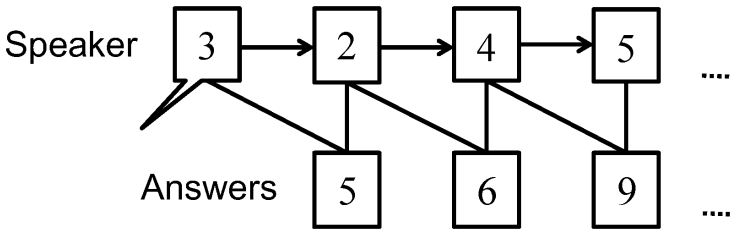

Figure 2.12: Flow of the PASAT [41].

2.7 Statistical Analysis

2.7.1 Kruskal-Wallis test

The Kruskal-Wallis 1-way analysis of variance by ranks is a non-parametric alternative test (H-test) to the 1-way ANOVA test. The 1-way ANOVA is used to determine whether there is any statistically significant difference between the means of two or more independent groups [42]. The null hypothesis of the ANOVA is that there is an absence of effect, such as no difference in the means between the baseline and the stress groups. The ANOVA produces an output, the F-value, which is a ratio between the "Between-group Variance"and the "Within-group Variance"(Eq.2.6), so a higher *F-value* produced means a large amount of variance between the baseline and stress group, and a larger significant effect [43]. The ANOVA test has important assumptions that must be satisfied [44]:

- The samples are independent.
- The observations within each group are normally distributed.
- The standard deviations of the groups are all equal (homoscedastic).

$$F-value = \frac{\text{Between-group Variance}}{\text{Within-group Variance}} \tag{2.6}$$

The Kruskal-Wallis test is a non-parametric test, so it means that is does not assume the normality of the data nor the homoscedaticity. The H-test uses ranked values, so the values observed are converted to their ranks in the data set: the smallest value gets a rank 1, the next smallest gets rank 2, and so on. The Kruskal-Wallis null-hypothesis is that the mean ranks of the different groups are the same [45], so as in the ANOVA-test, a *p-value* lower than the significance level is better, concluding that the null hypothesis may not adequately explain the observation - there is in fact variation between the ranked means of each group. The level of significance α is chosen by the user, usually being $\alpha = 1\%, 5\%$ or 10%. To quantify the statistical significance of the test, the *p-value* is used in the context of null hypothesis. So, the *p-value* is the probability, under the null hypothesis, of obtaining a result that would be equal to or more extreme than its observed value. In this case, it is expected to obtain significant difference between the two groups, concluding that a *p-value* lower than the significance level ($p-value < 0.05$), is

better and that the null hypothesis may not adequately explain the observation. The *H-value* is computed with equation 2.7, if there are no ties (no two observations are equal)[46, 47].

$$H-value = \frac{12}{N(N+1)} \sum_{i=1}^{C} \frac{R_i^2}{n_i} - 3(N+1) \tag{2.7}$$

where:

C = the number of groups.

n_i = the number of observation in the *i*th group.

N = $\sum n_i$ the number of observations in all groups combined.

R_i = the sum of the ranks in the *i*th group.

In case of ties, each observation is given the mean of the ranks for which it is tied, so the *H-value* needs to be corrected (Eq.2.9), by dividing it by equation 2.8, where the summation is over all groups of ties [46, 47].

$$1 - \frac{\sum T}{N^3 - N}, \qquad T = t^3 - t \quad \text{with t = number of tied observations in the group} \tag{2.8}$$

$$H_{ties} = \frac{H}{1 - \frac{\sum T}{N^3 - N}} \tag{2.9}$$

The degrees of freedom for the H-value are computed by *df1*=C-1, where C is the number of groups (2: Baseline and Stress). The interpretation of the resultant *H-value* is made by comparing it with the chi-square table. If there are more than five observations in each group, the *H-value* is distributed as a chi-square distribution with C-1 degrees of freedom - $\chi^2(1)$ [47]. The chi-square table shows that in order to obtain significant results (*p-value*<0.05) the *H-value* must be higher than 3.84.

2.7.2 Chi-square test for Goodness of Fit

The chi-square test (χ^2) is a test applied to determine whether a categorical variable from a single population is consistent with a hypothesized distribution. It is applicable to many situations in which experimental frequencies are compared to theoretical frequencies based on a hypothesis [48]. The null hypothesis for the χ^2 test is that the categorical data has the given frequencies. This test has some assumptions that must be satisfied: the sampling method is simple random sampling, the variable is categorical and the expected value for the number of observations is at least 5. The χ^2 statistic value is given by equation 2.10, where n is the number of observations, O_i is the *i*th observed value and E_i is the *i*th expected value [49]. The degrees

of freedom for the χ^2 value are computed by $k-1-ddof$, where k is the number of observations and $ddof$ is the adjustment to the degrees of freedom for the *p-value*, due to the linear regression performed, adding an extra constraint to the test ($ddof = 1$).

$$\chi^2 = \sum_{i=1}^{n} \left[\frac{(O_i - E_i)^2}{E_i} \right] \tag{2.10}$$

In the context of this thesis, the χ^2 test will be applied in section 5.7, to test the goodness of the linear regression line performed [50], by comparing the values observed calculated using the regression line obtained, with the expected values. In this situation, by contrast with the Kruskal-Wallis test, it is better to obtain a *p-value* higher than the significance level, that is, we expect to accept the null hypothesis, so that the difference between the observed values and the expected values is minimized.

2.8 Support Vector Machines (SVM)

Support Vector Machines (SVM) were developed by Vapnik et al. from statistical learning theory and machine learning [51]. SVMs are a family of algorithms for learning two-class discriminat functions from a set of training examples, in order to find a suitable boundary (called a hyperplane), in data space to separate the two classes. The basis of this boundary is the concept of margin, which is the minimal distance between the hyperplane separating the two classes and the closest points to it, defined as the support vectors. In linearly separable data, the kernel of SVM used is the maximal margin classifier or hard margin SVM. Considering a linearly separable data sample $S = \{(x_1, y_1), ..., (x_i, y_i)\}$ where i is the sample size, with a binary classification of the classes, such as $Y = \{-1, 1\}$, the support vectors are calculated based on equation 2.11 with a decision function given by equation 2.12 [52]. The points $\mathbf{x}$ are located in the hyperplane that satisfies equation 2.11, where the support vectors $\mathbf{w}$ define a direction perpendicular to the hyperplane, and the parameter b moves the hyperplane parallel to itself, as shown in Figure 2.13 . For the two different classes, it is possible to define that the decision function has a positive and a negative value (± 1), so considering two generic points x^+ and x^-, that belong, respectively, to the positive and negative class, have a decision function given by equations 2.13 and 2.14. The margin γ that maximizes the distance between the hyperplane and the two classes, can be achieved by minimizing the two-norm of $\mathbf{w}$ [53]. The expression to calculate this margin is given by equation 2.15. All these parameters are represented in Figure 2.13.

$$\langle \mathbf{w}, \mathbf{x} \rangle + b = 0, \quad \mathbf{w}, \mathbf{x} \in \mathbb{R}^n, b \in \mathbb{R} \tag{2.11}$$

$$f(x) = sign(\langle \mathbf{w}, \mathbf{x} \rangle + b) \tag{2.12}$$

$$\langle \mathbf{w}, x^+ \rangle + b = 1 \tag{2.13}$$

$$\langle \mathbf{w}, x^- \rangle + b = -1 \tag{2.14}$$

$$\gamma = \left\langle \frac{w}{\| w \|}, (x^+ - x^-) \right\rangle = \frac{2}{\| w \|} \tag{2.15}$$

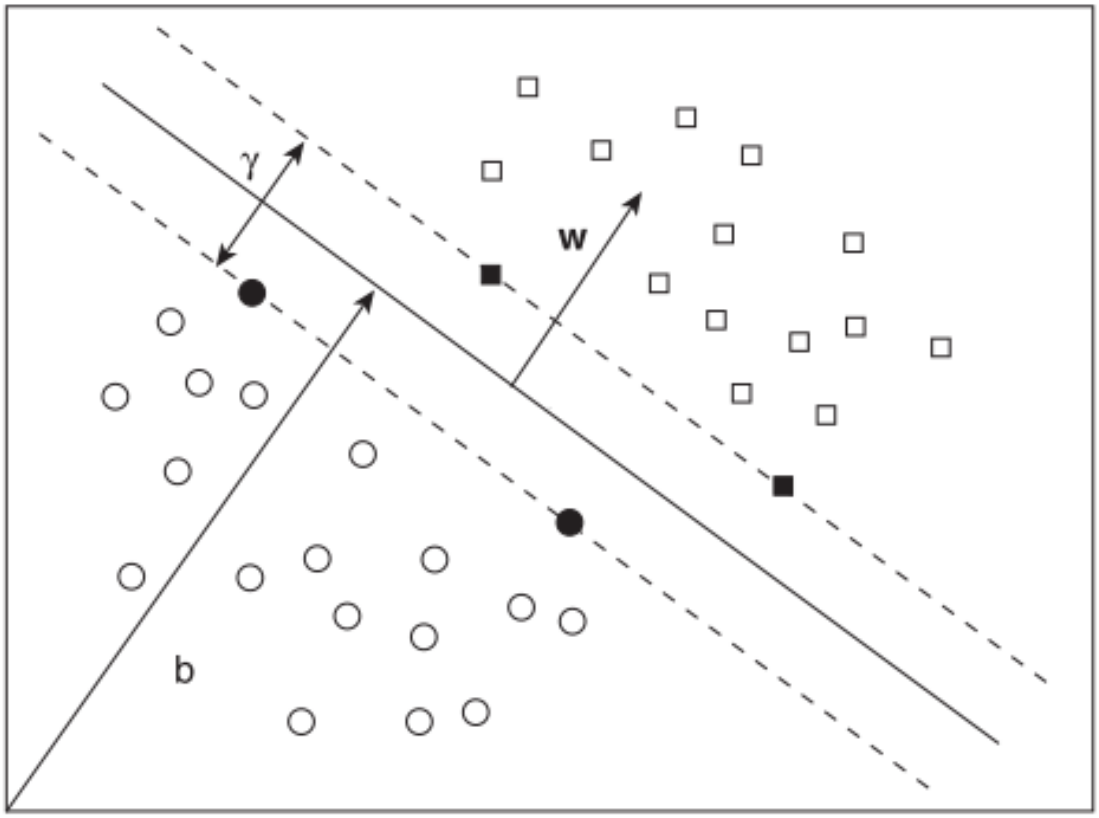

Figure 2.13: Support Vector Machine - The hyperplane separates the data into two classes: circles represent class -1 and squares represent class +1. The bold circles and squares represent the support vectors. The margin γ , the parameter b and the vectors w, are also represented [53].

2.9 Random Forest Classifier

Random Forest classifiers are based on the Decision Tree algorithm. Decision Trees are a supervised method of classification in machine learning, using pre-classified data. The division of the data is based on the values of features of the given data, by deciding which features, best divide it, creating a set of rules for the values of each feature. A decision tree has a root (the start of the tree), nodes (the positions where the branches divides), branches, and leaves. The nodes represent a certain characteristic for a feature while the branches represent different paths based on the values for those features. The leaves are the final step, where a classification is returned, taking into account whether that feature value is True or False in that node [54]. The structure of a tree is shown in figure 2.14. The Random Forest classifier is a combination of multiple decision trees, where each decision tree is made by randomly selecting portions of the data, reducing the correlation between trees, improving the prediction power and results with a higher efficiency. The Random Forest is appropriate for binary data, achieving a better result than decision trees, through the use of bagging on samples. This bagging method is used to reduce the variance of an estimator and improve overall generalization error, it aggregates the prediction from each tree and averaging to form a final prediction [55, 56]. For example, in a

random forest classifier with 10 decision trees, if 6 out of 10 trees classify the data as belonging to group 1, the random forest will output that classification. The structure of a random forest classifier is shown in figure 2.15.

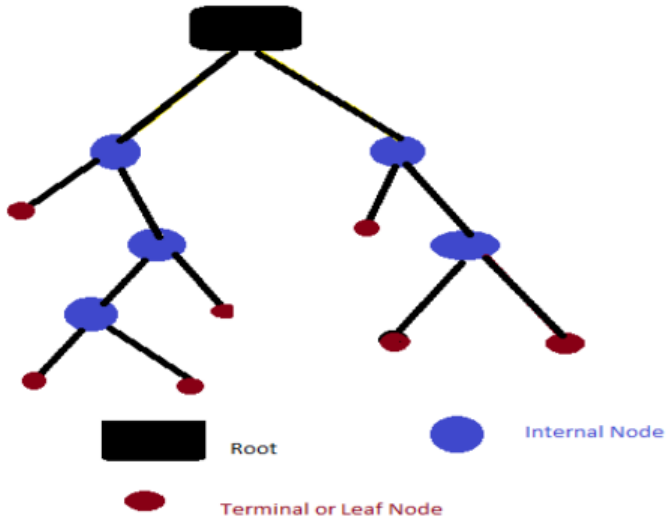

Figure 2.14: Structure of a Decision Tree [54].

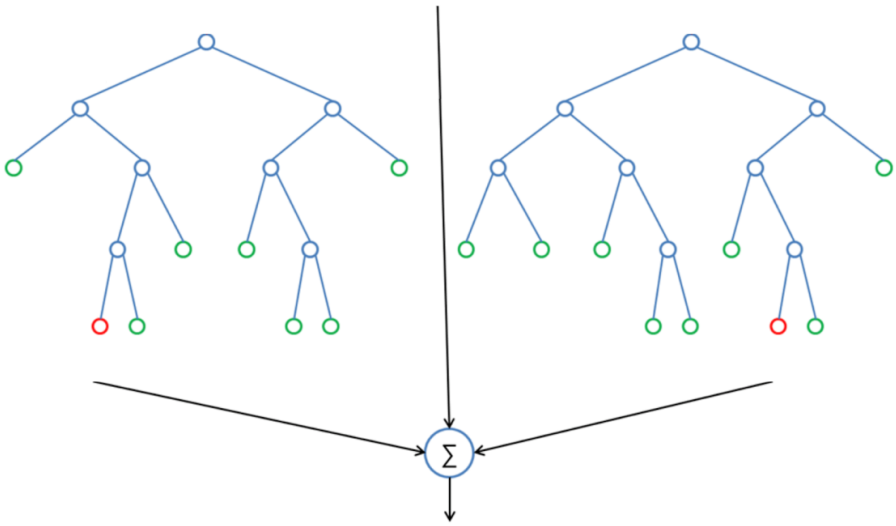

Figure 2.15: Structure of a Random Forest Classifier [57].

CHAPTER 3

MATERIALS AND PROCEDURE

In this chapter, it's described the wearable device used to acquire the EDA and PPG signals, as well as the software used to record and visualize the biosignals recorded. Also, a description of the acquisition protocol designed to implement the PVSAT is presented.

3.1 Study Population

Data was acquired from a group of healthy (reported) volunteer subjects. The total number of participants were fifteen (9 females and 6 males), ages from 21 to 55 years old (31 ± 11), height from 1.57 to 1.85 meters (1.73 ± 0.09) and weight from 52 to 94 kilograms (72 ± 13). This study was approved by FCT-UNL ethical committee and all subjects signed an informed consent. Table 3.1 gives the statistics for the study population.

Table 3.1: Study population characterization statistics for all subjects

	Mean	STD	Min	Max
Age (years)	31	11	21	55
Height (m)	1,72	0,09	1,57	1,85
Weight (kg)	72	13	52	94

3.2 Wearable Device

Data was acquired using a BITalino wearable wrist device with 6 different sensors, developed by PLUX - Wireless biosignals, with their resolutions, channels and sampling rates, described in table 3.2. The EDA sensor in channel 1,refers to that measured in the left distal wrist, whilst the sensor in channel 3 was used to measure EDA in the fingers (see Figure 3.1). The total volatile organic compound (TVOC), the CO2 and the temperature sensors were not used for the purpose of this thesis. All the signals were acquired with a sampling rate of 1000 Hz and with a 10-bit resolution. The EDA wrist sensor uses dry electrodes (two stainless steel stubs), the PPG sensor

is a green LED with a photodetector in reflection mode and the external EDA sensor uses Ag/Cl gel electrodes.

Figure 3.1: Wearable Device.

Table 3.2: Description of the wearable wrist device specifications.

Sensor	Channel	Resolution (bit)	Sampling Rate
EDA wrist	1	10	10 Hz 100 Hz 1000 Hz
PPG	2	10	
Spare	3	10	
TVOC	4	10	
CO2	5	6	
TEMP	6	6	

3.3 Acquisition Protocol

The experiment was performed in a quiet room, at ambient temperature, in order to avoid interference that would distract the participants. The total length of the protocol was 12 minutes (6-min baseline + 6-min stress). The subjects were asked to sit in a comfortable chair and avoid any movement during the entire experiment, specially in the left arm (where the wearable was strapped). PPG and EDA signals were recorded simultaneously, being the finger EDA attached to the anterior middle phalanges of the 2nd finger (Position 1 in Fig. 3.2a) and 3rd finger (Position 2 in Fig. 3.2a) of the left hand. The PPG signal was recorded on the posterior distal left wrist, as shown in Figure 3.2b.

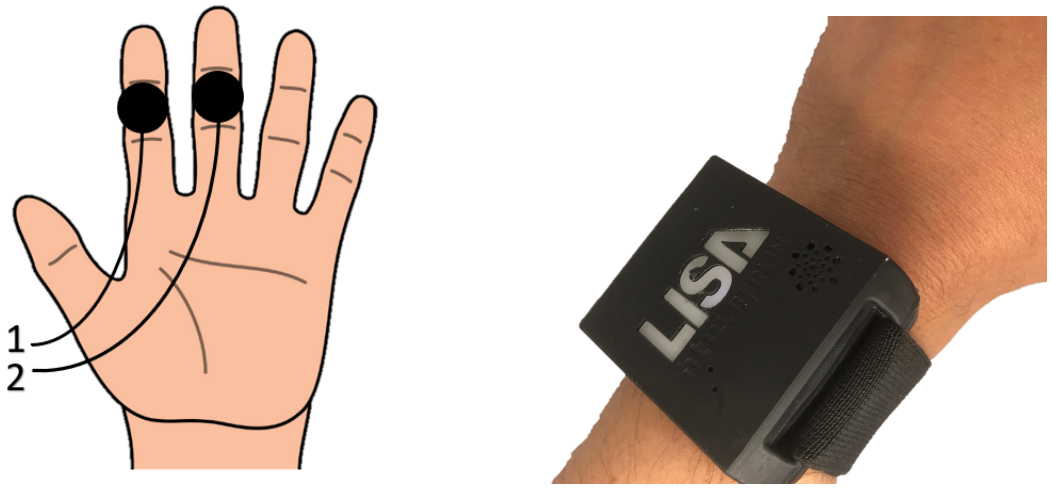

(a) EDA Recording Site. Adapted from [58].

(b) PPG Recording Site.

Figure 3.2: Visualization of the recording sites for both the PPG and EDA biosignals.

After placing the wearable device and the finger EDA sensor, the PVSAT test was explained to the subjects. Participants were presented with a series of single digits numbers and had to sum the two most recent digits, before the presentation of the next digit (see section 2.6). The PVSAT was performed to in the last 6-min, using a 12.2"tablet with white single numbers from 1 to 9, against a black screen (see Fig. 3.3). The digits were presented with a 3s rate for the first 2min, decreasing half a second every two minutes (2.5s and 2s). The subjects had to respond prior to the presentation of the next digit, and speak aloud each response. A 30s warning before the beginning of the PVSAT was given to all participants (Blue line in Fig. 3.4). During baseline measurements, the subjects were asked not to speak.

Figure 3.3: Example of the digit presentation in the PVSAT.

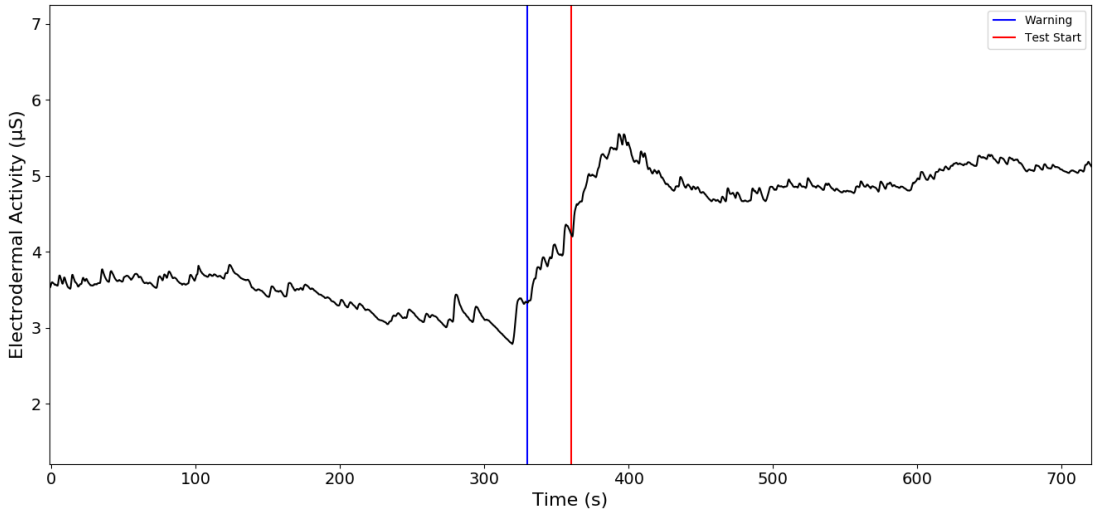

Figure 3.4: Representation of the warning and start of the PVSAT. EDA signal increases at the warning 30s before the PVSAT starts (Blue line). The start of the PVSAT is represented by the Red line.

3.4 Software

The software used to acquire the PPG and EDA data was PLUX's OpenSignals software. This software is easy-to-use, versatile and allows real-time biosignals visualization, being capable of direct interaction with all PLUX's devices via bluetooth. It is also capable to record simultaneous data for up to 24 channels, as well as loading pre-recorded signals.

All the processing of HRV and EDA in the following chapters was performed using Python programming language.

CHAPTER 4

DATA PROCESSING

4.1 HRV

The HRV data for all subjects was divided into two segments, one for each situation during the experiment: baseline and stress. As it is necessary to have 5-min recordings to compute frequency analysis of HRV, the baseline data goes from the start of the experiment to the 5th minute (Green band in Fig.4.1). The time between the 5th and the 7th minute (Red band in Fig. 4.1) was considered to be the transition band, where the heart rate changes significantly from baseline to stress, so this band was excluded. Finally, the stress data goes from the 7th minute, in which heart rate is already stable in the stress status, to the end of the experiment (Yellow band in Fig. 4.1). These bands are shown in Figure 4.1.

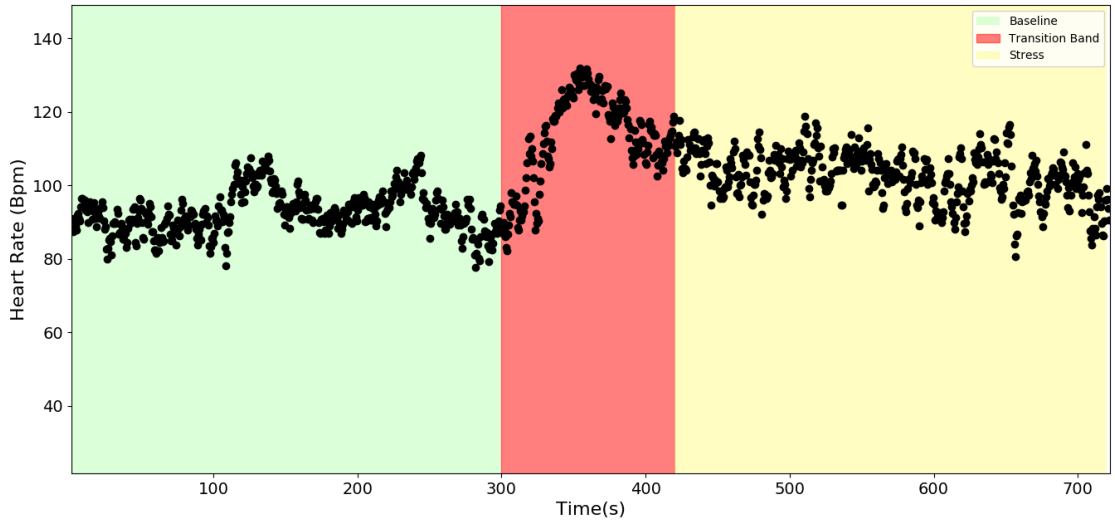

Figure 4.1: HRV data division in 5-min segments. Baseline status - 0-min to 5-min (Green band), Stress status - 7-min to 12-min (Yellow band). The Red band corresponds to the excluded Transition band.

4.1.1 Peak Detection Algorithm for PPG

The algorithm implemented to detect a peak in a PPG wave is based on the algorithm used in [59]. The characteristic PPG wave is composed by two waves: the systolic wave corresponding to the systole and the dicrotic wave corresponding to the diastole. The valley between these two waves is called the dicrotic notch (Fig. 2.3). First, it is necessary to filter the signal in order to remove noise. The signal was filtered with a 2nd order lowpass Butterworth filter with the cutoff frequency set at 2 Hz, followed by a 2nd order highpass Butterworth filter with a cutoff frequency of 0.1 Hz (Fig.4.2). Then, the algorithm detects all the peaks and valleys, as well as their locations, in the signal. Being the PPG signal a time series represented by $PPG(i) = \{PPG_1, PPG_2, ..., PPG_N\}$ where N is the length of the PPG signal, the peaks and the valleys are those points that satisfies the following criteria:

$$\text{Peaks PPG} = PPG(i) : PPG(i-1) < PPG(i) > PPG(i+1) \quad ; \quad i = 1, 2, ..., N \tag{4.1}$$

$$\text{Valleys PPG} = PPG(i) : PPG(i-1) > PPG(i) < PPG(i+1) \quad ; \quad i = 1, 2, ..., N \tag{4.2}$$

This step assumes that the processing of the signal starts with a valley. In case the first peak location comes first compared to the first valley location, the first peak location is discarded and the processing of the signal starts with a valley. Then, it calculates the difference in amplitude between the peaks (Eq. 4.1) and the valleys (Eq. 4.2) using equation 4.3.

$$\text{Peaks to Valleys Difference (i)} = \text{Peaks PPG (i)} - \text{Valleys PPG (i)} \quad ; \quad i = 1, 2, ..., k \tag{4.3}$$
$$\text{k = number of peaks}$$

After calculating these differences in amplitude, the algorithm will search for the differences that are greater than 50% of a 5-point window moving average (Eq. 4.4), discarding the lower points that do not verify this criteria, getting the final number of peaks with significance for heart rate computation (Fig.4.3). This last step is performed iteratively until the number of peaks from two iterations stays the same.

$$PVD(i) > 0.5 * \frac{PVD(i-2) + PVD(i-1) + PVD(i) + PVD(i+1) + PVD(i+2)}{5} \tag{4.4}$$
$$i = 1, 2, ..., k-2$$

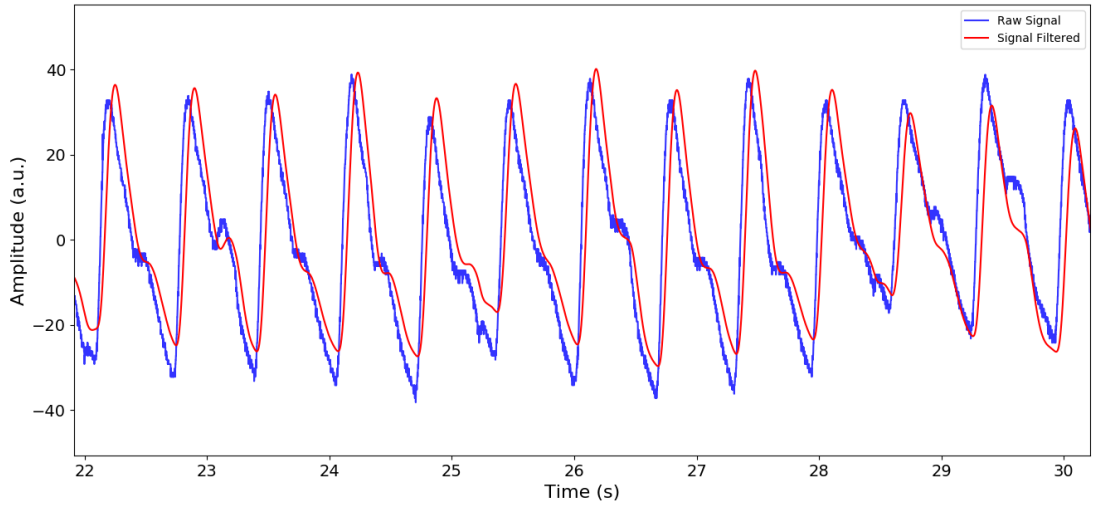

Figure 4.2: Comparison between the PPG raw signal acquired (blue line) and the PPG signal filtered (red line).

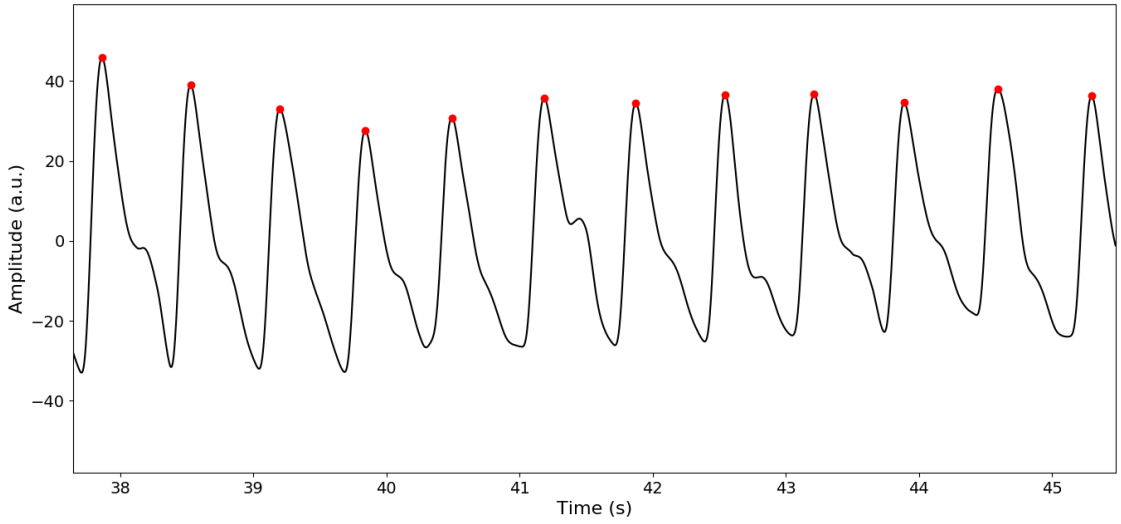

Figure 4.3: Peaks Detected (Red dots) with the algorithm implemented.

4.1.2 Heart Rate Computation

Heart rate is obtained by calculating the interval between two consecutive peaks, detected with the algorithm in section 4.1.1. In order to remove artifacts or errors in the detection of peaks, RR intervals lower than 380 ms were removed due to physiological conditioning, as a normal heart cycle (Fig.4.4), usually lasts at least 380 ms (PR interval: 120 ms - 200 ms, QRS width: 80 ms - 120 ms, QT interval: 350 ms - 430 ms). The instantaneous heart rate (IHR) is given by equation 4.5.

$$\text{IHR (Bpm)} = \frac{60}{\Delta RR} \quad ; \quad \Delta RR = RR_i - RR_{i-1} \quad ; \quad i = 1, 2, ..., k \tag{4.5}$$

Time-domain variables such as the average and the standard deviation for RR intervals and the IHR were also calculated.

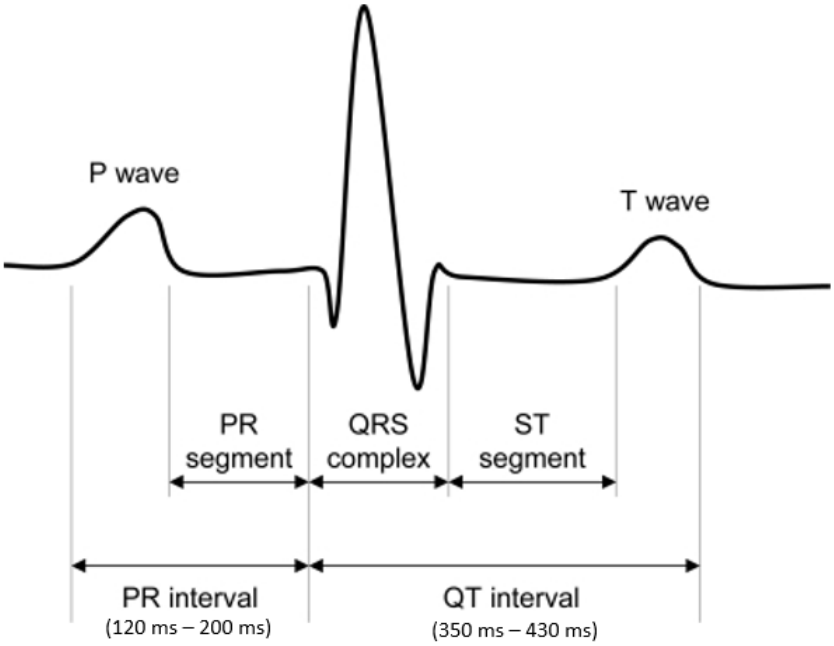

Figure 4.4: Normal Heart Cycle [60].

4.1.3 RR-interval series filtering

RR-interval series recorded from the wearable device PPG sensor are subject to different kinds of artifacts [61], with the most common, being motion artifact, breathing artifact and ectopic beats, thus leading to a wrong detection of the peak [62]. To correct the miscalculated RR-interval, a 7-point moving average window is computed, in respect to the RR-interval series. If a RR-interval differs more than 20% of the moving average or if the value RR_{i+1} is smaller than 75% of the value RR_{i-1}, those points are considered as a wrong detection. Then, a linear interpolation is computed for each miscalculated interval based on the points used for the moving average window, except for the miscalculated point, using the *interp1d* function from *Scipy's Interpolate* package (see Fig. 4.5). Finally, the IHR series is calculated using the new interpolated RR-interval series with the equation 4.5 in section 4.1.2.

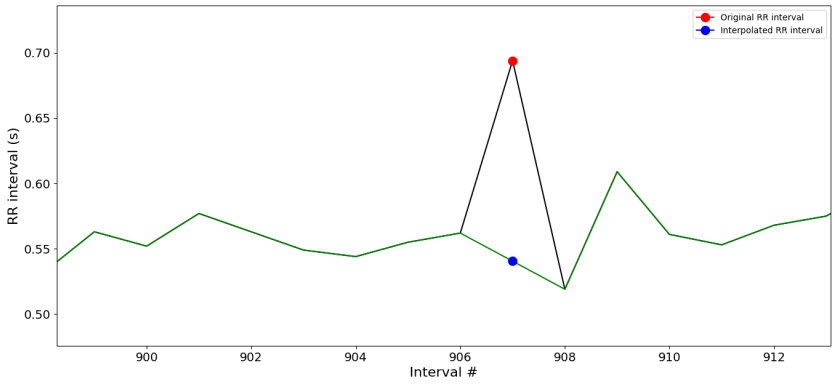

Figure 4.5: RR series linear interpolation. The black line represents the original RR series and the green line represents the interpolated RR series. The red circle is the miscalculated interval and the blue circle the interpolated interval.

4.1.4 Statistical Variables

The HRV statistical variables, related to the variance of the RR intervals obtained in section 4.1.2, are given by the following equations, where RR_i is the ith interval between peaks, $\overline{RR}$ is the average RR interval and n is the total number of intervals [27].

$$SDNN = \sqrt{\frac{1}{n-1}\sum_{i=1}^{n}(RR_i - \overline{RR})^2} \tag{4.6}$$

$$RMSSD = \sqrt{\frac{1}{n-1}\sum_{i=1}^{n-1}(RR_{i+1} - RR_i)^2} \tag{4.7}$$

$$NN50 = \#(\mid RR_i - RR_{i-1} \mid) > 50ms \tag{4.8}$$

$$pNN50 = \frac{NN50}{n} * 100\% \tag{4.9}$$

4.1.5 Non-linear Variables

The non-linear geometric variables derived from the Poincaré plot of the RR intervals are calculated with equations 4.10, and 4.11, where SDRR is the standard deviation of the RR intervals and SDSD is the standard deviation of the successive differences of the RR intervals [63]. The $SD2/SD1$ ratio was also computed.

$$SD1^2 = \frac{1}{2}Var(RR_n - RR_{n+1}) = \frac{1}{2}SDSD^2 \tag{4.10}$$

$$SD2^2 = 2SDRR^2 - \frac{1}{2}SDSD^2 \tag{4.11}$$

4.1.6 Frequency Components

The frequency components of HRV can be obtained by computing the power spectrum of the RR intervals. The RR-interval time series is an irregularly time-sampled series, thus it is necessary to interpolate and resample to avoid the appearance of additional harmonic components in the power spectrum. Therefore, and according to a person's IHR, which can go up to approximately 250 Bpm (4 Hz), and according to the Nyquist theorem, which states that the sampling frequency must be higher than the double of the signal frequency, a resampling frequency of 10 Hz was chosen. First, a cubic spline representation of the RR-interval time series was performed with *splrep* function from *Scipy's Interpolation* package, obtaining the vector of knots, the spline coefficients and the degree of the spline. Then, a new time array of 5-min was created with a sampling frequency of 10 Hz, instead of the original RR-interval frequency. Finally, the new regular time-sampled RR-interval series is obtained by evaluating the spline function at the points in the new time array with the given knots and coefficients, with *splev* function from *Scipy's Interpolation* package. Additionally, the mean of the signal was subtracted to remove any trend.

The power spectrum for baseline and stress (Figure 4.6) was computed using a periodogram, applying to each segment, a Hanning window. Then, the PSD was calculated for each windowed segment.

To calculate the power (ms^2) of each frequency component, the integrate of each component was computed using the function *trapz* from *Scipy's Integrate* package. The normalized frequency components were calculated by dividing the LF (Eq.4.12) or HF (Eq.4.13) power, by the total power minus the power of the VLF component. The ratio between the LF and HF components is calculated in equation 4.14.

$$LF(n.u) = \frac{LF}{\text{Total Power} - VLF} * 100 \tag{4.12}$$

$$HF(n.u) = \frac{HF}{\text{Total Power} - VLF} * 100 \tag{4.13}$$

$$\text{LF/HF ratio} = \frac{LF(n.u)}{HF(n.u)} \tag{4.14}$$

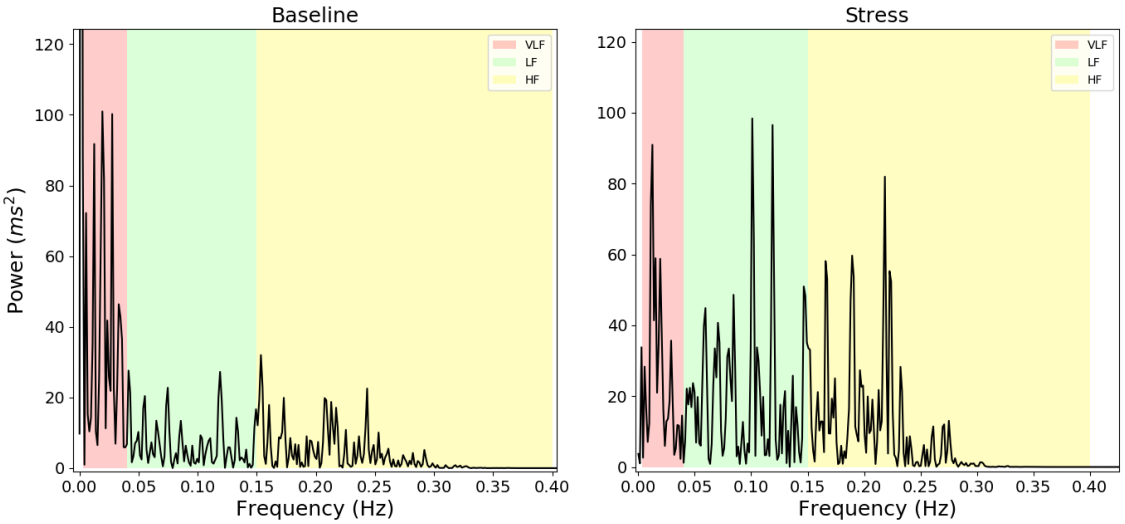

Figure 4.6: HRV power spectrum. The left spectrum corresponds to a Baseline status and the rigth spectrum corresponds to the Stress status. VLF (0.0033-0.04 Hz) - Red band, LF (0.04-0.15 Hz) - Green band, HF (0.15-0.4 Hz) - Yellow band.

4.2 EDA

In terms of EDA recordings, each subject's data was divided in five segments, each with 2 minutes duration: two bands in baseline, two bands in stress and a transition band. To perform frequency analysis on EDA it is necessary to divide the data into segments of 2-min: Baseline 1 goes from the start of the experiment to the 2nd minute (Green band in Fig. 4.7), Baseline 2 goes from the 2nd minute to the 4th minute (Blue band in Fig. 4.7), Stress 1 goes from the 6th minute to the 8th minute (Yellow band in Fig. 4.7) and Stress 2 goes from the 8th minute to the 10th minute (Purple band in Fig. 4.7). The Red band in Fig. 4.7, 4th minute to 6th minute, was considered the transition band, where the EDA level changes significantly, due to the warning of the start of the PVSAT test, 30s before the start of the test.

4.2.1 EDA Pre-Processing

In order to extract the EDA features from the recordings, a 4th order lowpass butterworth filter was used with the cutoff frequency set at 1 Hz. Then, the model applied mentioned in section 2.4.3, computed the impulsive response $h(t)$ for each peak, thus obtaining the SCR events.

4.2.2 SCL

The SCL was computed by subtracting the total EDA signal fitered by the SCR, giving a baseline level measure of EDA amplitude.

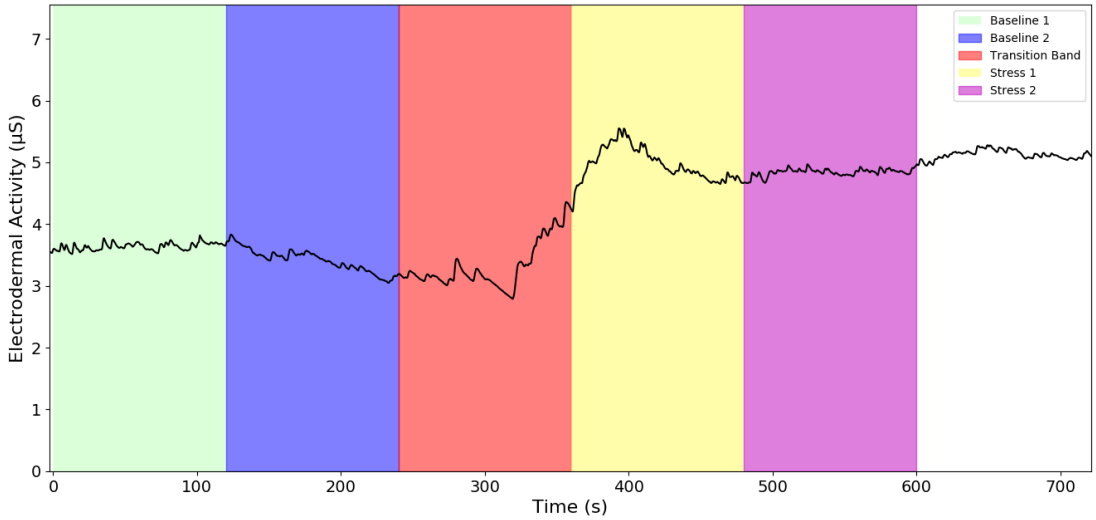

Figure 4.7: EDA data division in 2-min segments. Baseline 1 - 0-min to 2-min (Green Band), Baseline 2 - 2-min to 4-min (Blue band), Stress 1 - 6-min to 8min (Yellow band), Stress 2 - 8-min to 10-min (Purple band). The Red band corresponds to the Transition band.

4.2.3 SCR Features

SCR features reflects the response of the sympathetic nervous system, to an external stimuli. Time related features were calculated such as the rise time, corresponding to the latency from the initial instant (1% of the maximum value of the peak amplitude) until the maximum value of the corresponding peak. The latency from the maximum value of a peak to the value in which the peak amplitude decreases 50% and 63% in the descending zone, are called, respectively, SCR 50% Recovery time (Rec.t 50%) and SCR 63% Recovery time (Rec.t 63%). A threshold of 0.005 µS was applied. All these features are shown in Figure 4.8.

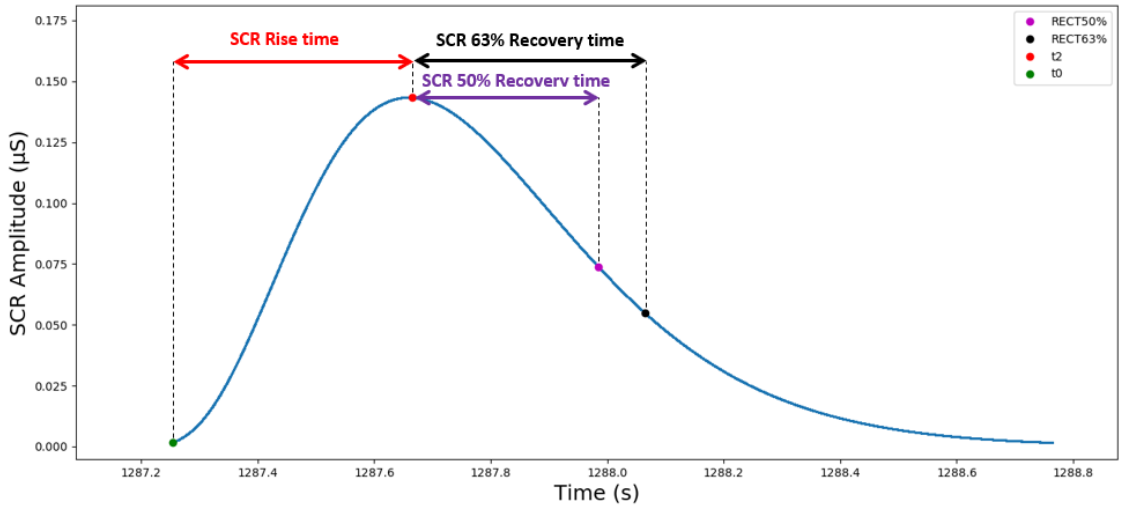

Figure 4.8: SCR features. The green mark corresponds to 1% of the maximum value (t0), the red mark corresponds to the maximum value of the peak (t2), the purple and the black mark correspond to the values in which the amplitude decreases, respectively, 50% and 63%.

4.2.4 Frequency Analysis

To compute frequency-domain analysis on EDA, the signal was filtered as mentioned in section 4.2.1, and then down-sampled. Down-sampling from 1000 Hz to 1 Hz was performed in three steps using consecutive factors of 1/10, with *decimate* function from *Scipy's Signal* package. Then the signal was highpass filtered with a 8th order Butterworth at 0.01 Hz, to remove any trend [64]. The power spectrum was computed using a periodogram, applying to each segment, a Blackman window. Then, the PSD was calculated for each windowed segment. The frequency band to assess the sympathetic nervous system through EDA used by Posada-Quintero et al. [1] was modified to the frequency band from 0.04 Hz to 0.35 Hz. Finally, the power of the bands of interest (Band 1 (0.04-0.35 Hz) and Band 2 (0.35-0.5 Hz)), was calculated to compare the changes in power in normalized units (nu) given by equations 4.15 and 4.16, in respect to baseline recordings and stress recording, to verify if there was an increase in power on Band 1 during the stress situation, to confirm the stimulation of the sympathetic nervous system.

$$\text{Band 1 (n.u)} = \frac{\text{Band 1}}{\text{Total Power}} * 100 \tag{4.15}$$

$$\text{Band 2 (n.u)} = \frac{\text{Band 2}}{\text{Total Power}} * 100 \tag{4.16}$$

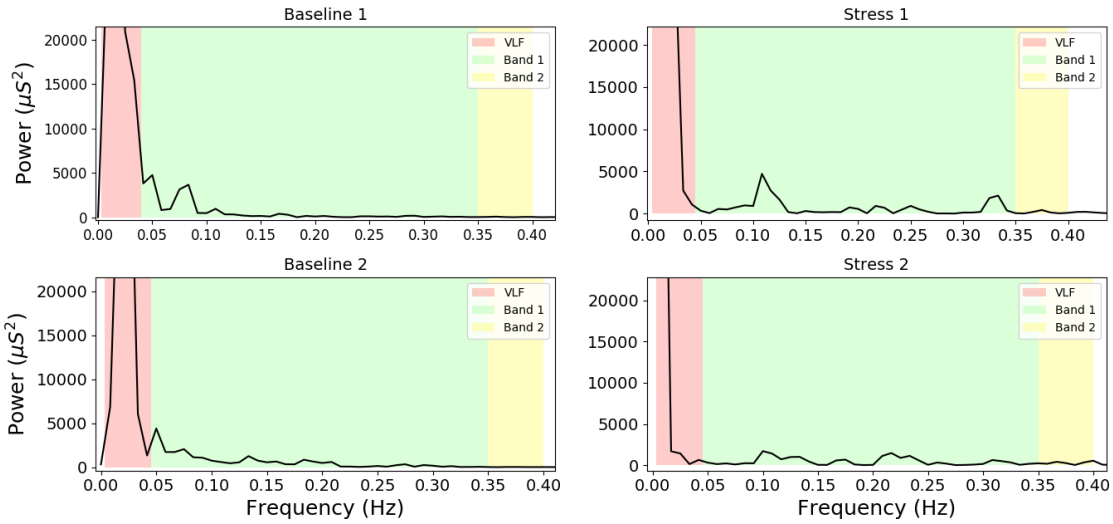

Figure 4.9: EDA power spectrum. VLF (0-0.045 Hz) - Red band, Band 1 (0.045-0.35 Hz) - Green band, Band 2 (0.35-0.5 Hz) - Yellow band.

CHAPTER 5

RESULTS

In this chapter, analysis of all the features extracted from the HRV and EDA signals in both time-domain and frequency-domain are presented, with special focus on the frequency-domain of both signals, in order to assess the changes in the sympathetic and parasympathetic nervous system. Statistical tests were also performed to evaluate the significance of variance between baseline and stress.

5.1 EDA Features

All EDA features extracted are described in Appendix B, with values such as Mean, Standard Error, Median, Min, Max and the percentiles. Baseline 1 (B1) features are described in Appendix B.1, Baseline 2 (B2) in Appendix B.2, Stress 1 (S1) in Appendix B.3 and Stress 2 (S2) in Appendix B.4. Finally, a comparison between mean values and standard error in the different segments mentioned are described in Appendix B.5

5.1.1 Time-domain Analysis

For EDA time-domain features the results reported an increase in the values of SCL, SCR, Rise time, Rec.t 50% and Rec.t 63% in stress. The Number of peaks didn't report any significant change between baseline and stress.

SCL values ranges from 1.3990 to 5.2439 µS (3.224 ± 1.1575) in B1, in B2 from 1.1200 to 5.1982 µS (2.7372 ± 1.1675), in S1 from 1.8323 to 6.6924 µS (4.0745 ± 1.3352) and S2 from 1.1279 to 8.8152 µS (3.7393 ± 1.6706). This increase can be seen from the boxplot in Fig.5.1a, as the mean and median values are slightly higher in stress.

SCR values ranges from 0.0089 to 0.2600 µS (0.0415 ± 0.0631) in B1, 0.0061 to 0.1996 µS (0.0339 ± 0.0539) in B2, 0.0106 to 0.3825 µS (0.0911 ± 0.1005) in S1 and 0.0085 to 0.2908 µS (0.0882 ± 0.0886) in S2. From Fig.5.1b it is possible to verify that the SCR values are always higher during stress compared to baseline, confirming the response to stress.

The **Number of peaks** in baseline and stress showed no significant change, as values ranges from 34 to 65 (50.8667 ± 7.3472) in B1, 36 to 67 (55.6667 ± 8.5328) in B2, 44 to 63 (53.6000 ± 5.1796) in S1 and from 36 to 80 (53.0667 ± 10.9118) in S2. In Fig.5.1c it is not possible to differentiate the number of peaks between baseline and stress.

Rise time values ranges from 0.5300 to 1.0400s (0.6693 ± 0.1346) in B1, 0.5200 to 0.9100s (0.6327 ± 0.1243) in B2, 0.5900 to 1.0900s (0.8133 ± 0.1529) in S1, 0.5500 to 1.0100s (0.7780 ± 0.1834) in S2.

Rec.t 50% values ranges from 0.4300 to 0.8500s (0.5427 ± 0.1105) in B1, 0.4200 to 0.7400s (0.5120 ± 0.1032) in B2, 0.4700 to 0.8800s (0.6593 ± 0.1247) in S1, 0.4400 to 0.8200s (0.6313 ± 0.1496) in S2.

Rec.t 63% values ranges 0.5300 to 1.0500s (0.6747 ± 0.1368) in B1, 0.5300 to 0.9200s (0.6367 ± 0.1261) in B2, 0.5900 to 1.1000s (0.8213 ± 0.1552) in S1 and from 0.5500 to 1.0200s (0.7840 ± 0.1848) in S2.

From the boxplots of Rise time, Rec.t 50% and Rec.t 63% in Figures 5.1d, 5.1e, 5.1f, the mean values are higher in a situation of stess, although there is a larger variation in this situation compared to baseline.

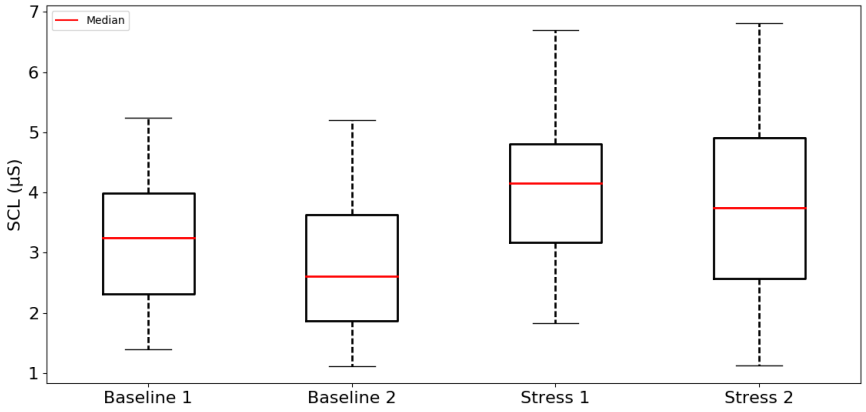

Figure 5.1a: Skin Conductance Level.

5.1.2 Frequency-domain Analysis

EDA frequency-domain features results showed an increase in power for all features in stress.

Band 1 power values varies between 1.9914 and 432.7505 µS² (56.9998 ± 109.7263) in B1, 0.0899 and 972.1302 µS² (126.8951 ± 270.6913) in B2, 4.7355 and 448.7866 µS² (116.9510 ± 130.6748) in S1, 3.9810 and 6189.3401 µS² (500.0602 ± 1577.1772) in S2. In Fig.5.2a shows that there is no visible difference between B2 and S1, and that in S2 the mean power is much higher than the ohter segments.

Band 2 power values varies between 0.0361 and 11.5802 µS² (1.0535 ± 2.9491) in B1, 0.0115 and 48.5909 µS² (3.5101 ± 12.4796) in B2, 0.1261 and 37.1645 µS² (4.8010 ± 9.8139) in S1, 0.0372

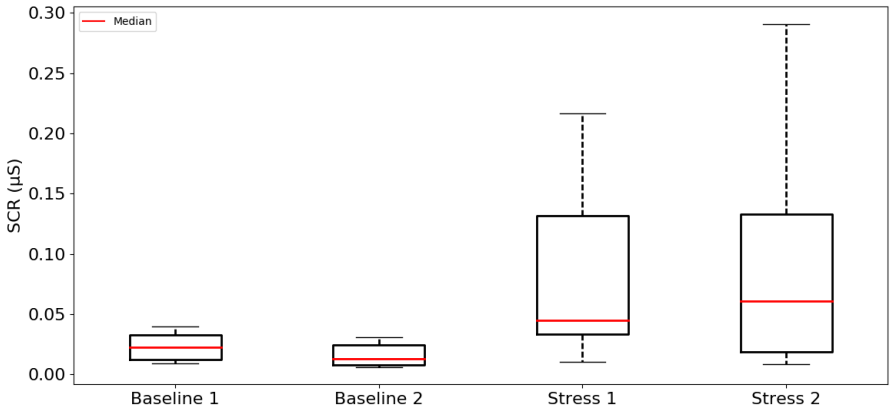

Figure 5.1b: Skin Conductance Response.

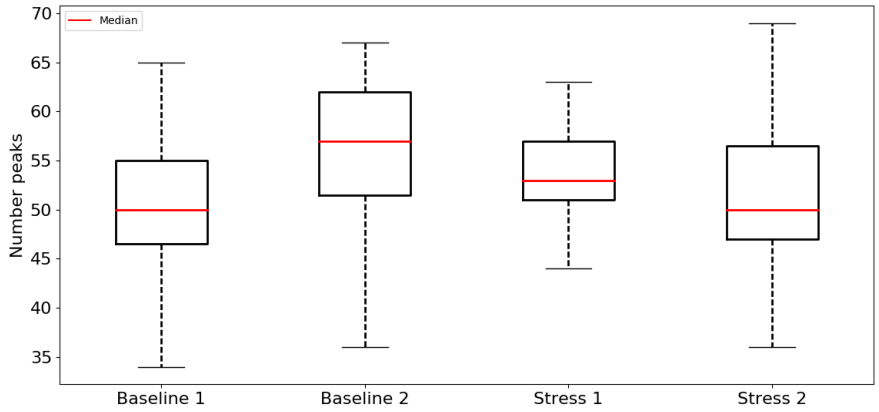

Figure 5.1c: SCR Number of Peaks.

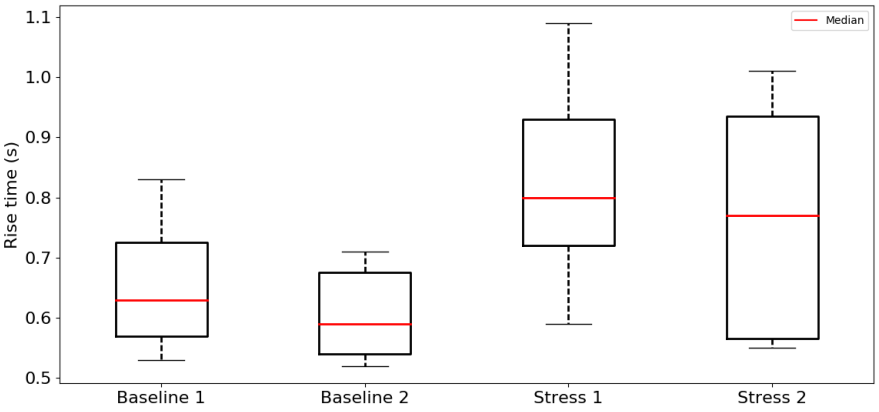

Figure 5.1d: SCR Rise Time.

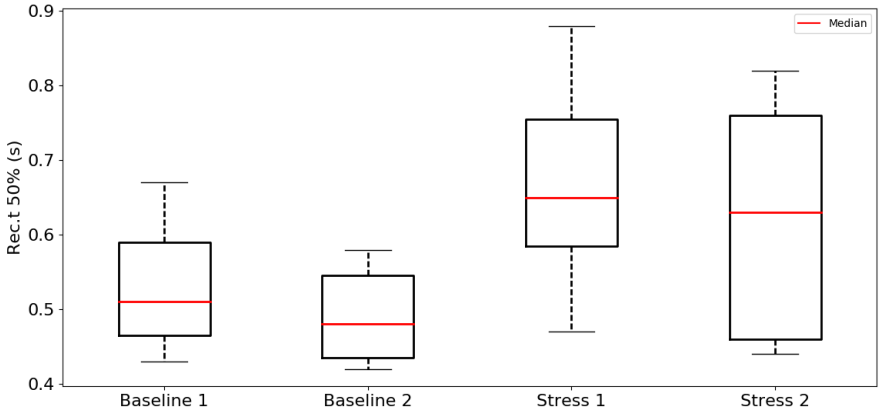

Figure 5.1e: SCR Rec.t 50%.

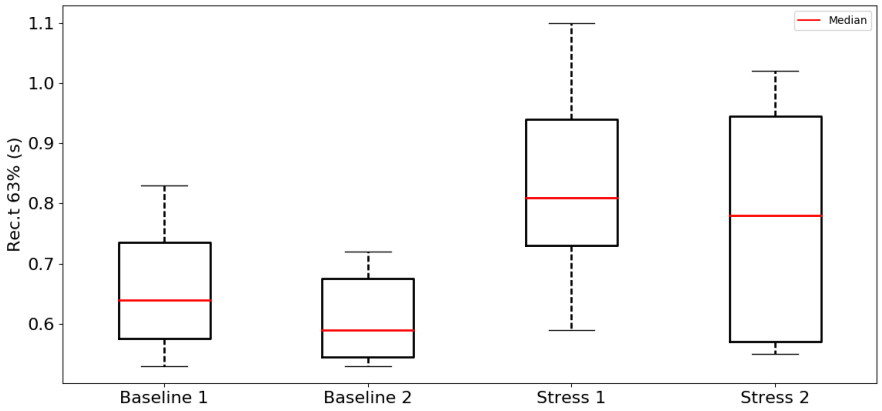

Figure 5.1f: SCR Rec.t 63%.

and 97.7843 μS² (10.5737 ± 25.3470) in S2. Fig.5.2b shows that the mean power increases during the experiment, although in segments B2 and S1, the mean power is similar, but with more variation in S1, as well as in S2.

Band 1 (nu) power values varies between 0.1200 and 21.2200 (6.5260 ± 6.0117) in B1, 0.0500 and 31.3900 (10.0480 ± 10.1175) in B2, 0.8700 and 42.7500 (8.9680 ± 10.9681) in S1, 1.0000 and 35.5700 (18.1633 ± 10.8429) in S2. Fig.5.2c shows that there is a slightly variation in the mean values between segments B1 and S1, and a significant increase between segments B1 and S2.

Band 2 (nu) power values varies between 0.0100 and 0.5700 (0.0853 ± 0.1428) in B1, 0.0100 and 1.4100 (0.1627 ± 0.3548) in B2, 0 and 1.2400 (0.1993 ± 0.3222) in S1, 0.0100 and 3.5300 (0.7420 ± 1.0495) in S2. Fig.5.2d shows that the mean values in segments B1,B2 and S1 are much similar, with significant increase in S2 compared to the other segments.

VLF power values varies between 112.1888 and 1682.1262 μS² (723.9877 ± 594.9969) in B1, 41.0887 and 5121.2986 μS² (737.0825 ± 1345.9756) in B2, 59.5796 and 8509.7223 μS² (2189.2165

± 2399.0016) in S1, 54.2928 and 14146.6983 µS² (1293.2019 ± 3566.3403) in S2.

Total Power values varies between 125.2853 and 2039.2808 µS² (789.6398 ± 658.3265) in B1, 42.2526 and 6009.9971 µS² (902.5581 ± 1652.4247) in B2, 113.7103 and 8509.7223 µS² (2327.6836 ± 2475.1542) in S1, 58.7455 and 21205.9638 µS² (1867.8397 ± 5362.4193) in S2.

From the boxplots of the VLF power and Total Power in Figures 5.2e and 5.2f, it is possible to verify that there is an increase in power, for both features in stress, with a greater variation in segment S1.

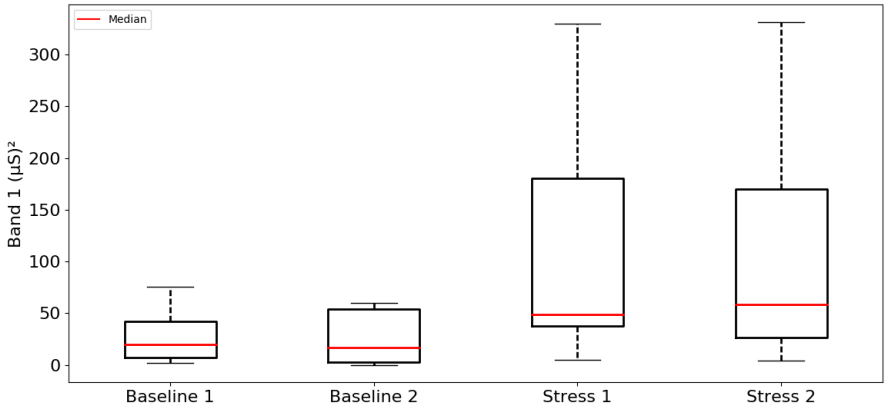

Figure 5.2a: EDA Band 1 Power.

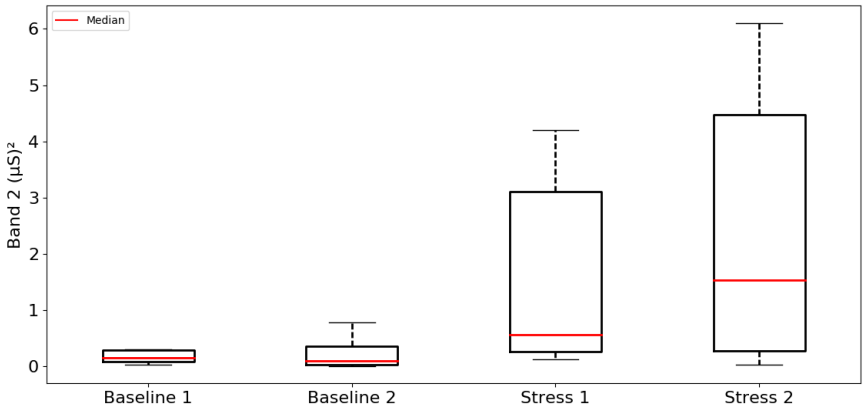

Figure 5.2b: EDA Band 2 Power.

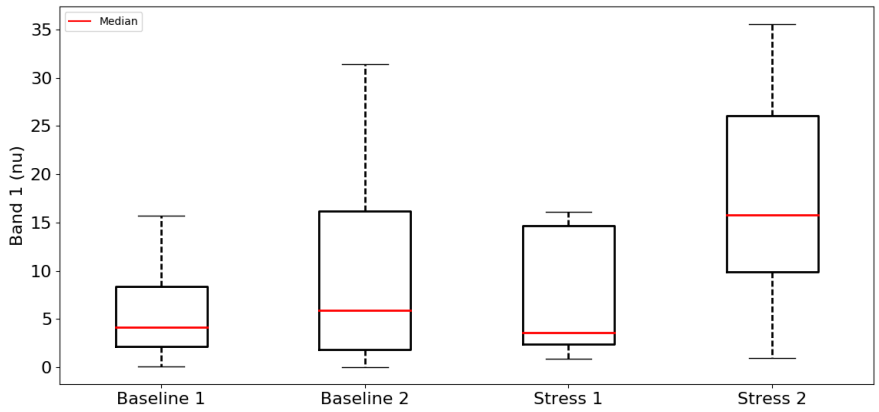

Figure 5.2c: EDA Band 1 Power in normalized units.

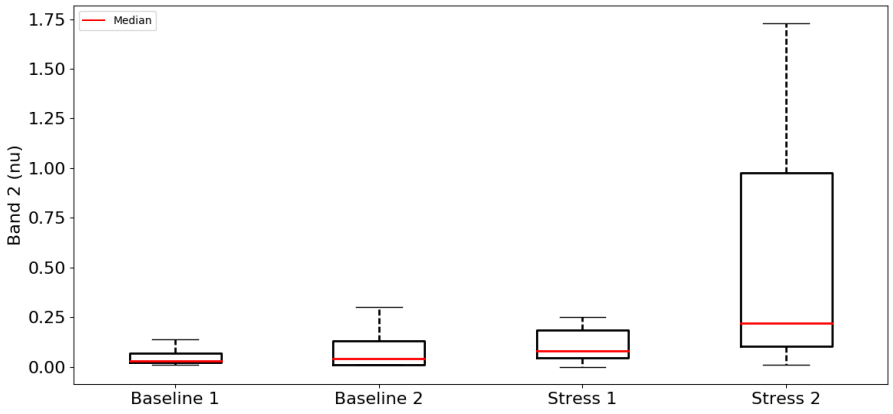

Figure 5.2d: EDA Band 2 Power in normalized units.

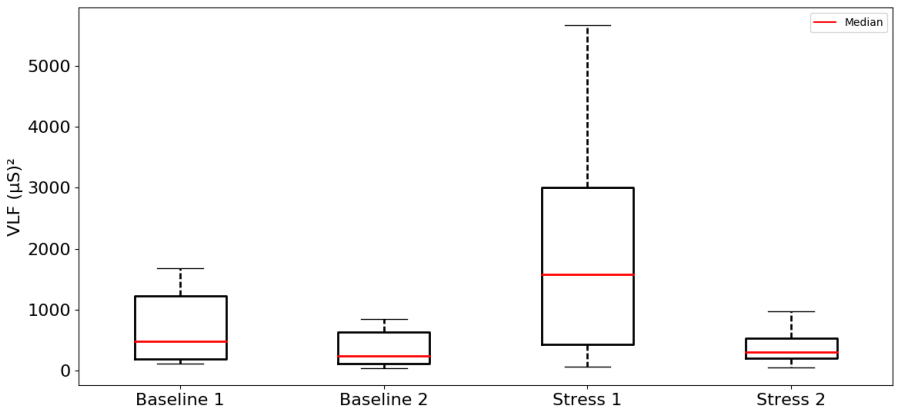

Figure 5.2e: EDA VLF Power.

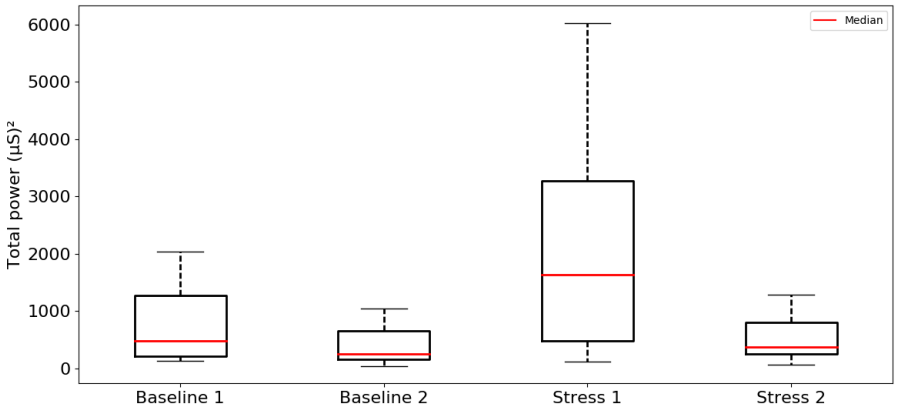

Figure 5.2f: EDA Total Power.

5.2 HRV Features

All HRV features extracted are described in Appendix A, with values such as Mean, Standard Error, Median, Min, Max and the percentiles. Baseline features are described in Appendix A.1 while Stress features are described in Appendix A.2. The comparison between mean values and standard error in baseline and stress are described in Appendix A.3

5.2.1 Time-domain Analysis

HRV time-domain features results showed an increase in heart rate (Bpm), RMSSD, NN50, and pNN50 during stress. RR-intervals and SDNN decreased in stress compared to baseline.

Bpm values goes from 60.9000 to 96.5700 (78.9427 ± 10.9216) in Baseline and from 64.0500 to 106.3200 (88.5820 ± 11.5948) in Stress. Fig.5.3a shows the increase in heart rate during stress.

RR interval values goes from 0.6270 to 0.9910 s (0.7791 ± 0.1116) in Baseline and from 0.5750 to 0.9470 s (0.6937 ± 0.0980) in Stress. Fig.5.3b shows the decrease in RR interval during stress.

RMSSD values goes from 18.1031 to 91.5776 ms (50.0909 ± 20.5628) in Baseline and from 21.2120 to 96.1536 ms (53.4927 ± 26.2762) in Stress. Fig.5.3c shows that although there is a small increase in RMSSD, it is not possible to clearly differentiate the mean values between baseline and stress.

SDNN values goes from 36.6147 to 90.1643 ms (58.4755 ± 16.1007) in Baseline and from 27.4345 to 89.2802 ms (54.6565 ± 17.9574) in Stress. Fig.5.3d shows the small decrease in mean value between baseline and stress.

NN50 values goes from 3 to 186 (91.0000 ± 49.9028) in Baseline and from 12 to 240 (105.8000 ± 71.3835) in Stress.

pNN50 values goes from 0.6593 to 59.7403% (25.4757 ± 16.5910) in Baseline and from 2.3810 to 56.1605% (27.2245 ± 19.3110) in Stress.

From the boxplots in Figures 5.3e and 5.3f, there is a small increase during stress but with greater variation within the values observed for both features.

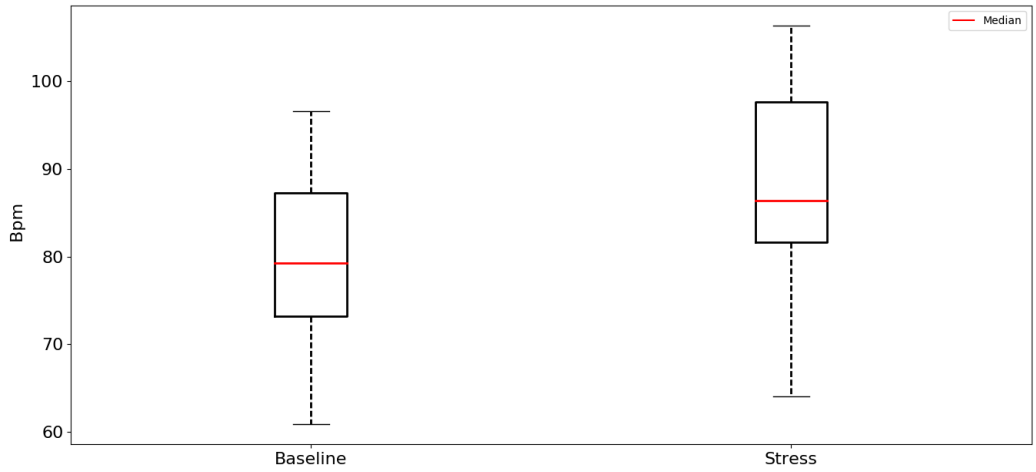

Figure 5.3a: Heart Rate (Bpm)

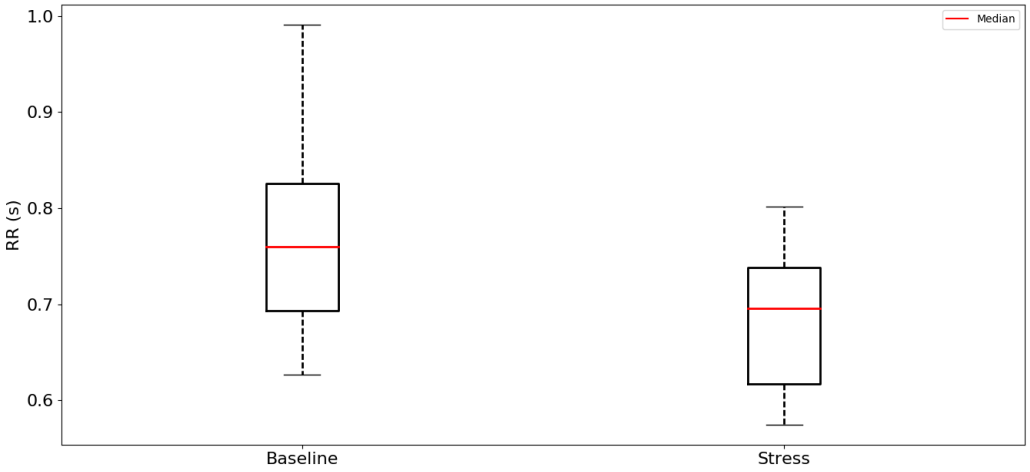

Figure 5.3b: RR intervals.

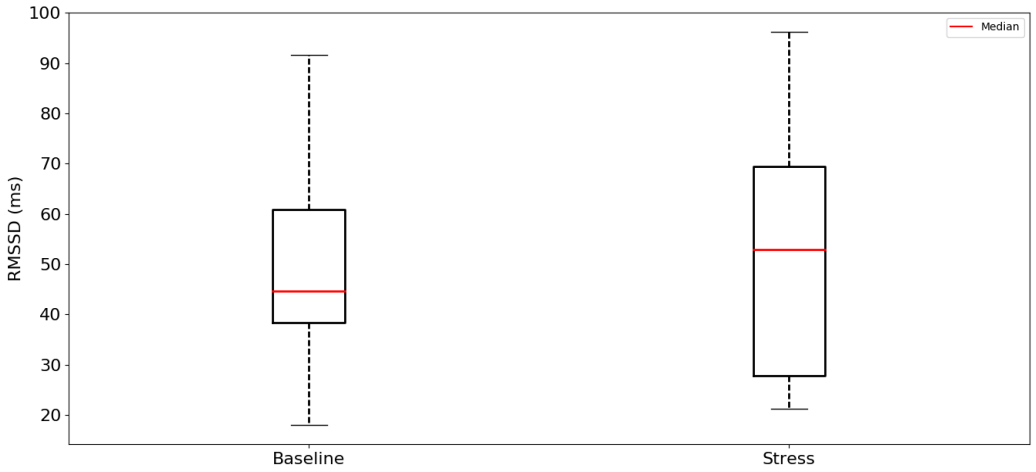

Figure 5.3c: RMSSD.

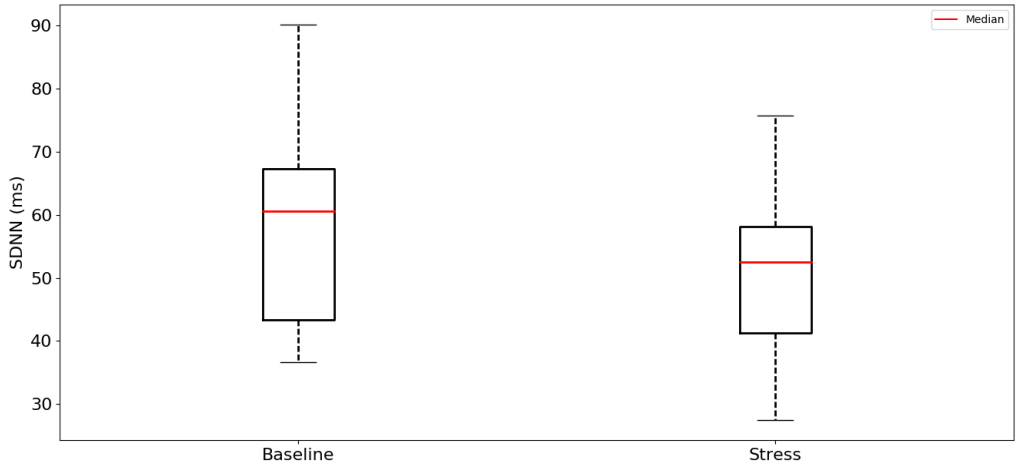

Figure 5.3d: SDNN.

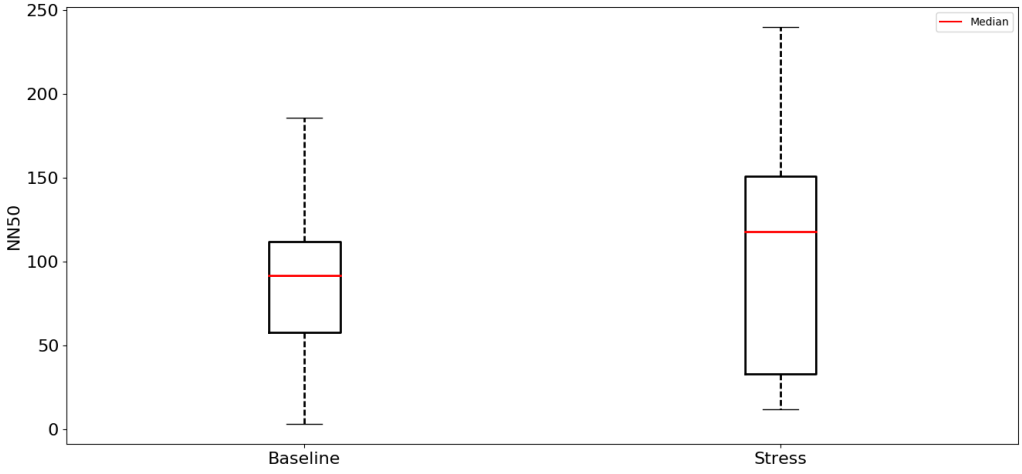

Figure 5.3e: NN50.

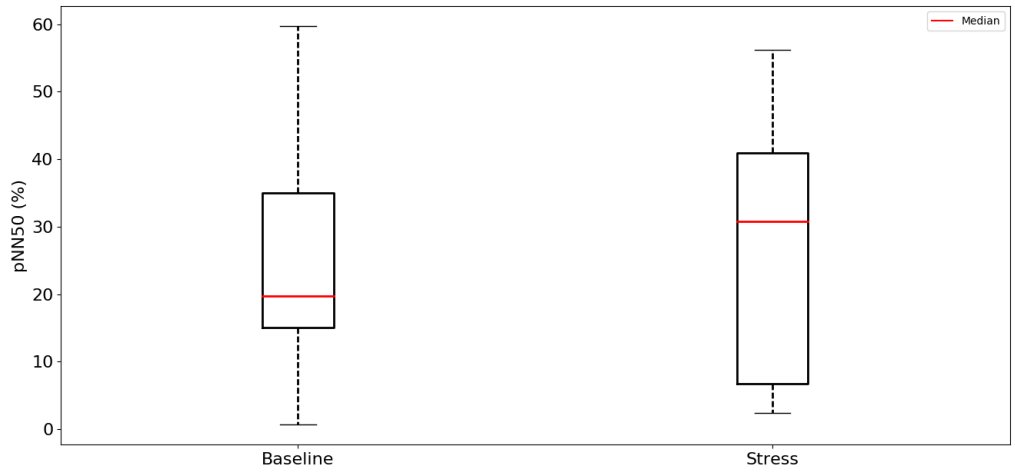

Figure 5.3f: pNN50.

5.2.2 Frequency-domain Analysis

HRV frequency-domain features results showed an increase in LF power, HF and HF(nu) power in stress. LF(nu) power, VLF power and LF/HF ratio decreased during stress. Total power remained constant during baseline and stress.

LF power values ranges from 0.4910 to 4.9303 ms² (2.2422 ± 1.1515) in baseline and from 0.3270 to 9.4205 ms² (2.3234 ± 2.2709) in stress. Fig.5.4a shows that the increase in LF power during stress is not significant, in comparison to baseline.

HF power values ranges from 0.0459 to 2.3855 ms² (0.5967 ± 0.5914) in baseline and from 0.0910 to 2.9087 ms² (1.0087 ± 0.8958) in stress. Fig.5.4b shows that there is a significant increase in HF power during stress

LF (nu) power values ranges from 46.6800 to 93.1000 (75.2767 ± 14.3799) in baseline and from 19.1100 to 93.2000 (66.8740 ± 19.4732) in stress. Fig.5.4c shows that there is a small decrease in LF(nu) power, with more values deviation in stress.

HF (nu) power values ranges from 6.3000 to 51.4400 (19.9720 ± 16.0623) in baseline and from 5.9300 to 80.4300 (30.2613 ± 20.5290) in stress. Fig.5.4d shows that HF(nu) power increases during stress.

LF/HF ratio values ranges from 0.9100 to 14.7800 (6.9787 ± 4.7953) in baseline and from 0.2400 to 15.7200 (4.4953 ± 4.6061) in stress. Fig.5.4e shows that there is a decrease in LF/HF ratio during stress.

VLF power values ranges from 0.5843 to 4.3614 ms² (2.3702 ± 1.2790) in baseline and from 0.3129 to 6.9203 ms² (1.9072 ± 1.9645) in stress. Fig.5.4f shows that there is a decrease in VLF power with less deviation of values during stress

Total power values rages from 2.1786 to 9.0212 ms² (5.3376 ± 2.3858) in baseline and from 1.5832 to 18.1589 ms² (5.3189 ± 4.6208) in stress. Fig.5.4g shows that the mean value for total power doesn't change between baseline and stress.

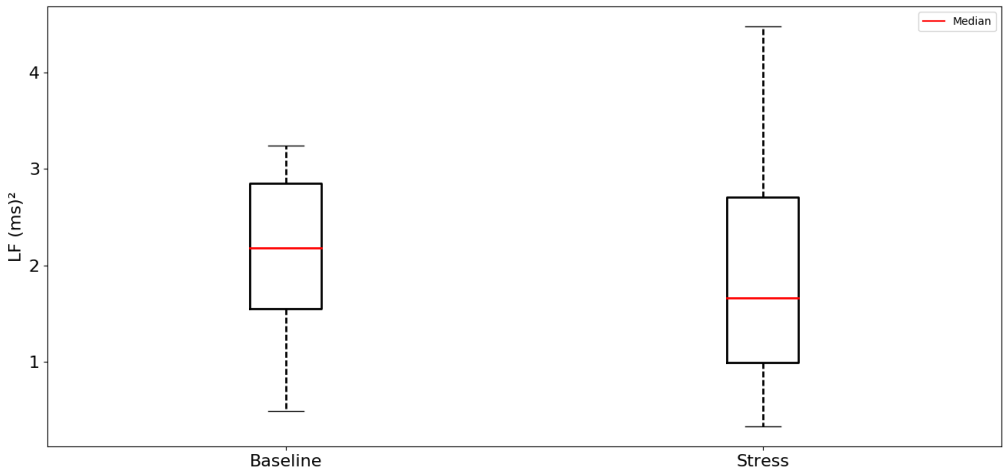

Figure 5.4a: HRV LF Power

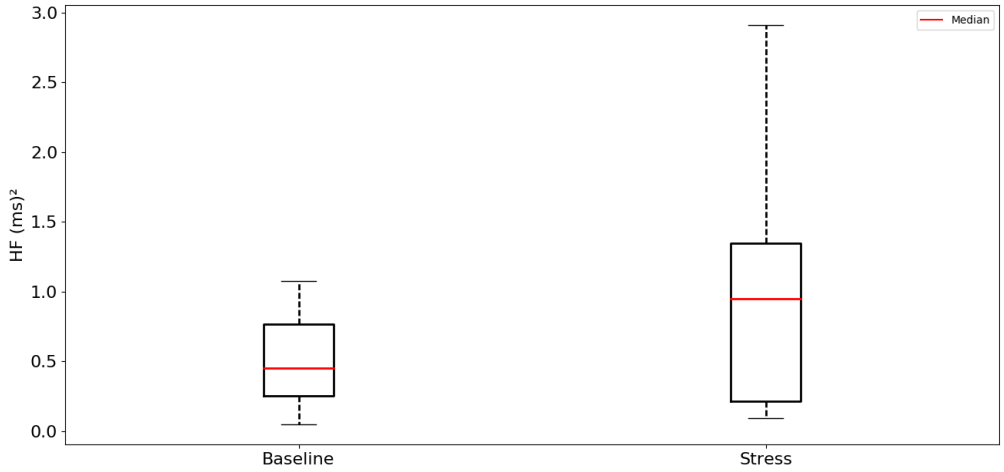

Figure 5.4b: HRV HF Power.

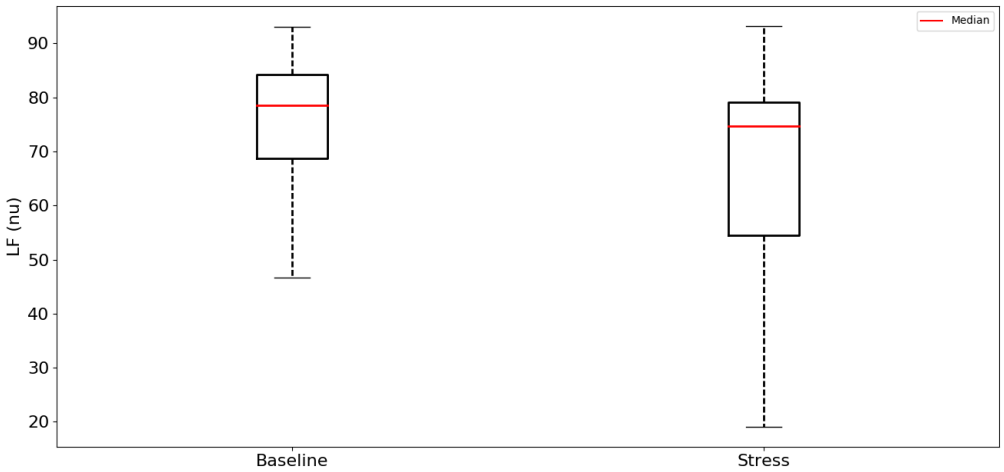

Figure 5.4c: HRV LF Power in normalized units.

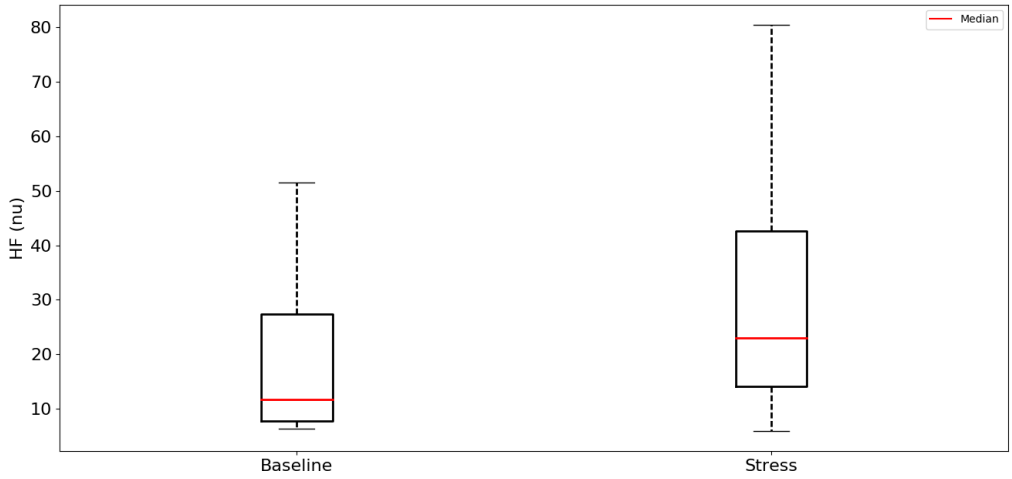

Figure 5.4d: HRV HF Power in normalized units.

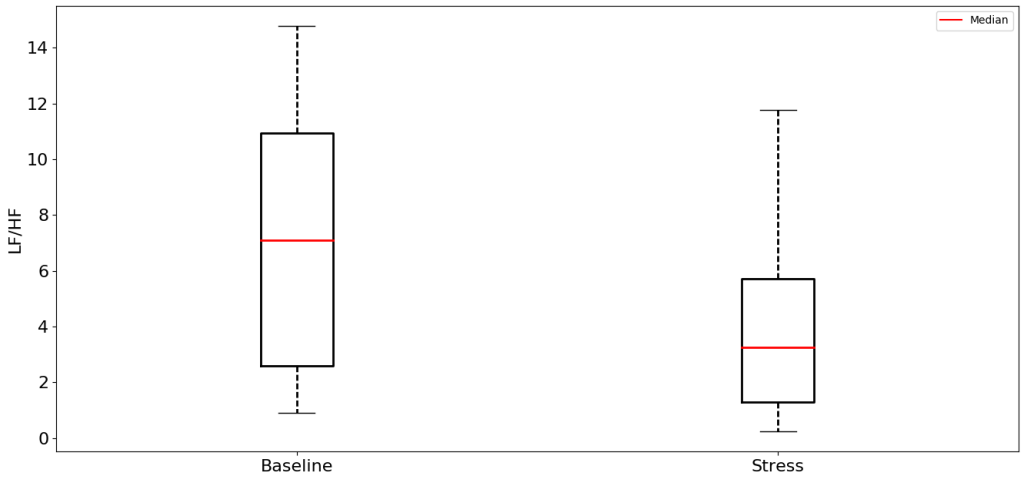

Figure 5.4e: HRV LF/HF ratio.

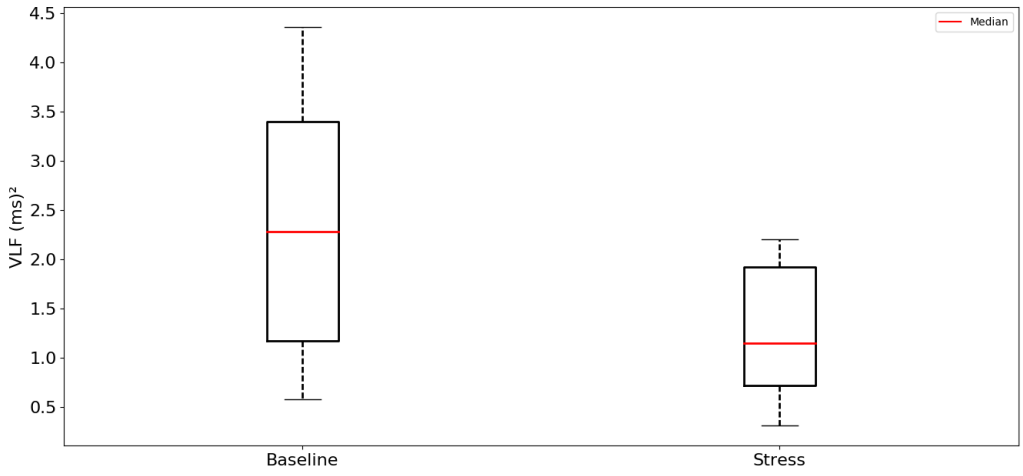

Figure 5.4f: HRV VLF Power.

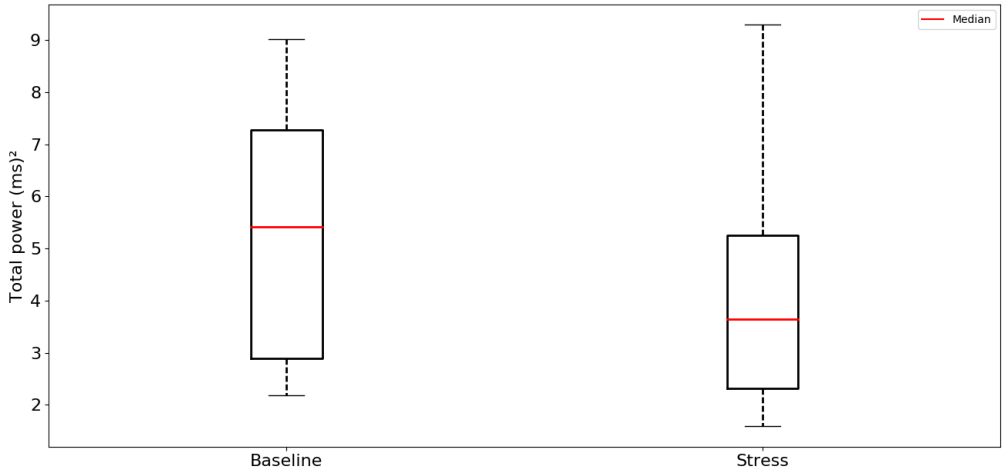

Figure 5.4g: HRV Total Power.

5.3 HRV Non-linear Variables Boxplots

HRV Non-linear features results shows an increase in SD1 and a decrease in SD2 and SD2/SD1 ratio.

SD1 values ranges from 0.0128 to 0.0648 s (0.0354 ± 0.0145) in baseline and from 0.0150 to 0.0680 s (0.0378 ± 0.0186) in stress.

SD2 values ranges from 0.0421 to 0.1099 s (0.0742 ± 0.0199) in baseline and from 0.0346 to 0.1083 s (0.0662 ± 0.0218) in stress.

SD2/SD1 ratio values ranges from 1.2954 to 4.1562 (2.2960 ± 0.7738) in baseline and from 0.8382 to 3.8365 (2.0751 ± 0.9510) in stress.

From the boxplots of SD1, SD2 and SD2/SD1 in Figures 5.5a, 5.5b and 5.5c, it is possible to see that these values don't differ significantly between baseline and stress.

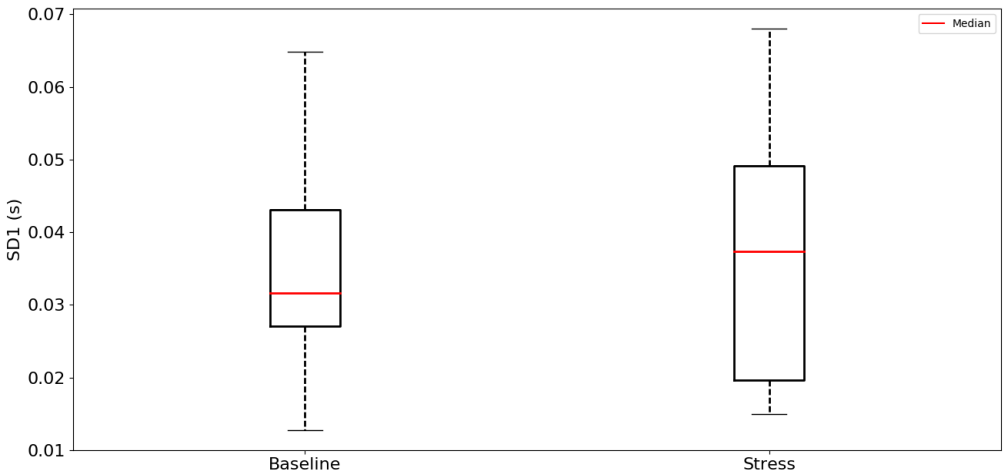

Figure 5.5a: HRV SD1.

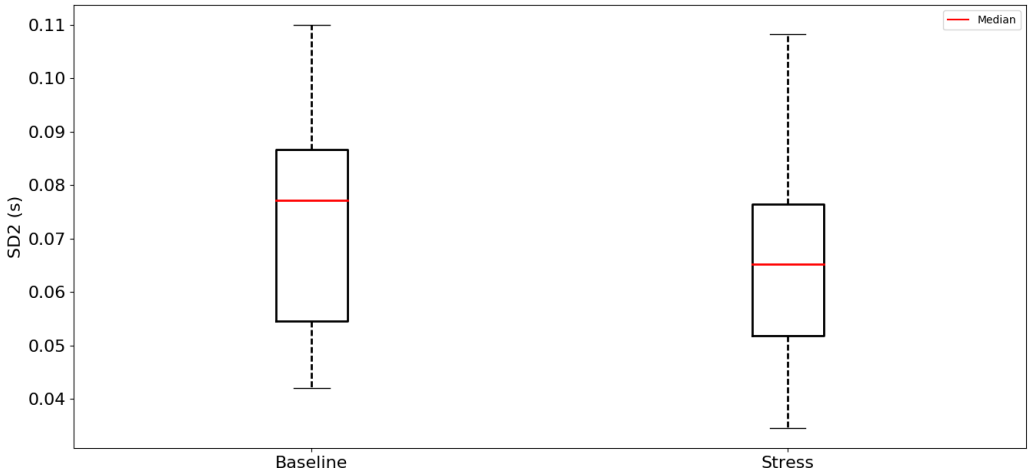

Figure 5.5b: HRV SD2.

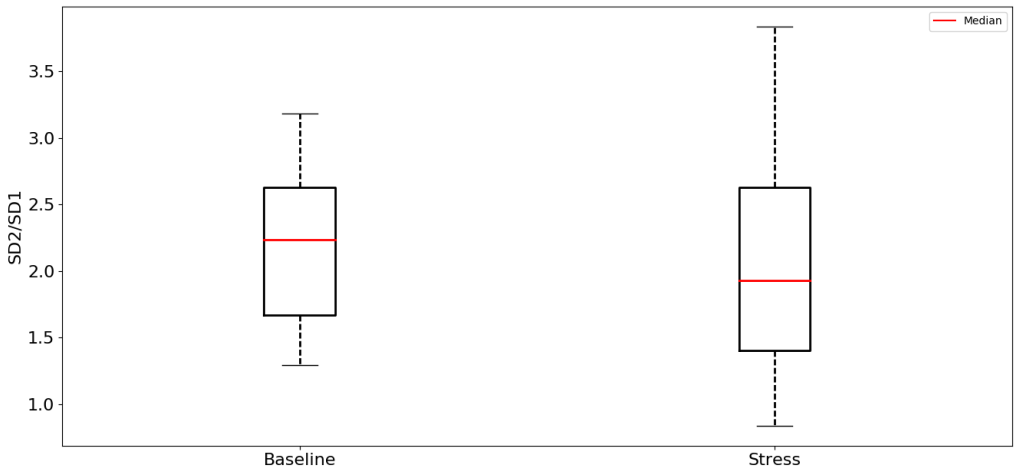

Figure 5.5c: HRV SD2/SD1.

5.4 Kruskal-Wallis test

Kruskal-Wallis test was performed instead of the 1-way ANOVA, since from the number of observations of each group (n=15), it is not possible to assume the normality of the data. To confirm this statement, a Kolmogorov-Smirnov test was performed using *kstest* from *Scipy's Stats* package. The Kolmogorov-Smirnov tests the distribution of an observed variable against a given distribution. Under the null hypothesis, the two distributions are identical, so we hypothesized that the observed samples have a normal distribution. The results for all HRV and EDA features showed *p-values* lower than a significance level of 1% (p-*value*<0.01), so the null-hypothesis that the data has a normal distribution is rejected, making it inappropriate to use the 1-way ANOVA.

5.4.1 EDA Kruskal-Wallis test

EDA Kruskal-Wallis test was performed between each segment (B1,B2,S1 and S2), to test for statistical significance between the medians of each group. A p-value of 0.05 was used as a significance level. The results for the *H-value* and *p-value* are described in Appendix G.

No significant result was found between segments **B1-B2**.

In **B1-S1**, significant effect was shown in the following features: **SCR** ($H(1) = 6.2972; p = 0.0121$), **Rise time** ($H(1) = 7.1686; p = 0.0074$), **Rec.t 50%** ($H(1) = 6.9465; p = 0.0084$), **Rec.t 63%** ($H(1) = 7.0579; p = 0.0079$), **Band 2** power ($H(1) = 6.4031; p = 0.0114$) and **Band 1** power ($H(1) = 4.9243; p = 0.0265$).

In **B1-S2**, significant effect was shown in the following features: **Band 2** power ($H(1) = 4.7419; p = 0.0294$), **Band 2(nu)** ($H(1) = 8.4678; p = 0.0036$) and **Band 1(nu)** ($H(1) = 9.0430; p = 0.0026$).

In **B2-S1**, significant effect was shown in the following features: **SCL** ($H(1) = 6.5071; p = 0.0107$), **SCR** ($H(1) = 8.7972; p = 0.0030$), **Rise time** ($H(1) = 10.4951; p = 0.0012$), **Rec.t 50%** ($H(1) = 10.3587; p = 0.0013$), **Rec.t 63%** ($H(1) = 10.6254; p = 0.0011$), **VLF** power ($H(1) = 6.7204; p = 0.0095$) and **Total Power** ($H(1) = 6.9372; p = 0.0084$).

In **B2-S2**, significant effect was shown in the following features: **SCR** ($H(1) = 5.4933; p = 0.0191$), **Rise time** ($H(1) = 4.8510; p = 0.0276$), **Rec.t 50%** ($H(1) = 4.9375; p = 0.0263$), **Rec.t 63%** ($H(1) = 5.0313; p = 0.0249$), **Band 2** power ($H(1) = 5.8877; p = 0.0152$) and **Band 2(nu)** ($H(1) = 6.9948; p = 0.0082$).

In **S1-S2**, significant effect was shown in the following features: **Band 1(nu)** ($H(1) = 5.4933; p = 0.0191$), **VLF** power ($H(1) = 5.1101; p = 0.0238$) and **Total Power** ($H(1) = 4.7419; p = 0.0294$).

5.4.2 HRV Kruskal-Wallis test

HRV Kruskal-Wallis test was performed between baseline and stress, to test for statistical significance between the medians of each group. A p-value of 0.05 was used as a significance level. The results for the *H-value* and *p-value* are described in Appendix A.3.

The results showed significant effect only for **Bpm** ($H(1) = 4.9243; p = 0.0265$) and **RR** interval ($H(1) = 4.9243; p = 0.0265$).

Despite no significance was obtained in frequency-domain features for HRV, a thorough analysis of these spectral characteristics, revealed that in some subjects the LF(nu) decreased in stress, while in other subjects there was an increase in stress. Actually, within the 15 subjects that were analyzed, there was a division of 8 subjects in which LF(nu) decreased during stress, and 7 subjects that LF(nu) increased during stress. So, when analyzing the group as a whole, it is possible that the opposite responses cancels out the LF(nu) results. Therefore, two distinct groups were formed: group 1 consisted of subjects which LF(nu) decreased during stress, and group 2 consisted of subjects which LF(nu) increased during stress. Then, all features for HRV and EDA were analyzed for each group. The results will be shown in the next sections.

5.5 Group 1 Features

Group 1 consists of subjects (N=8) who responded to stress with a decrease in LF(nu). A level of significance of 5% was used to assess the significance of the results, using the Kruskal-Wallis test.

5.5.1 HRV Features

All HRV features for Group 1 are described in Appendix C. Baseline features are described in Appendix C.1, while Stress features are described in Appendix C.2.

For group 1, the results showed a significant increase in HF(nu) power, LF(nu) power and LF/HF ratio.

HF(nu) power significantly increases ($H(1) = 5.3382; p = 0.0209$) during stress, with values varying between 6.3000 and 45.9800 (16.1000 ± 13.5085) in baseline and between 11.9000 and 80.4300 (37.0525 ± 22.1569) in stress.

LF(nu) power significantly decreases ($H(1) = 5.8346; p = 0.0157$) during stress, with values varying between 53.8700 and 93.1000 (80.5038 ± 12.4098) in baseline and between 19.1100 and 76.9200 (59.9038 ± 20.4281) in stress.

LF/HF ratio significantly decreases ($H(1) = 5.3382; p = 0.0209$) during stress, with values varying between 1.1700 and 14.7800 (8.0325 ± 4.8162) in baseline and between 0.2400 and 6.4000 (2.5438 ± 2.0179) in stress.

5.5.2 EDA Features

All EDA features for Group 1 are described in Appendix E. Baseline 1 features are described in Appendix E.1, Baseline 2 in Appendix E.2, Stress 1 in Appendix E.3 and Stress 2 in Appendix E.4.

For group 1, the results showed a significant increase between the following segments:

In **B2-S1**, **SCL** ($H(1) = 3.9816; p = 0.0460$) with values ranging from 1.4874 to 5.1982 µS (2.9848 ± 1.1778) in B2 and from 3.0617 to 6.6924 µS (4.3421 ± 1.1802) in S1. **Rise time** ($H(1) = 4.6556; p = 0.0310$) with values ranging from 0.5300 to 0.9100 s (0.6713 ± 0.1520) in B2 and from 0.5900 to 1.0100 s (0.8263 ± 0.1621) in S1. **Rec.t 50%** ($H(1) = 4.6488; p = 0.0311$) with values ranging from 0.4300 to 0.7400 s (0.5425 ± 0.1270) in B2 and from 0.4700 to 0.8200 s (0.6700 ± 0.1328) in S1. **Rec.t 63%** ($H(1) = 4.6488; p = 0.0311$) with values ranging from 0.5400 to 0.9200s (0.6750 ± 0.1550) in B2 and from 0.5900 to 1.0200 s (0.8338 ± 0.1649) in S1.

In **S1-S2**, **VLF power** ($H(1) = 5.8346; p = 0.0157$) with values ranging from 366.9861 to 8288.1823 µS² (2411.8345 ± 2614.2274) in S1 and from 79.2185 to 971.2627 µS² (454.5952 ± 317.5892) in S2. **Total Power** ($H(1) = 5.8346; p = 0.0157$) with values from 435.2971 to 8509.7223 µS² (2578.7961 ± 2663.9292) in S1 and from 124.1221 to 1287.1544 µS² (584.1263 ± 432.7657) in S2.

5.6 Group 2 Features

Group 2 consists of subjects (N=7) who responded to stress with an increase in LF(nu). A level of significance of 5% was used to assess the significance of the results, using the Kruskal-Wallis test.

5.6.1 HRV Features

All HRV features for Group 2 are described in Appendix D. Baseline features are described in Appendix D.1, while Stress features are described in Appendix D.2.

For group 2, the results showed significant effect only for **Bpm** ($H(1) = 4.4449$; $p = 0.0350$) with values from 60.9000 to 84.7600 (75.0257 ± 7.6175) in baseline and from 64.0500 to 102.9600 (84.3357 ± 11.5130) in stress and **RR** interval ($H(1) = 4.4449$; $p = 0.0350$) with values from 0.7120 to 0.9910 s (0.8129 ± 0.0900) in baseline and from 0.5890 to 0.9470 s (0.7287 ± 0.1087) in stress.

5.6.2 EDA Features

All EDA features for Group 2 are described in Appendix F. Baseline 1 features are described in Appendix F.1, Baseline 2 in Appendix F.2, Stress 1 in Appendix F.3 and Stress 2 in Appendix F.4.

For group 2, the results showed significant effect in the following segments:

In **B1-S1**, significant increase was found in the following features: **SCR** ($H(1) = 5.000$; $p = 0.0253$) with values from 0.0089 to 0.0399 µS (0.0216 ± 0.0119) in B1 and from 0.0151 to 0.1503 µS (0.0666 ± 0.0561) in S1. **Rise time** ($H(1) = 5.5878$; $p = 0.0181$) with values from 0.5300 to 0.7300 s (0.6314 ± 0.0793) in B1 and from 0.6000 to 1.0900 s (0.7986 ± 0.1529) in S1. **Rec.t 50%** ($H(1) = 5.3132$; $p = 0.0212$) with values from 0.4300 to 0.5900 s (0.5114 ± 0.0657) in B1 and from 0.4800 to 0.8800 s (0.6471 ± 0.1241) in S1. **Rec.t 63%** ($H(1) = 5.5878$; $p = 0.0181$) with values from 0.5300 to 0.7400 s (0.6371 ± 0.0840) in B1 and from 0.6000 to 1.1000 s (0.8071 ± 0.1551) in S1. **Band 2** power ($H(1) = 4.4449$; $p = 0.0350$) with values from 0.0361 to 0.6177 µS² (0.1935 ± 0.1976) in B1 and from 0.1315 to 10.2737 µS² (2.3663 ± 3.7677) in S1.

In **B1-S2**, significant increase was found in **Band 1(nu)** ($H(1) = 6.8612$; $p = 0.0088$) with values from 1.0500 to 15.7500 (5.7014 ± 4.9219) in B1 and from 6.7800 to 29.1900 (19.7214 ± 8.1362) in S2. **Band 2** power ($H(1) = 4.449$; $p = 0.0350$) with values from 0.0361 to 0.6177 µS² (0.1935 ± 0.1976) in B1 and from 0.0554 to 97.7843 µS² (15.2685 ± 36.4489) in S2. **Band 2(nu)** ($H(1) = 8.6749$; $p = 0.0032$) with values from 0.0100 to 0.0800 (0.0386 ± 0.0254) in B1 and from 0.0600 to 2.3200 (0.5057 ± 0.8129) in S2.

In **B2-S1**, significant increase was found in the following features: **SCR** ($H(1) = 7.5636$; $p = 0.0060$) with values from 0.0070 to 0.0309 µS (0.0139 ± 0.0086) in B2 and from 0.0151 to 0.1503 µS (0.0666 ± 0.0561) in S1. **Rise time** ($H(1) = 7.2318$; $p = 0.0072$) with values from 0.5200 to 0.7100 s (0.5886 ± 0.0696) in B2 and from 0.6000 to 1.0900 s (0.7986 ± 0.1529) in S1. **Rec.t 50%** ($H(1) = 6.9375$; $p = 0.0084$) with values from 0.4200 to 0.5800 s (0.4771 ± 0.0579) in B2 and from 0.4800 to 0.8800 s (0.6471 ± 0.1241) in S1. **Rec.t 63%** ($H(1) = 7.2318$; $p = 0.0072$) with values from 0.5300 to 0.7200 s (0.5929 ± 0.0697) in B2 and from 0.6000 to 1.1000 s (0.8071 ±

0.1551) in S1. **Band 2** power ($H(1) = 6.2082$; $p = 0.0127$) with values from 0.0115 to 0.4459 μS² (0.1453 ± 0.1577) in B2 and from 0.1315 to 10.2737 μS² (2.3663 ± 3.7677) in S1. **Total Power** ($H(1) = 3.9224$; $p = 0.0476$) with values from 42.2526 to 906.6900 μS² (300.0222 ± 294.6788) in B2 and from 113.7103 to 6026.4462 μS² (2040.6980 ± 2415.6717) in S1.

In **B2-S2**, significant increase was found in the following features: **SCR** ($H(1) = 4.4547$; $p = 0.0348$) with values from 0.0070 to 0.0309 μS (0.0139 ± 0.0086) in B2 and from 0.0098 to 0.2908 μS (0.0788 ± 0.0991) in S2. **Band 2** power ($H(1) = 5.0000$; $p = 0.0253$) with values from 0.0115 to 0.4459 μS² (0.1453 ± 0.1577) in B2 and from 0.0554 to 97.7843 μS² (15.2685 ± 36.4489) in S2. **Band 2(nu)** ($H(1) = 5.0433$; $p = 0.0247$) with values from 0.0100 to 0.3000 (0.0771 ± 0.1072) in B2 and from 0.0600 to 2.3200 (0.5057 ± 0.8129) in S2.

5.7 Groups Separation

In this section, SVM were applied to try separate by a hyperplane into two different responses of the subjects to stress: decrease in LF(nu) and increase in LF(nu). This separation is based on the work of Vuksanovic et al. [65], that verified this distinct response to stress, but in respect to HF power.

First, a binary classification of each group was applied: Group 1 - Decrease in LF(nu) was classified as $Y = -1$ and Group 2 - Increase in LF(nu) was classified as $Y = 1$. Using *SVC* function from *SKlearn SVM* package, with a linear kernel, a penalty parameter $C = 1$ and an automatic γ, it was possible to separate the two different groups by a hyperplane, as shown in figure 5.6. The decision function obtained to separate the two groups is given by equation 5.1, where w_1 and w_2 represents, respectively, the weights for groups 1 and 2, $\vec{x}_1$ and $\vec{x}_2$ represents, respectively, a point for group 1 (Blue circles in Fig.5.6) and group 2 (Red circles in Fig.5.6).

$$w_1.\vec{x}_1 + w_2.\vec{x}_2 + b = 0 \tag{5.1}$$

The results obtained for the weights and the b parameter were: $w_1 = -0.31$, $w_2 = 0.25$ and $b = 4.85$. The number of support vectors for each group were: Group 1 - 1 support vector, Group 2 - 2 support vectors. The coordinates ([LF(nu) Baseline, LF(nu) Stress]) of the support vectors (Black not filled circles in Fig.5.6) for each group were: Group 1 - [78.48,74.64] and in Group 2 - [77.35,81.25];[63.08,63.41].

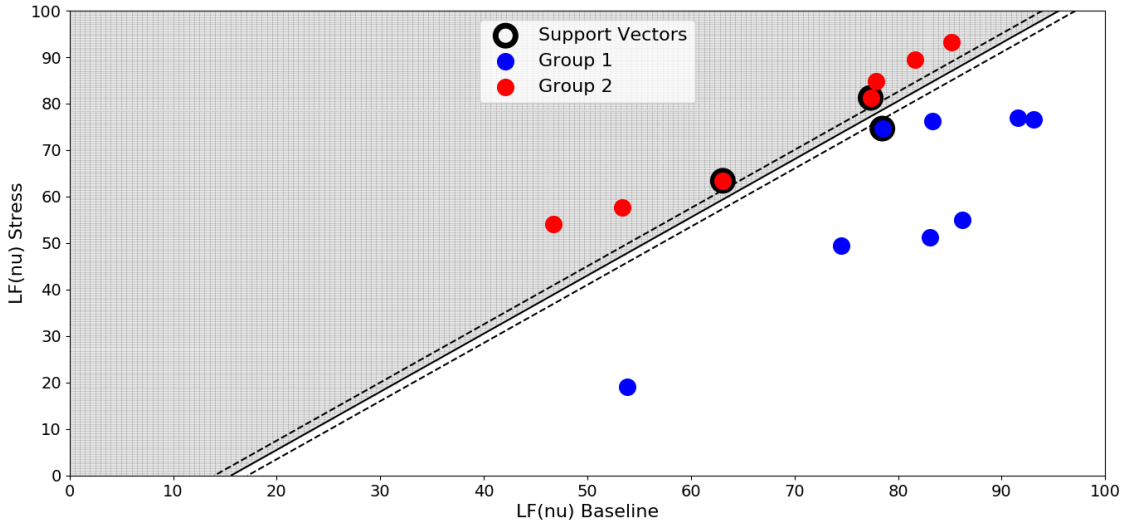

Figure 5.6: SVM Group Separation by the hyperplane: $-0.31.\vec{x}_1 + 0.25.\vec{x}_2 + 4.85 = 0$. Blue circles - Group 1. Red circles - Group 2. The support vectors are the points with black border.

Then, a linear regression was computed for each group (Fig.5.7) using *LinearRegression* function from *SKlearn linear_model* package. For Group 1 regression (Red line in Fig.5.7), the following regression line was obtained: LF(nu) Stress = $1.40 \times$ LF(nu) Baseline $- 53.15$, $r^2 = 0.728$. For Group 2 regression (Blue line in Fig.5.7), the regression line obtained was LF(nu) Stress = $1.06 \times$ LF(nu) Baseline $+ 1.48$, $r^2 = 0.972$.

Finally, a chi-squared test for goodness of fit was applied to the regression lines, comparing the expected values with the observed values using the regression line obtained. For group 1 the chi-square result was $\chi^2(6) = 12.785$; $p = 0.047$ and for group 2 was $\chi^2(5) = 0.674$; $p = 0.984$. With the results obtained for the χ^2 statistic, it is possible to reject at a significance level of 5%, the null hypothesis for group 1, concluding that the fit of the regression line is not adequate, while for group 2, with a *p-value*=0.984 it is possible to accept the null hypothesis, concluding that the fit of the regression line is suitable.

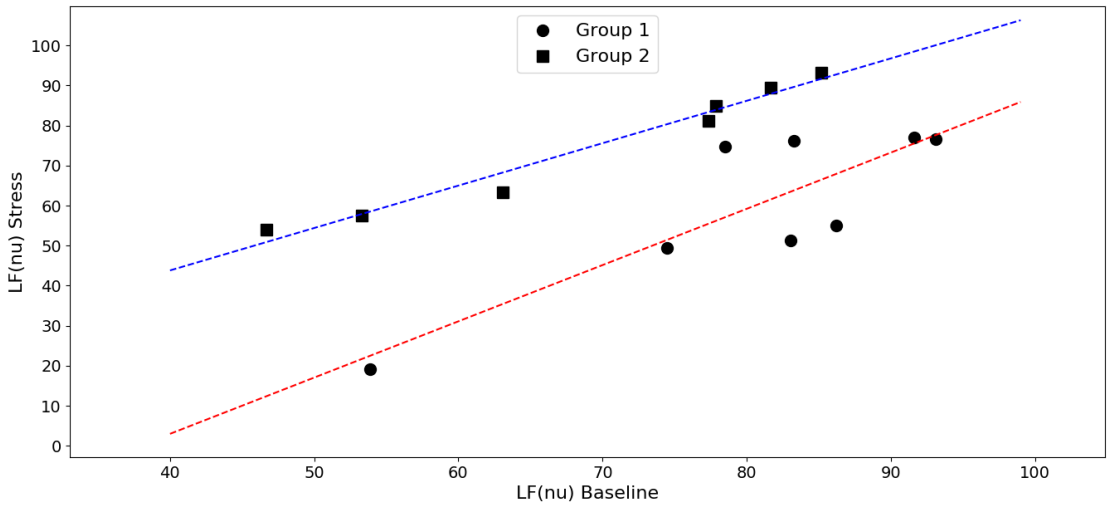

Figure 5.7: Linear Regression for each group. Group 1 regression line (Red line): LF(nu) Stress = 1.40 × LF(nu) Baseline − 53.15, $r^2 = 0.728$; Group 2 regression line (Blue line): LF(nu) Stress = 1.06 × LF(nu) Baseline + 1.48, $r^2 = 0.972$.

5.8 Classification

In section 5.7, it was possible to separate the subjects into two groups, by evaluating their response to stress, with an increase or a decrease in LF(nu) during stress. As this separation is based on a frequency-domain feature, requiring the recording of the data for at least 10 minutes (5-min in baseline, 5-min in stress), in order to predict the subject's response to a situation of stress in a shorter recording time, a classification of the subjects using only time-domain features for both HRV and EDA, was performed, to classify the subjects into the two different groups obtained in the previous section.

This classification was performed with a random forest classifier (section 2.9), using *RandomForestClassifier* function from *SKlearn Ensemble* package, with 10 decision trees, and the Gini criteria to assess the impurity and the quality of the split. Training of the classifier was performed with a cross validation method, using 6 different random splits and a test sample of 30% of the subjects. This process was repeated 100 times, so that it was possible to choose the model that best classifies the data, that is, the model with a higher accuracy score for the cross validation training method.

5.8.1 HRV features Random Forest Classifier

First, a random forest classifier using only the following time-domain features for HRV was performed: Bpm, RR-interval and SD2/SD1 ratio. After iterating 100 times, the estimators for the model with a higher accuracy score were selected, and the decision trees were visualized, such as in figure 5.8. All the 10 trees obtained with the random forest classifier are shown in Appendix I. Then, the importance of each feature is plotted in figure 5.9. From this figure, we

verify that RR-interval is the most important feature in this model, followed by the SD2/SD1 ratio and the Bpm. The accuracy score for this model to classify correctly each subject to the corresponding group was approximately 80%. In order to obtain a better visualization of the regions defined by the random forest classifier, the features boundaries are shown in a 3D graph (Fig. 5.10). A subject with features coordinates that belong to the blue region will be assigned to group 1 - decrease in LF(nu), and subjects that belong to the red region will be assigned to group 2 - Increase in LF(nu). Then, the same regions were visualized for each pair of features selected, by giving the mean value recorded for the extra feature. These boundaries can be seen in Figure 5.11.

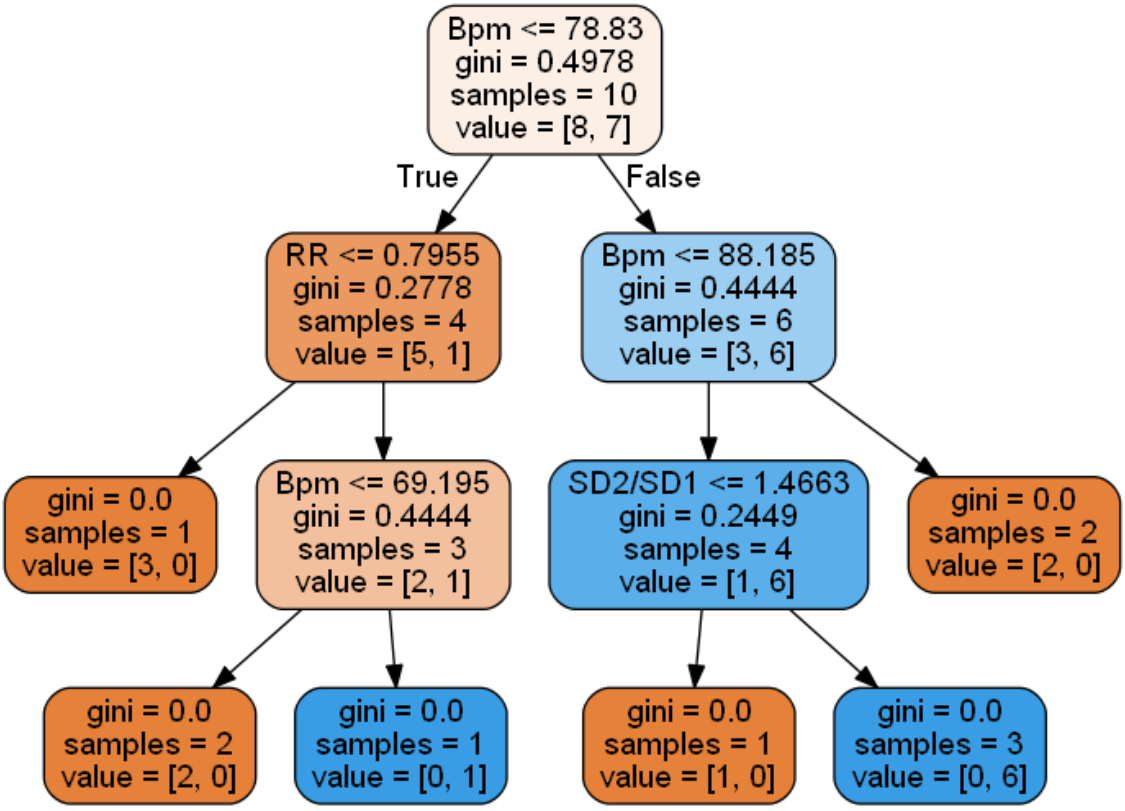

Figure 5.8: Decision tree obtained with a random forest classifier using only HRV features.

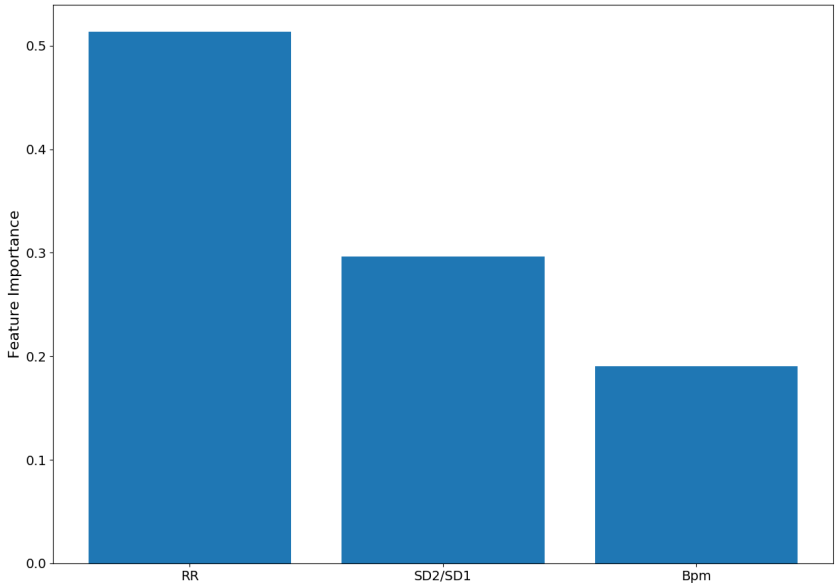

Figure 5.9: Feature Importance for HRV features obtained with the random forest classifier.

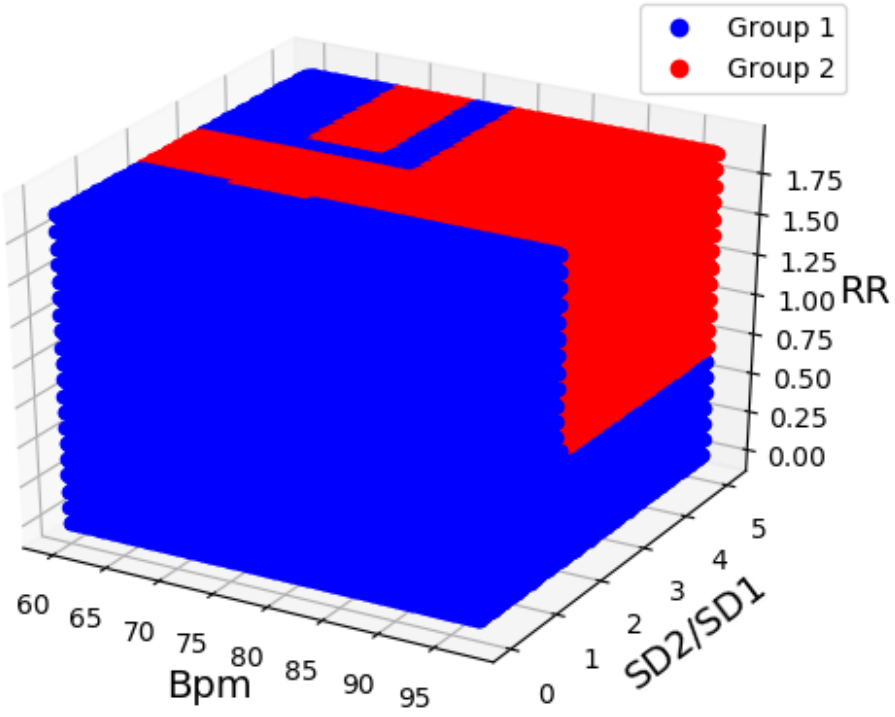

Figure 5.10: 3D Decision Surface for the Random Forest Classifier. Features selected: Bpm, SD2/SD1 and RR-interval (s). Blue region - Group 1 and Red region - Group 2.

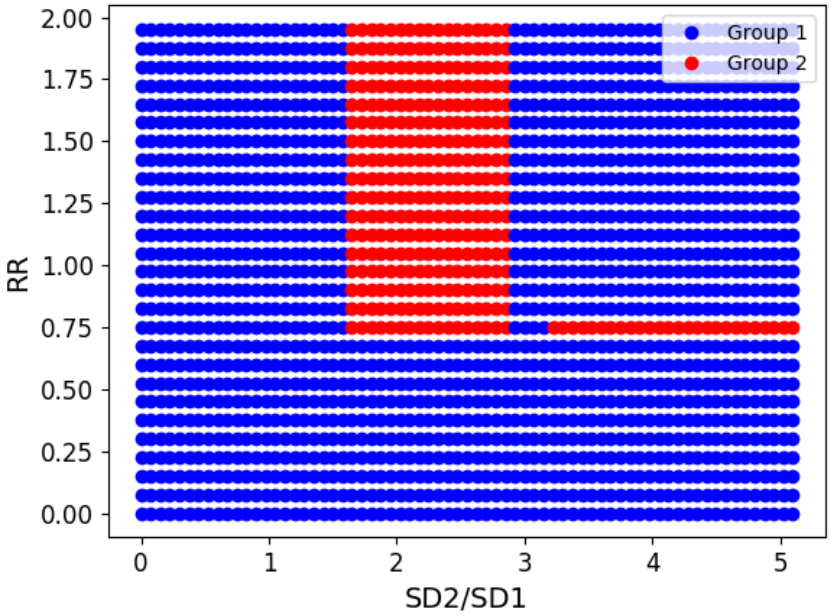

(a) Decision regions for pair SD2/SD1 - RR.

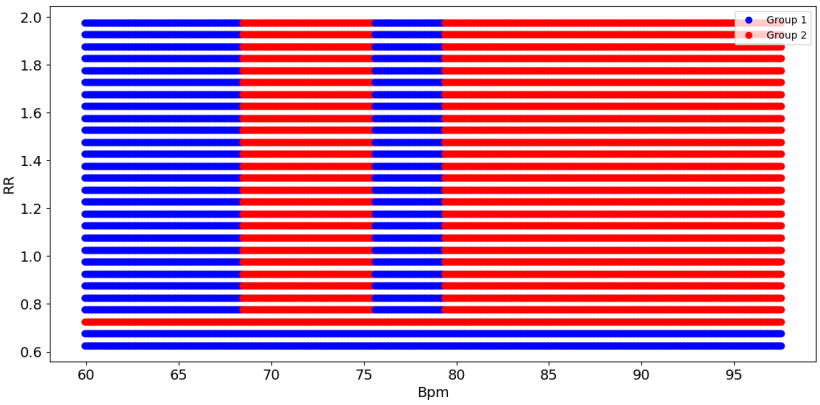

(b) Decision regions for pair Bpm - RR.

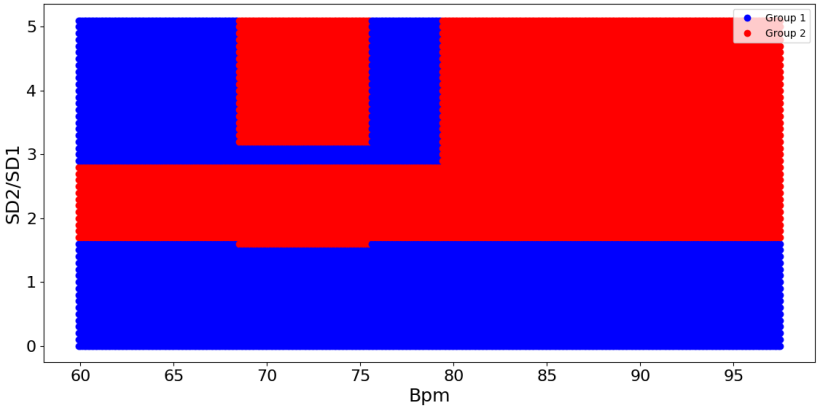

(c) Decision regions for pair Bpm - SD2/SD1.

Figure 5.11: 2D Decision Boundaries.

5.8.2 HRV-EDA features Random Forest Classifier

In section 5.8.1, only HRV features were used to classify the subjects into the two different groups. The accuracy score obtained was approximately 80%. In this section, to classify the subjects, information related to EDA was added to the classifier. Similarly to the previous classifier, in order to reduce the recording time, only time-domain features for EDA were added to the classifier. The following features for EDA were selected: SCR, SCL and Rise Time. The more accurate estimators were selected, and the decision trees were visualized, such as in figure 5.12. All 10 trees obtained with this classifier are shown in J. The importance of each feature in plotted in figure 5.13. The accuracy score for this model was approximately 77%.

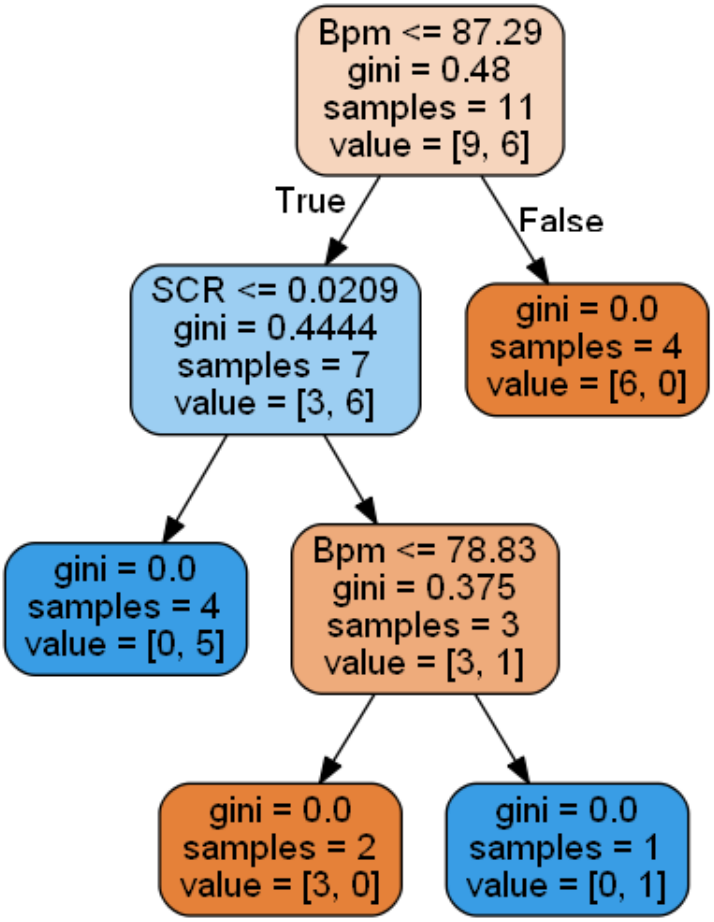

Figure 5.12: Decision tree obtained with a random forest classifier using both HRV and EDA features.

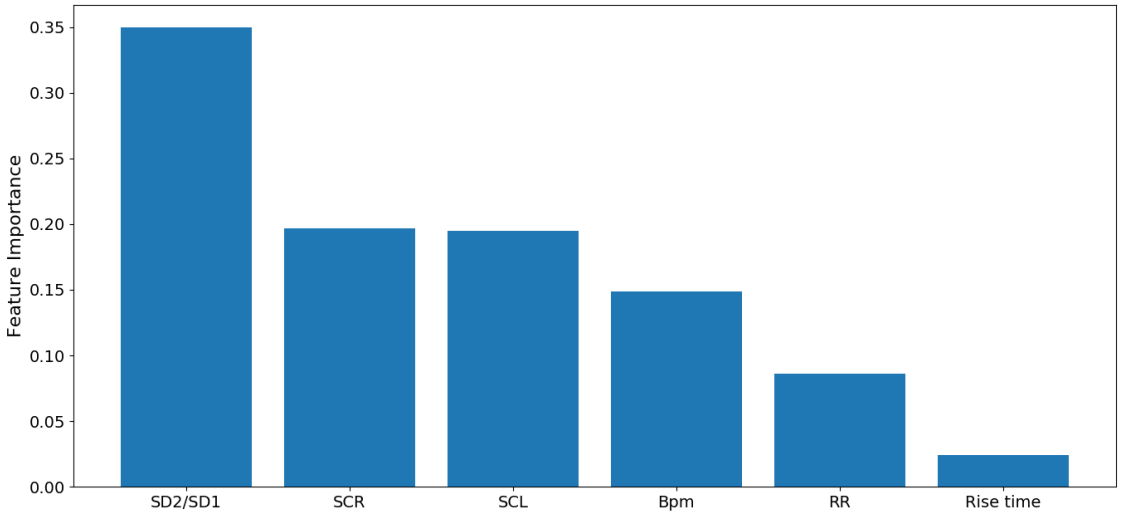

Figure 5.13: Feature Importance for HRV and EDA features obtained with the random forest classifier.

CHAPTER 6

DISCUSSION

The results obtained in section 5, showed that the arithmetic test (PVSAT) induced stress to the subjects, reflected by the increase in heart rate (Bpm) and in EDA features, such as, SCR and SCL, during stress.

For EDA features, SCR, SCL, Rise time, Rec.t 50% and Rec.t 63%, revealed to be good markers of stress, with the increase of values during all the segments studied during stress compared to the baseline segments. In section 4.2.4, the frequency analysis of EDA signals confirmed the activation of the sympathetic nervous system with an increase in power for low frequency bands. The results obtained showed that there was a significant increase in Band 1 power. This confirms that the dynamics of the sympathetic nervous system are confined to low frequencies, in agreement with the work performed by Posada et al., although in this thesis the frequency band studied was extended more 0.10 Hz, the increase in power was also verified, making frequency analysis of EDA a potential marker of quantitative assessment of the level of stress and sympathetic nervous system impairments [1].

For HRV, the results obtained for spectral measures were opposite to the expected. The inducement of stress in subjects was expected to increase LF(nu) and LF/HF ratio [33, 65, 66]. Contrarily to the expectation, the results obtained showed that there was a decrease in LF(nu) and LF/HF ratio during stress, results also reported by [65–67]. Vuksanovic et al. reported that vocalization of the answers, assigned to parasympathetic activity, during the PVSAT interfered with the spectral analysis and concealed out the changes in spectral measures of HRV [65]. Langewitz et al. showed that the breathing pattern for some subjects during vocalization affects the low frequency band power, as the breathing frequency falls in the 0.1 Hz frequency band, the resonance phenomenon will not increase the power in the LF band [68], concluding that the fact subjects answered the PVSAT aloud might have influenced the spectral measures of HRV. These facts also show that the LF band does not reflect purely the cardiac response to the activation of the sympathetic nervous system, but a mixture of the sympathetic and parasympathetic systems, with counteracting effects of activation of the sympathetic system and withdrawal of the parasympathetic system [69]. From the point of view of humoral mechanisms, these results

can be explained, as, during a situation of stress, the sympathetic nervous system affects the heart through release of catecholamines [70], such as epinephrine, leading to an increase in heart rate without changing heart rate variability measures, as the release of epinephrine does not affect spectral measures [71].

In section 5.7, despite the results for HRV were concealed out when analyzing the subjects as a whole, it was possible to verify significant changes in spectral measures for HRV after separating the subjects into the two different groups, taking into account that subjects can exhibit distinct response when submitted to stress. From figure 5.7, it is possible to see that the slopes for each group do not intercept with one another, so the two responses are parallel. For group 2, the results obtained were in agreement with the expectations that during stress, the LF(nu) and the LF/HF ratio increased with a small decrease in HF(nu) power with no significance. This group responds to stress with the withdrawal of the parasympathetic nervous system and the activation of the sympathetic nervous system. For group 1, the results showed significant decrease in LF(nu) and LF/HF ratio during stress and significant increase in HF(nu) power. The simultaneous increase in HF(nu) and heart rate is more difficult to explain, although it could be an influence of complex respiratory pattern [65], or it could be the effect of different co-activation humoral mechanims, caused by compensatory sympatho-adrenal activation with catecholamine release into the circulation [70].

In terms of EDA, both groups showed an increase in Band 1 power, although significance was only found in group 2 between baseline 2 and stress 1 segments. It is possible to conclude that even if there is a distinct response to stress in terms of HRV, there is activation of the sympathetic nervous system during the stress situation, due to the fact that the sympathetic nervous system influences the heart and sweat through distinct hormones, respectively, epinephrine and acetylcholine.

Finally, the classification model implemented in section 5.8, showed that it was possible to predict the type of response for each subject during stress, using only their baseline features for both HRV and EDA features, making it possible to classify the subjects into the two different groups, with an accuracy of approximately 80% for HRV features in baseline and an accuracy of approximately 77% for HRV and EDA simultaneous features. This model assumes to be a good asset for future assessment of the type of response when the subjects are under a stress situation.

CHAPTER 7

FUTURE EXPECTATIONS

There are some improvements that can be made. First it is necessary to acquire data from a greater number of subjects in order to confirm the significance of the results obtained.

All the volunteers in this thesis were considered healthy subjects, so it would be interesting to test the model implemented to classify the subjects into the groups, on subjects that are clinically classified with psychological stress, and see if there are any changes on HRV and EDA parameters on those patients compared to healthy subjects.

The stress test implemented (PVSAT) with the vocalization of the answers during the test, interfered with HRV spectral analysis due to the phenomenon of resonance in the LF band, so it is necessary to remove this influence in spectral analysis, by applying this test without vocalization of the answers, or even perform a different stress test than the PVSAT, a test that could induce a higher level of stress to the participants.

In terms of EDA, frequency-domain analysis to assess the sympathetic nervous system tone, is not yet a reliable marker. Only Posada et al. performed this kind of analysis on EDA, showing that the activity of the sympathetic nervous system is confined to low frequencies (0.04-0.25 Hz), which is in agreement with the work performed on this thesis, although the frequency band analyzed was of 0.04 Hz to 0.35 Hz. It is necessary to fully elucidate the frequency band in which it is possible to assess the activation of the sympathetic nervous system during a stress situation, using EDA.

Finally, the classification method used was the Random Forest Classifier with an accuracy score of approximately 80%. Other classification methods could be used to classify the subjects into the two groups, and try to obtain a higher accuracy score to avoid misclassification errors.

BIBLIOGRAPHY

[1] H. F. Posada-Quintero, J. P. Florian, A. D. Orjuela-Cañón, T. Aljama-Corrales, S. Charleston-Villalobos, and K. H. Chon. "Power Spectral Density Analysis of Electrodermal Activity for Sympathetic Function Assessment." In: *Annals of Biomedical Engineering* 44.10 (2016), pp. 3124–3135. ISSN: 15739686. DOI: 10.1007/s10439-016-1606-6.

[2] J. L. Hamilton and L. B. Alloy. *Atypical reactivity of heart rate variability to stress and depression across development: Systematic review of the literature and directions for future research.* 2016. DOI: 10.1016/j.cpr.2016.09.003. URL: http://dx.doi.org/10.1016/j.cpr.2016.09.003.

[3] H. F. Posada-quintero and S. Hall. "Electrodermal Activity : What it can contribute to the Assessment of the Autonomic Nervous System." In: (2016), p. 24.

[4] H. F. Posada-Quintero, J. P. Florian, Á. D. Orjuela-Cañón, and K. H. Chon. "Highly sensitive index of sympathetic activity based on time-frequency spectral analysis of electrodermal activity." In: *American Journal of Physiology - Regulatory, Integrative and Comparative Physiology* 311.3 (2016), R582–R591. ISSN: 0363-6119. DOI: 10.1152/ajpregu.00180.2016. URL: http://ajpregu.physiology.org/lookup/doi/10.1152/ajpregu.00180.2016.

[5] D. Bansal, M. Khan, and A. Salhan. "A Review of Measurement and Analysis of Heart Rate Variability." In: *2009 International Conference on Computer and Automation Engineering*. 2009, pp. 243–246. ISBN: 978-0-7695-3569-2. DOI: 10.1109/ICCAE.2009.70. URL: http://ieeexplore.ieee.org/document/4804526/.

[6] M. P. Wachowiak, D. C. Hay, and M. J. Johnson. "Assessing heart rate variability through wavelet-based statistical measures." In: *Computers in Biology and Medicine* 77 (2016), pp. 222–230. ISSN: 18790534. DOI: 10.1016/j.compbiomed.2016.07.008. URL: http://dx.doi.org/10.1016/j.compbiomed.2016.07.008.

[7] C. H. Hsu, M. Y. Tsai, G. S. Huang, T. C. Lin, K. P. Chen, S. T. Ho, L. Y. Shyu, and C. Y. Li. "Poincaré plot indexes of heart rate variability detect dynamic autonomic modulation during general anesthesia induction." In: *Acta Anaesthesiologica Taiwanica* 50.1 (2012),

pp. 12–18. ISSN: 18754597. DOI: 10.1016/j.aat.2012.03.002. URL: http://dx.doi.org/10.1016/j.aat.2012.03.002.

[8] G.-S. Zoltan. "Wavelet transform based HRV analysis." In: *The 7th International Conference Interdisciplinarity in Engineering (INTER-ENG 2013)* 12 (2013), pp. 105–111. ISSN: 2212-0173. DOI: 10.1016/j.protcy.2013.12.462. URL: http://dx.doi.org/10.1016/j.protcy.2013.12.462http://ac.els-cdn.com/S2212017313006476/1-s2.0-S2212017313006476-main.pdf?_tid=8941ead6-9824-11e7-9778-00000aab0f02&acdnat=1505267014_14fa3d485d21743f69e69ba97dedc2a5.

[9] J. Allen. "Photoplethysmography and its application in clinical physiological measurement." In: *Physiological Measurement* 28.3 (2007). ISSN: 09673334. DOI: 10.1088/0967-3334/28/3/R01.

[10] Guidelines. "Guidelines Heart rate variability." In: *European Heart Journal* 17 (1996), pp. 354–381. ISSN: 0195-668X. DOI: 10.1161/01.CIR.93.5.1043. arXiv: WOS:A1996UF54400011. URL: http://www.mendeley.com/research/guidelines-heart-rate-variability-2/.

[11] A. Bouziane, B. Yagoubi, and M. Malika. "A hybrid method for Heart Rate Variability analysis." In: *2014 1st International Conference on Advanced Technologies for Signal and Image Processing (ATSIP)* (2014), pp. 305–309. DOI: 10.1109/ATSIP.2014.6834626. URL: http://ieeexplore.ieee.org/lpdocs/epic03/wrapper.htm?arnumber=6834626.

[12] I. R. Kleckner, R. M. Jones, O. Wilder-Smith, J. B. Wormwood, M. Akcakaya, K. S. Quigley, C. Lord, and M. S. Goodwin. *Simple, Transparent, and Flexible Automated Quality Assessment Procedures for Ambulatory Electrodermal Activity Data.* 2017. DOI: 10.1109/TBME.2017.2758643.

[13] H. Gamboa and A. Fred. "Electrodermal Activity Model." In: *Psychophysiology* April (2008), p. 30.

[14] W. Boucsein. *Electodermal Activity.* Second Edi. 2012. ISBN: 9781461411253. DOI: 10.1007/978-1-4614-1126-0.

[15] M. van Dooren, J. J. J. de Vries, and J. H. Janssen. "Emotional sweating across the body: Comparing 16 different skin conductance measurement locations." In: *Physiology and Behavior* 106.2 (2012), pp. 298–304. ISSN: 00319384. DOI: 10.1016/j.physbeh.2012.01.020. URL: http://dx.doi.org/10.1016/j.physbeh.2012.01.020.

[16] H. F. Posada-quintero, S. Member, K. H. Chon, and S. Member. "Frequency - Domain Electrodermal Activity Index of Sympathetic Function." In: (2016), pp. 497–500.

[17] A. C. Guyton and J. E. Hall. *Textbook of Medical Physiology.* 2011, pp. 101–153. ISBN: 9781416045748. arXiv: arXiv:1011.1669v3.

[18] P. T. Figures and H. P. Germann. *Introduction to the ANS.* URL: http://tmedweb.tulane.edu/pharmwiki/doku.php/introduction_to_the_ans (visited on 01/29/2018).

[19] *CH 14 ANS Histology & Pharmacology*. URL: http://www.apsubiology.org/anatomy/2010/2010_Exam_Reviews/Exam_5_Final_Review/CH_14_ANS_Histology-Pharmacology.htm (visited on 01/29/2018).

[20] M Bolanos, H Nazeran, and E Haltiwanger. "Comparison of heart rate variability signal features derived from electrocardiography and photoplethysmography in healthy individuals." In: *Annual International Conference of the IEEE Engineering in Medicine and Biology - Proceedings*. 2006, pp. 4289–4294. ISBN: 1424400325. DOI: 10.1109/IEMBS.2006.260607.

[21] D. Jarchi and A. J. Casson. "Towards Photoplethysmography-Based Estimation of Instantaneous Heart Rate during Physical Activity." In: *IEEE Transactions on Biomedical Engineering* 64.9 (2017), pp. 2042–2053. ISSN: 15582531. DOI: 10.1109/TBME.2017.2668763.

[22] S. W. Weinschenk, R. D. Beise, and J. Lorenz. "Heart rate variability (HRV) in deep breathing tests and 5-min short-term recordings: agreement of ear photoplethysmography with ECG measurements, in 343 subjects." In: *European Journal of Applied Physiology* 116.8 (2016), pp. 1527–1535. ISSN: 14396319. DOI: 10.1007/s00421-016-3401-3.

[23] D. J. Plews, B. Scott, M. Altini, M. Wood, A. E. Kilding, and P. B. Laursen. "Comparison of heart-rate-variability recording with smartphone photoplethysmography, polar H7 chest strap, and electrocardiography." In: *International Journal of Sports Physiology and Performance* 12.10 (2017), pp. 1324–1328. ISSN: 15550265. DOI: 10.1123/ijspp.2016-0668.

[24] S. Lu, H. Zhao, K. Ju, K. Shin, M. Lee, K. Shelley, and K. H. Chon. "Can photoplethysmography variability serve as an alternative approach to obtain heart rate variability information?" In: *Journal of Clinical Monitoring and Computing* 22.1 (2008), pp. 23–29. ISSN: 13871307. DOI: 10.1007/s10877-007-9103-y.

[25] J.-q. Ke, S.-m. Shao, Y.-Y. Zheng, F.-w. Fu, G.-q. Zheng, and C.-f. Liu. "Sympathetic skin response and heart rate variability in predicting autonomic disorders in patients with Parkinson disease." In: *Medicine* 96.18 (2017), e6523. ISSN: 0025-7974. DOI: 10.1097/MD.0000000000006523. URL: http://insights.ovid.com/crossref?an=00005792-201705050-00004.

[26] M. Paniccia, L. Verweel, S. Thomas, T. Taha, M. Keightley, K. E. Wilson, and N. Reed. "Heart rate variability in healthy non-concussed youth athletes: Exploring the effect of age, sex, and concussion-like symptoms." In: *Frontiers in Neurology* 8.JAN (2018), pp. 1–11. ISSN: 16642295. DOI: 10.3389/fneur.2017.00753.

[27] M. Vollmer. "A robust, simple and reliable measure of heart rate variability using relative RR intervals." In: *Computing in Cardiology* 42.6 (2015), pp. 609–612. ISSN: 2325887X. DOI: 10.1109/CIC.2015.7410984.

[28] F. Shaffer and J. P. Ginsberg. “An Overview of Heart Rate Variability Metrics and Norms.” In: *Frontiers in Public Health* 5.September (2017), pp. 1–17. ISSN: 2296-2565. DOI: 10.3389/fpubh.2017.00258. URL: http://journal.frontiersin.org/article/10.3389/fpubh.2017.00258/full.

[29] B Bussmann. “Differentiation of autonomic nervous activity in different stages of coma displayed by power spectrum analysis of heart rate variability.” In: (1998), pp. 46–52.

[30] E. Miranda Dantas, M. Lima Sant'Anna, R. Varejão Andreão, C. Pereira Gonçalves, E. Aguiar Morra, M. Perim Baldo, S. Lamĉgo Rodrigues, and J. Geraldo Mill. “Spectral analysis of heart rate variability with the autoregressive method: What model order to choose?” In: *Computers in Biology and Medicine* 42.2 (2012), pp. 164–170. ISSN: 00104825. DOI: 10.1016/j.compbiomed.2011.11.004.

[31] M. Benedek and C. Kaernbach. “A continuous measure of phasic electrodermal activity.” In: *Journal of Neuroscience Methods* 190.1 (2010), pp. 80–91. ISSN: 01650270. DOI: 10.1016/j.jneumeth.2010.04.028. arXiv: 1606.01836. URL: http://dx.doi.org/10.1016/j.jneumeth.2010.04.028.

[32] A. Greco, G. Valenza, and E. P. Scilingo. “Advances in electrodermal activity processing with applications for mental health: From heuristic methods to convex optimization.” In: *Advances in Electrodermal Activity Processing with Applications for Mental Health: From Heuristic Methods to Convex Optimization* (2016), pp. 1–138. DOI: 10.1007/978-3-319-46705-4.

[33] Z Visnovcova, A Calkovska, and I Tonhajzerova. “Heart Rate Variability and Electrodermal Activity As Noninvasive Indices of Sympathovagal Balance in Response To Stress.” In: *Acta Medica Martiniana* 13.1 (2013), pp. 5–13. ISSN: 13358421. DOI: 10.2478/acm-2013-0006. URL: 10.2478/acm-2013-0006%5Cnhttp://ezproxy.net.ucf.edu/login?url=http://search.ebscohost.com/login.aspx?direct=true&db=aph&AN=87347381&site=ehost-live.

[34] J. Kettunen, N. Ravaja, P. Näätänen, P. Keskivaara, and L. Keltikangas-Järvinen. “The synchronization of electrodermal activity and heart rate and its relationship to energetic arousal: A time series approach.” In: *Biological Psychology* 48.3 (1998), pp. 209–225. ISSN: 03010511. DOI: 10.1016/S0301-0511(98)00017-9.

[35] S Ward, M Brickley, J Sharry, G Mcdarby, and C Heneghan. “Assessment of Heart Rate and Electrodermal Activity during Sustained Attention to Response Tests Media Lab Europe , Dublin , Ireland.” In: (2004), pp. 473–476. ISSN: 02766574.

[36] T. Rachow, S. Berger, M. K. Boettger, S. Schulz, S. Guinjoan, V. K. Yeragani, A. Voss, and K. J. Bär. “Nonlinear relationship between electrodermal activity and heart rate variability in patients with acute schizophrenia.” In: *Psychophysiology* 48.10 (2011), pp. 1323–1332. ISSN: 00485772. DOI: 10.1111/j.1469-8986.2011.01210.x.

[37] T. N. Tombaugh. "A comprehensive review of the Paced Auditory Serial Addition Test (PASAT)." In: *Archives of Clinical Neuropsychology* 21.1 (2006), pp. 53–76. ISSN: 08876177. DOI: 10.1016/j.acn.2005.07.006.

[38] T. D. Parsons and C. G. Courtney. "An initial validation of the Virtual Reality Paced Auditory Serial Addition Test in a college sample." In: *Journal of Neuroscience Methods* 222 (2014), pp. 15–23. ISSN: 01650270. DOI: 10.1016/j.jneumeth.2013.10.006. URL: http://dx.doi.org/10.1016/j.jneumeth.2013.10.006.

[39] B. N. Axelrod, J. Aharon-Peretz, R. Tomer, and T. Fisher. "Creating Interpretation Guidelines for the Hebrew Trail Making Test." In: *Applied Neuropsychology* 7.March 2015 (2000), pp. 186–188. ISSN: 0908-4282. DOI: 10.1207/S15324826AN0703.

[40] J. Royan, T. N. Tombaugh, L. Rees, and M. Francis. "The Adjusting-Paced Serial Addition Test (Adjusting-PSAT): Thresholds for speed of information processing as a function of stimulus modality and problem complexity." In: *Archives of Clinical Neuropsychology* 19.1 (2004), pp. 131–143. ISSN: 08876177. DOI: 10.1016/S0887-6177(02)00216-0.

[41] K. Nakano, K. Park, R. Zheng, F. Fang, M. Ohori, H. Nakamura, Y. Kumagai, H. Okada, K. Teramura, S. Nakayama, A. Irimajiri, H. Taoka, and S. Okada. "Leukoaraiosis significantly worsens driving performance of ordinary older drivers." In: *PLoS ONE* 9.10 (2014). Ed. by P. Allen, e108333. ISSN: 19326203. DOI: 10.1371/journal.pone.0108333. URL: http://dx.plos.org/10.1371/journal.pone.0108333.

[42] J. H. McDonald. *One-way anova - Handbook of Biological Statistics*. 2014. URL: http://www.biostathandbook.com/onewayanova.html (visited on 06/18/2018).

[43] B. Winter. "The F distribution and the basic principle behind ANOVAs Bodo." In: *Bodowinter.Com* (2015), pp. 1–30. ISSN: 1098-6596. DOI: 10.1017/CBO9781107415324.004. arXiv: arXiv:1011.1669v3.

[44] Laerd Statistics. *One-way ANOVA in SPSS Statistics - Step-by-step procedure including testing of assumptions*. 2013. URL: https://statistics.laerd.com/spss-tutorials/one-way-anova-using-spss-statistics.php.

[45] J. H. McDonald. *Kruskal–Wallis test - Handbook of Biological Statistics*. 2014. URL: http://www.biostathandbook.com/kruskalwallis.html (visited on 06/18/2018).

[46] Y Chan and R. P. Walmsley. "Learning and understanding the Kruskal-Wallis one-way analysis-of-variance-by-ranks test for differences among three or more independent groups." In: *Physical therapy* 77.12 (1997), pp. 1755–62. ISSN: 0031-9023. DOI: 10.1093/ptj/77.12.1755. URL: http://www.ncbi.nlm.nih.gov/pubmed/9413454.

[47] W. H. Kruskal and W. A. Wallis. "Use of Ranks in One-Criterion Variance Analysis." In: *Journal of the American Statistical Association* 47.260 (1952), pp. 583–621. ISSN: 1537274X. DOI: 10.1080/01621459.1952.10483441. arXiv: NIHMS150003.

[48] W. G. Cochran. "The χ2 Test of Goodness of Fit." In: *The Annals of Mathematical Statistics* 23.3 (2013), pp. 315–345.

[49] M. R. Tallarida R.J. "Chi-Square Test." In: *Manual of Pharmacologic Calculations. Springer, New York, NY* (1987), pp. 140–142.

[50] R. L. Plackett. "Karl Pearson and the Chi-Squared Test." In: *International Statistical Review / Revue Internationale de Statistique* 51.1 (1983), p. 59. ISSN: 03067734. DOI: 10.2307/1402731. URL: http://www.jstor.org/stable/1402731?origin=crossref.

[51] V. N. Vapnik. "An overview of statistical learning theory." In: *IEEE transactions on neural networks / a publication of the IEEE Neural Networks Council* 10.5 (1999), pp. 988–99. ISSN: 1045-9227. DOI: 10.1109/72.788640. URL: http://www.ncbi.nlm.nih.gov/pubmed/18252602.

[52] L. Discriminants. "Support Vector Machines." In: *Kernel Methods and Machine Learning* (2010), pp. 343–379. ISSN: 00775762. DOI: 10.1016/j.aca.2011.07.027. arXiv: arXiv:1011.1669v3. URL: http://dx.doi.org/10.1017/CBO9781139176224.

[53] A. Mammone, M. Turchi, and N. Cristianini. "Support Vector Machines." In: *Challenge* 1.December (2009), pp. 1–8. ISSN: 18732380. DOI: 10.1002/wics.049. URL: http://dx.doi.org/10.1002/wics.49.

[54] J Ali, R Khan, N Ahmad, and I Maqsood. "Random forests and decision trees." In: *IJCSI International Journal of Computer Science Issues* 9.5 (2012), pp. 272–278.

[55] P. O. Gislason, J. A. Benediktsson, and J. R. Sveinsson. "Random forests for land cover classification." In: *Pattern Recognition Letters* 27.4 (2006), pp. 294–300. ISSN: 01678655. DOI: 10.1016/j.patrec.2005.08.011.

[56] L. Breiman. "Random forests." In: *Machine Learning* 45.1 (2001), pp. 5–32. ISSN: 08856125. DOI: 10.1023/A:1010933404324. arXiv: /dx.doi.org/10.1023%2FA%3A1010933404324 [http:].

[57] N. Donges. *The Random Forest Algorithm*. 2018. URL: https://machinelearning-blog.com/2018/02/06/the-random-forest-algorithm/https://towardsdatascience.com/the-random-forest-algorithm-d457d499ffcd (visited on 06/29/2018).

[58] *Left Hand Cartoon Hd, Palm, Five Fingers, Left Hand PNG Image and Clipart for Free Download*. URL: https://pngtree.com/freepng/left-hand-cartoon-hd_3009837.html (visited on 06/06/2018).

[59] S. Kuntamalla, L Ram, and G. Reddy. "An Efficient and Automatic Systolic Peak Detection Algorithm for Photoplethysmographic Signals." In: *International Journal of Computer Applications* 97.19 (2014), pp. 975–8887. ISSN: 0975-8887.

[60] *A typical ECG signal for a single heartbeat*. URL: https://openi.nlm.nih.gov/detailedresult.php?img=PMC3312444_sensors-09-06273f4&req=4 (visited on 03/21/2018).

[61] D.-G. Jang, S. Park, M. Hahn, and S.-H. Park. "A Real-Time Pulse Peak Detection Algorithm for the Photoplethysmogram." In: *International Journal of Electronics and Electrical Engineering* 2.1 (2014), pp. 45–49. ISSN: 2301380X. DOI: 10.12720/ijeee.2.1.45-49. URL: http://www.ijeee.net/index.php?m=content&c=index&a=show&catid=36&id=85.

[62] R Logier, J De Jonckheere, and A Dassonneville. "An efficient algorithm for R-R intervals series filtering." In: *Conference proceedings : ... Annual International Conference of the IEEE Engineering in Medicine and Biology Society. IEEE Engineering in Medicine and Biology Society. Conference* 6 (2004), pp. 3937–3940. ISSN: 1557-170X. DOI: 10.1109/IEMBS.2004.1404100.

[63] M. Brennan, M. Palaniswami, and P. Kamen. "Do existing measures of Poincareé plot geometry reflect nonlinear features of heart rate variability?" In: *IEEE Transactions on Biomedical Engineering* 48.11 (2001), pp. 1342–1347. ISSN: 00189294. DOI: 10.1109/10.959330.

[64] H. Posada-Quintero, J. Florian, A. Orjuela-Cañón, and K. Chon. "Electrodermal activity is sensitive to cognitive stress under water." In: *Frontiers in Physiology* 8.JAN (2018), pp. 1–8. ISSN: 1664042X. DOI: 10.3389/fphys.2017.01128.

[65] V. Vuksanović and V. Gal. "Heart rate variability in mental stress aloud." In: *Medical Engineering and Physics* 29.3 (2007), pp. 344–349. ISSN: 13504533. DOI: 10.1016/j.medengphy.2006.05.011.

[66] N. Hjortskov, D. Rissén, A. K. Blangsted, N. Fallentin, U. Lundberg, and K. Søgaard. "The effect of mental stress on heart rate variability and blood pressure during computer work." In: *European Journal of Applied Physiology* 92.1-2 (2004), pp. 84–89. ISSN: 14396319. DOI: 10.1007/s00421-004-1055-z. arXiv: WOS:A1996UF54400011.

[67] E. Tharion, S. Parthasarathy, and N. Neelakantan. "Short-term heart rate variability measures in students during examinations." In: *National Medical Journal of India* 22.2 (2009), pp. 63–66. ISSN: 0970258X.

[68] W Langewitz and H Ruddel. "Spectral analysis of heart rate variability under mental stress." In: *J Hypertens Suppl* 7.6 (1989), S32–3. ISSN: 0952-1178. DOI: NLM;19900511. URL: http://www.ncbi.nlm.nih.gov/pubmed/2632731.

[69] R. P. Sloan, J. B. Korten, and M. M. Myers. "Components of heart rate reactivity during mental arithmetic with and without speaking." In: *Physiology and Behavior* 50.5 (1991), pp. 1039–1045. ISSN: 00319384. DOI: 10.1016/0031-9384(91)90434-P.

[70] A. J. Terkelsen, H. Mølgaard, J. Hansen, O. K. Andersen, and T. S. Jensen. "Acute pain increases heart rate: Differential mechanisms during rest and mental stress." In: *Autonomic Neuroscience: Basic and Clinical* 121.1-2 (2005), pp. 101–109. ISSN: 15660702. DOI: 10.1016/j.autneu.2005.07.001.

[71] M. W. Ahmed, A. H. Kadish, M. A. Parker, and J. J. Goldberger. "Effect of physiologic and pharmacologic adrenergic stimulation on heart rate variability." In: *Journal of the American College of Cardiology* 24.4 (1994), pp. 1082–1090. ISSN: 07351097. DOI: 10.1016/0735-1097(94)90874-5.

APPENDIX A - HRV FEATURES

Table A.1: HRV Features Baseline

Variable	Mean	SE	Median	Min	Max	25th Percentile	50th Percentile	75th Percentile
Bpm	78,9427	10,9216	79,2300	60,9000	96,5700	73,1850	79,2300	87,2900
RR (s)	0,7791	0,1116	0,7600	0,6270	0,9910	0,6930	0,7600	0,8260
RMSSD (ms)	50,0909	20,5628	44,6943	18,1031	91,5776	38,3091	44,6943	60,9298
SDNN (ms)	58,4755	16,1007	60,5799	36,6147	90,1643	43,3959	60,5799	67,3082
NN50	91,0000	49,9028	92,0000	3,0000	186,0000	58,0000	92,0000	112,0000
pNN50 (%)	25,4757	16,5910	19,7849	0,6593	59,7403	15,0325	19,7849	34,9638
HF (ms^2)	0,5967	0,5914	0,4517	0,0459	2,3855	0,2494	0,4517	0,7640
HF (nu)	19,9720	16,0623	11,6900	6,3000	51,4400	7,7650	11,6900	27,3400
LF (ms^2)	2,2422	1,1515	2,1847	0,4910	4,9303	1,5492	2,1847	2,8513
LF (nu)	75,2767	14,3799	78,4800	46,6800	93,1000	68,7750	78,4800	84,2350
VLF (ms^2)	2,3702	1,2790	2,2803	0,5843	4,3614	1,1717	2,2803	3,4030
Total Power (ms^2)	5,3376	2,3858	5,4097	2,1786	9,0212	2,8907	5,4097	7,2798
LF/HF	6,9787	4,7953	7,1000	0,9100	14,7800	2,5900	7,1000	10,9500
SD1 (s)	0,0354	0,0145	0,0316	0,0128	0,0648	0,0271	0,0316	0,0431
SD2 (s)	0,0742	0,0199	0,0772	0,0421	0,1099	0,0546	0,0772	0,0867
SD2/SD1	2,2960	0,7738	2,2343	1,2954	4,1562	1,6666	2,2343	2,6265

Table A.2: HRV Features Stress

Variable	Mean	SE	Median	Min	Max	25th Percentile	50th Percentile	75th Percentile
Bpm	88,5820	11,5948	86,4000	64,0500	106,3200	81,6450	86,4000	97,6250
RR (s)	0,6937	0,0980	0,6960	0,5750	0,9470	0,6170	0,6960	0,7380
RMSSD (ms)	53,4927	26,2762	52,9161	21,2120	96,1536	27,8050	52,9161	69,4797
SDNN (ms)	54,6565	17,9574	52,4972	27,4345	89,2802	41,3392	52,4972	58,1211
NN50	105,8000	71,3835	118,0000	12,0000	240,0000	33,0000	118,0000	151,0000
pNN50 (%)	27,2245	19,3110	30,8094	2,3810	56,1605	6,6862	30,8094	40,9543
HF (ms^2)	1,0087	0,8958	0,9500	0,0910	2,9087	0,2142	0,9500	1,3447
HF (nu)	30,2613	20,5290	23,0500	5,9300	80,4300	14,0700	23,0500	42,6600
LF (ms^2)	2,3234	2,2709	1,6620	0,3270	9,4205	0,9921	1,6620	2,7037
LF (nu)	66,8740	19,4732	74,6400	19,1100	93,2000	54,5450	74,6400	79,0850
VLF (ms^2)	1,9072	1,9645	1,1535	0,3129	6,9203	0,7253	1,1535	1,9263
Total Power (ms^2)	5,3189	4,6208	3,6461	1,5832	18,1589	2,3128	3,6461	5,2469
LF/HF	4,4953	4,6061	3,2400	0,2400	15,7200	1,2800	3,2400	5,7000
SD1 (s)	0,0378	0,0186	0,0374	0,0150	0,0680	0,0197	0,0374	0,0492
SD2 (s)	0,0662	0,0218	0,0652	0,0346	0,1083	0,0518	0,0652	0,0764
SD2/SD1	2,0751	0,9510	1,9306	0,8382	3,8365	1,4029	1,9306	2,6265

Table A.3: HRV Features Baseline-Stress

Variables	Baseline		Stress		H-value	p-value
	Mean	SE	Mean	SE		
Bpm	78,9427	10,9216	88,5820	11,5948	4,9243	0,0265*
RR (s)	0,7791	0,1116	0,6937	0,0980	4,9243	0,0265*
RMSSD (ms)	50,0909	20,5628	53,4927	26,2762	0,0727	0,7875
SDNN (ms)	58,4755	16,1007	54,6565	17,9574	1,0327	0,3095
NN50	91,0000	49,9028	105,8000	71,3835	0,3135	0,5755
pNN50 (%)	25,4757	16,5910	27,2245	19,3110	0,0108	0,9174
HF (ms^2)	0,5967	0,5914	1,0087	0,8958	1,3011	0,2540
HF (nu)	19,9720	16,0623	30,2613	20,5290	1,9308	0,1647
LF (ms^2)	2,2422	1,1515	2,3234	2,2709	0,5888	0,4429
LF (nu)	75,2767	14,3799	66,8740	19,4732	1,6004	0,2058
VLF (ms^2)	2,3702	1,2790	1,9072	1,9645	2,2920	0,1300
Total Power (ms^2)	5,3376	2,3858	5,3189	4,6208	1,0327	0,3095
LF/HF	6,9787	4,7953	4,4953	4,6061	1,8172	0,1776
SD1 (s)	0,0354	0,0145	0,0378	0,0186	0,0727	0,7875
SD2 (s)	0,0742	0,0199	0,0662	0,0218	1,3011	0,2540
SD2/SD1	2,2960	0,7738	2,0751	0,9510	0,7953	0,3725

p-value<0.05

APPENDIX B - EDA FEATURES

Table B.1: EDA Features Baseline 1

Variable	Mean	SE	Median	Min	Max	25th Percentile	50th Percentile	75th Percentile
SCL (µS)	3,2224	1,1575	3,2459	1,3990	5,2439	2,3152	3,2459	3,9843
SCR (µS)	0,0415	0,0631	0,0227	0,0089	0,2600	0,0121	0,0227	0,0329
Number of peaks	50,8667	7,3472	50,0000	34,0000	65,0000	46,5000	50,0000	55,0000
Rise time (s)	0,6693	0,1346	0,6300	0,5300	1,0400	0,5700	0,6300	0,7250
Rec.t 50% (s)	0,5427	0,1105	0,5100	0,4300	0,8500	0,4650	0,5100	0,5900
Rec.t 63% (s)	0,6747	0,1368	0,6400	0,5300	1,0500	0,5750	0,6400	0,7350
Band 2 $(\mu S)^2$	1,0535	2,9491	0,1592	0,0361	11,5802	0,0873	0,1592	0,2967
Band 2 (nu)	0,0853	0,1428	0,0300	0,0100	0,5700	0,0200	0,0300	0,0700
Band 1 $(\mu S)^2$	56,9998	109,7263	19,8981	1,9914	432,7505	7,0675	19,8981	42,4270
Band 1 (nu)	6,5260	6,0117	4,1800	0,1200	21,2200	2,1650	4,1800	8,4050
VLF $(\mu S)^2$	723,9877	594,9969	480,2268	112,1888	1682,1262	189,2500	480,2268	1223,0480
Total Power $(\mu S)^2$	789,6398	658,3265	485,6550	125,2853	2039,2808	211,9408	485,6550	1269,3813

Table B.2: EDA Features Baseline 2

Variable	Mean	SE	Median	Min	Max	25th Percentile	50th Percentile	75th Percentile
SCL (µS)	2,7372	1,1675	2,6105	1,1200	5,1982	1,8711	2,6105	3,6268
SCR (µS)	0,0339	0,0539	0,0129	0,0061	0,1996	0,0077	0,0129	0,0245
Number of peaks	55,6667	8,5328	57,0000	36,0000	67,0000	51,5000	57,0000	62,0000
Rise time (s)	0,6327	0,1243	0,5900	0,5200	0,9100	0,5400	0,5900	0,6750
Rec.t 50% (s)	0,5120	0,1032	0,4800	0,4200	0,7400	0,4350	0,4800	0,5450
Rec.t 63% (s)	0,6367	0,1261	0,5900	0,5300	0,9200	0,5450	0,5900	0,6750
Band 2 $(\mu S)^2$	3,5101	12,4796	0,1082	0,0115	48,5909	0,0315	0,1082	0,3676
Band 2 (nu)	0,1627	0,3548	0,0400	0,0100	1,4100	0,0100	0,0400	0,1300
Band 1 $(\mu S)^2$	126,8951	270,6913	17,2068	0,0899	972,1302	2,4272	17,2068	53,7689
Band 1 (nu)	10,0480	10,1175	5,8800	0,0500	31,3900	1,8300	5,8800	16,1550
VLF $(\mu S)^2$	737,0825	1345,9756	241,6063	41,0887	5121,2986	116,0237	241,6063	627,0645
Total Power $(\mu S)^2$	902,5581	1652,4247	246,3089	42,2526	6009,9971	160,9228	246,3089	658,6880

Table B.3: EDA Features Stress 1

Variable	Mean	SE	Median	Min	Max	25th Percentile	50th Percentile	75th Percentile
SCL (µS)	4,0745	1,3352	4,1615	1,8323	6,6924	3,1755	4,1615	4,8061
SCR (µS)	0,0911	0,1005	0,0448	0,0106	0,3825	0,0332	0,0448	0,1318
Number of peaks	53,6000	5,1796	53,0000	44,0000	63,0000	51,0000	53,0000	57,0000
Rise time (s)	0,8133	0,1529	0,8000	0,5900	1,0900	0,7200	0,8000	0,9300
Rec.t 50% (s)	0,6593	0,1247	0,6500	0,4700	0,8800	0,5850	0,6500	0,7550
Rec.t 63% (s)	0,8213	0,1552	0,8100	0,5900	1,1000	0,7300	0,8100	0,9400
Band 2 $(\mu S)^2$	4,8010	9,8139	0,5642	0,1261	37,1645	0,2728	0,5642	3,1105
Band 2 (nu)	0,1993	0,3222	0,0800	0,0000	1,2400	0,0450	0,0800	0,1850
Band 1 $(\mu S)^2$	116,9510	130,6748	48,6134	4,7355	448,7866	37,4124	48,6134	180,2865
Band 1 (nu)	8,9680	10,9681	3,6200	0,8700	42,7500	2,4050	3,6200	14,6700
VLF $(\mu S)^2$	2189,2165	2399,0016	1579,0083	59,5796	8288,1823	421,9942	1579,0083	3009,1358
Total Power $(\mu S)^2$	2327,6836	2475,1542	1627,7638	113,7103	8509,7223	478,1952	1627,7638	3277,5194

Table B.4: EDA Features Stress 2

Variable	Mean	SE	Median	Min	Max	25th Percentile	50th Percentile	75th Percentile
SCL (µS)	3,7393	1,6706	3,7474	1,1279	6,8152	2,5679	3,7474	4,9025
SCR (µS)	0,0882	0,0886	0,0607	0,0085	0,2908	0,0187	0,0607	0,1328
Number of peaks	53,0667	10,9118	50,0000	36,0000	80,0000	47,0000	50,0000	56,5000
Rise time (s)	0,7780	0,1834	0,7700	0,5500	1,0100	0,5650	0,7700	0,9350
Rec.t 50% (s)	0,6313	0,1496	0,6300	0,4400	0,8200	0,4600	0,6300	0,7600
Rec.t 63% (s)	0,7840	0,1848	0,7800	0,5500	1,0200	0,5700	0,7800	0,9450
Band 2 $(\mu S)^2$	10,5737	25,3470	1,5314	0,0372	97,7843	0,2859	1,5314	4,4791
Band 2 (nu)	0,7420	1,0495	0,2200	0,0100	3,5300	0,1050	0,2200	0,9750
Band 1 $(\mu S)^2$	500,0602	1577,1772	58,8064	3,9810	6189,3401	26,4814	58,8064	170,0922
Band 1 (nu)	18,1633	10,8429	15,7700	1,0000	35,5700	9,8800	15,7700	26,0500
VLF $(\mu S)^2$	1293,2019	3566,3403	300,3935	54,2928	14146,6983	196,7919	300,3935	530,3139
Total Power $(\mu S)^2$	1867,8397	5362,4193	373,0023	58,7455	21205,9638	251,0736	373,0023	805,4503

Table B.5: EDA Features Baseline-Stress

Variables	Baseline 1		Baseline 2		Stress 1		Stress 2	
	Mean	SE	Mean	SE	Mean	SE	Mean	SE
SCL (µS)	3,2224	1,1575	2,7372	1,1675	4,0745	1,3352	3,7393	1,6706
SCR (µS)	0,0415	0,0631	0,0339	0,0539	0,0911	0,1005	0,0882	0,0886
Number of peaks	50,8667	7,3472	55,6667	8,5328	53,6000	5,1796	53,0667	10,9118
Rise time (s)	0,6693	0,1346	0,6327	0,1243	0,8133	0,1529	0,7780	0,1834
Rec.t 50% (s)	0,5427	0,1105	0,5120	0,1032	0,6593	0,1247	0,6313	0,1496
Rec.t 63% (s)	0,6747	0,1368	0,6367	0,1261	0,8213	0,1552	0,7840	0,1848
Band 2 $(\mu S)^2$	1,0535	2,9491	3,5101	12,4796	4,8010	9,8139	10,5737	25,3470
Band 2 (nu)	0,0853	0,1428	0,1627	0,3548	0,1993	0,3222	0,7420	1,0495
Band 1 $(\mu S)^2$	56,9998	109,7263	126,8951	270,6913	116,9510	130,6748	500,0602	1577,1772
Band 1 (nu)	6,5260	6,0117	10,0480	10,1175	8,9680	10,9681	18,1633	10,8429
VLF	723,9877	594,9969	737,0825	1345,9756	2189,2165	2399,0016	1293,2019	3566,3403
Total Power	789,6398	658,3265	902,5581	1652,4247	2327,6836	2475,1542	1867,8397	5362,4193

APPENDIX C - GROUP 1 HRV FEATURES

Table C.1: Group 1 - HRV Features Baseline

Variable	Mean	SE	Median	Min	Max	25th Percentile	50th Percentile	75th Percentile
Bpm	82,3700	12,6515	85,2500	64,1000	96,5700	75,0000	85,2500	91,9675
RR (s)	0,7496	0,1258	0,7100	0,6270	0,9420	0,6553	0,7100	0,8108
RMSSD (ms)	47,3314	21,8417	43,8662	18,1031	85,5509	35,6130	43,8662	52,6261
SDNN (ms)	55,6806	15,2273	59,4436	37,6258	81,6945	41,4191	59,4436	61,8740
NN50	84,3750	54,8555	84,0000	3,0000	184,0000	50,5000	84,0000	103,5000
pNN50 (%)	23,2483	18,6320	18,6281	0,6593	59,7403	12,7822	18,6281	28,3206
HF (ms^2)	0,4378	0,3299	0,3740	0,0459	1,0301	0,2139	0,3740	0,6059
HF (nu)	16,1000	13,5085	9,7950	6,3000	45,9800	7,7325	9,7950	19,3500
LF (ms^2)	2,3756	1,3927	2,2800	0,4910	4,9303	1,7321	2,2800	2,9789
LF (nu)	80,5038	12,4098	83,1600	53,8700	93,1000	77,4775	83,1600	87,5475
VLF (ms^2)	2,2112	1,2074	2,2050	0,5843	4,0993	1,3958	2,2050	2,9921
Total Power (ms^2)	5,1195	2,5041	5,3475	2,1786	9,0212	2,7884	5,3475	6,7862
LF/HF	8,0325	4,8162	8,9000	1,1700	14,7800	4,0725	8,9000	11,2000
SD1 (s)	0,0335	0,0154	0,0310	0,0128	0,0605	0,0252	0,0310	0,0372
SD2 (s)	0,0705	0,0185	0,0767	0,0421	0,0984	0,0549	0,0767	0,0805
SD2/SD1	2,4034	0,9486	2,4430	1,2954	4,1562	1,5953	2,4430	2,7578

Table C.2: Group 1 - HRV Features Stress

Variable	Mean	SE	Median	Min	Max	25th Percentile	50th Percentile	75th Percentile
Bpm	92,2975	11,0208	93,7850	75,5700	106,3200	84,7200	93,7850	100,6850
RR (s)	0,6631	0,0825	0,6430	0,5750	0,8020	0,5988	0,6430	0,7113
RMSSD (ms)	53,4291	28,2694	55,7593	21,2120	91,8566	25,8560	55,7593	68,1310
SDNN (ms)	52,2543	21,2277	46,1940	27,4345	89,2802	37,9259	46,1940	62,4104
NN50	113,7500	86,0278	131,5000	12,0000	240,0000	23,7500	131,5000	163,0000
pNN50 (%)	27,8566	21,7165	31,8446	2,3810	56,1605	4,9714	31,8446	40,9479
HF (ms^2)	1,2205	1,0881	1,1317	0,1428	2,9087	0,2027	1,1317	1,6991
HF (nu)	37,0525	22,1569	31,9450	11,9000	80,4300	22,2625	31,9450	48,0425
LF (ms^2)	2,1861	3,0113	1,0975	0,3270	9,4205	0,7255	1,0975	1,7341
LF (nu)	59,9038	20,4281	64,8500	19,1100	76,9200	50,8025	64,8500	76,2875
VLF (ms^2)	1,7291	1,8878	0,8100	0,3129	5,5380	0,7087	0,8100	1,8157
Total Power (ms^2)	5,2225	5,8054	2,7816	1,5832	18,1589	1,9367	2,7816	4,9341
LF/HF	2,5438	2,0179	2,2950	0,2400	6,4000	1,0575	2,2950	3,4475
SD1 (s)	0,0378	0,0200	0,0394	0,0150	0,0650	0,0183	0,0394	0,0482
SD2 (s)	0,0625	0,0255	0,0576	0,0346	0,1083	0,0454	0,0576	0,0761
SD2/SD1	1,9310	0,8683	1,8091	0,8382	3,6267	1,3970	1,8091	2,1436

Table C.3: Group 1 - HRV Features Baseline-Stress

Variables	Baseline		Stress		H-value	p-value
	Mean	SE	Mean	SE		
Bpm	82,3700	12,6515	92,2975	11,0208	2,1618	0,1415
RR (s)	0,7496	0,1258	0,6631	0,0825	2,1618	0,1415
RMSSD (ms)	47,3314	21,8417	53,4291	28,2694	0,2757	0,5995
SDNN (ms)	55,6806	15,2273	52,2543	21,2277	0,7059	0,4008
NN50	84,3750	54,8555	113,7500	86,0278	0,5404	0,4622
pNN50 (%)	23,2483	18,6320	27,8566	21,7165	0,0993	0,7527
HF (ms²)	0,4378	0,3299	1,2205	1,0881	1,8640	0,1722
HF (nu)	16,1000	13,5085	37,0525	22,1569	5,3382	0,0209*
LF (ms²)	2,3756	1,3927	2,1861	3,0113	1,3346	0,2480
LF (nu)	80,5038	12,4098	59,9038	20,4281	5,8346	0,0157*
VLF (ms²)	2,2112	1,2074	1,7291	1,8878	1,1029	0,2936
Total Power (ms²)	5,1195	2,5041	5,2225	5,8054	1,1029	0,2936
LF/HF	8,0325	4,8162	2,5438	2,0179	5,3382	0,0209*
SD1 (s)	0,0335	0,0154	0,0378	0,0200	0,2757	0,5995
SD2 (s)	0,0705	0,0185	0,0625	0,0255	0,7059	0,4008
SD2/SD1	2,4034	0,9486	1,9310	0,8683	0,7059	0,4008

p-value<0.05

APPENDIX D - GROUP 2 HRV FEATURES

Table D.1: Group 2 - HRV Features Baseline

Variable	Mean	SE	Median	Min	Max	25th Percentile	50th Percentile	75th Percentile
Bpm	75,0257	7,6175	73,6800	60,9000	84,7600	73,1850	73,6800	79,7350
RR (s)	0,8129	0,0900	0,8210	0,7120	0,9910	0,7570	0,8210	0,8260
RMSSD (ms)	53,2445	20,2058	46,3816	32,5236	91,5776	40,1848	46,3816	60,9298
SDNN (ms)	61,6696	17,6646	66,2708	36,6147	90,1643	50,7809	66,2708	68,5378
NN50	98,5714	46,6328	97,0000	40,0000	186,0000	71,5000	97,0000	112,0000
pNN50 (%)	28,0212	14,9362	25,0646	11,2360	54,3860	17,7673	25,0646	34,9638
HF (ms^2)	0,7784	0,7855	0,5690	0,0944	2,3855	0,2690	0,5690	0,9310
HF (nu)	24,3971	18,6082	20,4200	6,8200	51,4400	7,9150	20,4200	38,1350
LF (ms^2)	2,0898	0,8833	2,1847	0,7140	3,0641	1,6172	2,1847	2,7159
LF (nu)	69,3029	14,9920	77,3500	46,6800	85,1900	58,2000	77,3500	79,7500
VLF (ms^2)	2,5519	1,4297	2,8321	0,9730	4,3614	1,1717	2,8321	3,6768
Total Power (ms^2)	5,5869	2,4145	6,2911	2,4623	8,1067	3,4885	6,2911	7,6357
LF/HF	5,7743	4,8393	3,7900	0,9100	11,4200	1,6050	3,7900	10,5450
SD1 (s)	0,0377	0,0143	0,0328	0,0230	0,0648	0,0285	0,0328	0,0431
SD2 (s)	0,0783	0,0220	0,0847	0,0464	0,1099	0,0646	0,0847	0,0891
SD2/SD1	2,1734	0,5606	2,0174	1,6372	3,1851	1,7607	2,0174	2,4262

Table D.2: Group 2 - HRV Features Stress

Variable	Mean	SE	Median	Min	Max	25th Percentile	50th Percentile	75th Percentile
Bpm	84,3357	11,5130	85,4400	64,0500	102,9600	81,6450	85,4400	87,3050
RR (s)	0,7287	0,1087	0,7060	0,5890	0,9470	0,6915	0,7060	0,7380
RMSSD (ms)	53,5654	26,0512	48,9561	24,1061	96,1536	33,3914	48,9561	69,4797
SDNN (ms)	57,4019	14,4992	53,2013	42,7875	88,2248	51,2018	53,2013	57,5980
NN50	96,7143	55,4518	93,0000	17,0000	157,0000	58,5000	93,0000	146,5000
pNN50 (%)	26,5021	17,8546	23,4257	4,2289	50,1672	12,8923	23,4257	40,9543
HF (ms^2)	0,7666	0,6025	0,8942	0,0910	1,7481	0,2453	0,8942	1,0713
HF (nu)	22,5000	16,6986	16,2400	5,9300	44,4800	8,0250	16,2400	37,4000
LF (ms^2)	2,4804	1,1829	2,1233	1,0700	4,4748	1,7317	2,1233	3,1156
LF (nu)	74,8400	16,0978	81,2500	54,0300	93,2000	60,5050	81,2500	87,1950
VLF (ms^2)	2,1106	2,1809	1,2821	0,6407	6,9203	1,0394	1,2821	1,9263
Total Power (ms^2)	5,4291	3,2367	4,8239	2,5422	12,4276	3,8581	4,8239	5,2469
LF/HF	6,7257	5,8199	5,0000	1,2100	15,7200	1,6300	5,0000	10,9450
SD1 (s)	0,0379	0,0184	0,0346	0,0170	0,0680	0,0236	0,0346	0,0492
SD2 (s)	0,0704	0,0178	0,0668	0,0492	0,1046	0,0617	0,0668	0,0744
SD2/SD1	2,2397	1,0823	1,9306	0,9609	3,8365	1,4613	1,9306	3,0137

Table D.3: Group 2 - HRV Features Baseline-Stress

Variables	Baseline		Stress		H-value	p-value
	Mean	SE	Mean	SE		
Bpm	75,0257	7,6175	84,3357	11,5130	4,4449	0,0350*
RR (s)	0,8129	0,0900	0,7287	0,1087	4,4449	0,0350*
RMSSD (ms)	53,2445	20,2058	53,5654	26,0512	0,0041	0,9491
SDNN (ms)	61,6696	17,6646	57,4019	14,4992	0,6898	0,4062
NN50	98,5714	46,6328	96,7143	55,4518	0,0041	0,9491
pNN50 (%)	28,0212	14,9362	26,5021	17,8546	0,1020	0,7494
HF (ms^2)	0,7784	0,7855	0,7666	0,6025	0,0041	0,9491
HF (nu)	24,3971	18,6082	22,5000	16,6986	0,1020	0,7494
LF (ms^2)	2,0898	0,8833	2,4804	1,1829	0,0367	0,8480
LF (nu)	69,3029	14,9920	74,8400	16,0978	0,9184	0,3379
VLF (ms^2)	2,5519	1,4297	2,1106	2,1809	0,6898	0,4062
Total Power (ms^2)	5,5869	2,4145	5,4291	3,2367	0,2000	0,6547
LF/HF	5,7743	4,8393	6,7257	5,8199	0,3306	0,5653
SD1 (s)	0,0377	0,0143	0,0379	0,0184	0,0041	0,9491
SD2 (s)	0,0783	0,0220	0,0704	0,0178	0,6898	0,4062
SD2/SD1	2,1734	0,5606	2,2397	1,0823	0,1020	0,7494

p-value<0.05

APPENDIX E - GROUP 1 EDA FEATURES

Table E.1: Group 1 - EDA Features Baseline 1

Variable	Mean	SE	Median	Min	Max	25th Percentile	50th Percentile	75th Percentile
SCL (µS)	3,2892	1,0320	3,1973	1,7488	4,7984	2,7545	3,1973	3,8347
SCR (µS)	0,0589	0,0842	0,0277	0,0101	0,2600	0,0191	0,0277	0,0449
Number of peaks	47,8750	6,9166	47,5000	34,0000	56,0000	45,7500	47,5000	53,2500
Rise time (s)	0,7025	0,1678	0,6550	0,5300	1,0400	0,6025	0,6550	0,7625
Rec.t 50% (s)	0,5700	0,1374	0,5300	0,4300	0,8500	0,4875	0,5300	0,6175
Rec.t 63% (s)	0,7075	0,1696	0,6600	0,5300	1,0500	0,6050	0,6600	0,7700
Band 2 $(\mu S)^2$	1,8061	3,9967	0,2196	0,0467	11,5802	0,0951	0,2196	0,7087
Band 2 (nu)	0,1263	0,1901	0,0350	0,0100	0,5700	0,0250	0,0350	0,1500
Band 1 $(\mu S)^2$	85,0437	146,9753	26,2142	1,9914	432,7505	7,0275	26,2142	69,4975
Band 1 (nu)	7,2475	7,0882	5,4000	0,1200	21,2200	2,0825	5,4000	10,5275
VLF $(\mu S)^2$	893,4613	641,3577	1021,5303	112,1888	1682,1262	226,2571	1021,5303	1377,1053
Total Power $(\mu S)^2$	989,0162	725,3802	1132,9178	125,2853	2039,2808	234,9387	1132,9178	1433,5291

Table E.2: Group 1 - EDA Features Baseline 2

Variable	Mean	SE	Median	Min	Max	25th Percentile	50th Percentile	75th Percentile
SCL (µS)	2,9848	1,1778	2,8531	1,4874	5,1982	2,2400	2,8531	3,5298
SCR (µS)	0,0515	0,0707	0,0117	0,0061	0,1996	0,0088	0,0117	0,0663
Number of peaks	53,0000	9,7688	55,5000	36,0000	64,0000	45,7500	55,5000	61,0000
Rise time (s)	0,6713	0,1520	0,6100	0,5300	0,9100	0,5575	0,6100	0,7550
Rec.t 50% (s)	0,5425	0,1270	0,4900	0,4300	0,7400	0,4475	0,4900	0,6100
Rec.t 63% (s)	0,6750	0,1550	0,6100	0,5400	0,9200	0,5575	0,6100	0,7575
Band 2 $(\mu S)^2$	6,4543	17,0362	0,1854	0,0246	48,5909	0,0639	0,1854	1,0312
Band 2 (nu)	0,2375	0,4776	0,0750	0,0100	1,4100	0,0175	0,0750	0,1400
Band 1 $(\mu S)^2$	214,2972	356,8060	16,6679	0,0899	972,1302	2,4388	16,6679	261,7270
Band 1 (nu)	9,2463	9,2874	7,3700	0,0500	28,2100	3,1550	7,3700	11,3975
VLF $(\mu S)^2$	1148,2186	1772,0061	250,0687	60,3249	5121,2986	170,0024	250,0687	1218,0176
Total Power $(\mu S)^2$	1429,7771	2169,3008	260,2532	63,1898	6009,9971	176,0178	260,2532	1647,0929

Table E.3: Group 1 - EDA Features Stress 1

Variable	Mean	SE	Median	Min	Max	25th Percentile	50th Percentile	75th Percentile
SCL (µS)	4,3421	1,1802	4,3372	3,0617	6,6924	3,3778	4,3372	4,7526
SCR (µS)	0,1125	0,1280	0,0564	0,0106	0,3825	0,0326	0,0564	0,1433
Number of peaks	52,3750	4,1726	52,5000	44,0000	58,0000	51,5000	52,5000	55,0000
Rise time (s)	0,8263	0,1621	0,8400	0,5900	1,0100	0,7250	0,8400	0,9475
Rec.t 50% (s)	0,6700	0,1328	0,6800	0,4700	0,8200	0,5900	0,6800	0,7725
Rec.t 63% (s)	0,8338	0,1649	0,8500	0,5900	1,0200	0,7275	0,8500	0,9575
Band 2 $(\mu S)^2$	6,9314	13,0131	1,0880	0,1261	37,1645	0,3134	1,0880	4,8726
Band 2 (nu)	0,2350	0,4143	0,0900	0,0000	1,2400	0,0275	0,0900	0,1825
Band 1 $(\mu S)^2$	148,0975	162,3756	54,0599	21,2583	448,7866	41,5835	54,0599	232,8581
Band 1 (nu)	7,7775	6,3433	5,6050	0,8700	16,0800	2,3600	5,6050	14,5150
VLF $(\mu S)^2$	2411,8345	2614,2274	1773,9867	366,9861	8288,1823	589,1765	1773,9867	2753,5517
Total Power $(\mu S)^2$	2578,7961	2663,9292	1992,1162	435,2971	8509,7223	632,9884	1992,1162	3136,9465

Table E.4: Group 1 - EDA Features Stress 2

Variable	Mean	SE	Median	Min	Max	25th Percentile	50th Percentile	75th Percentile
SCL (µS)	4,3644	1,6237	4,2814	2,0371	6,8152	3,1327	4,2814	5,5409
SCR (µS)	0,0965	0,0844	0,0851	0,0085	0,2395	0,0222	0,0851	0,1576
Number of peaks	48,1250	6,7493	47,5000	36,0000	60,0000	46,5000	47,5000	50,5000
Rise time (s)	0,8363	0,1868	0,9050	0,5600	1,0100	0,7175	0,9050	0,9900
Rec.t 50% (s)	0,6800	0,1518	0,7350	0,4500	0,8200	0,5875	0,7350	0,8025
Rec.t 63% (s)	0,8438	0,1878	0,9150	0,5600	1,0200	0,7275	0,9150	0,9925
Band 2 $(\mu S)^2$	6,4658	10,2412	1,8363	0,0372	27,7648	0,4247	1,8363	6,3403
Band 2 (nu)	0,9488	1,2376	0,3150	0,0100	3,5300	0,1400	0,3150	1,5500
Band 1 $(\mu S)^2$	110,2360	128,3767	49,7732	4,2447	331,5710	16,5271	49,7732	172,7693
Band 1 (nu)	16,8000	13,1851	13,9500	1,0000	35,5700	6,6525	13,9500	27,5250
VLF $(\mu S)^2$	454,5952	317,5892	359,4525	79,2185	971,2627	275,1952	359,4525	574,8295
Total Power $(\mu S)^2$	584,1263	432,7657	398,4556	124,1221	1287,1544	291,3705	398,4556	872,5420

Table E.5: Group 1 - EDA Features Baseline - Stress

Variables	Baseline 1		Baseline 2		Stress 1		Stress 2	
	Mean	SE	Mean	SE	Mean	SE	Mean	SE
SCL (µS)	3,2892	1,0320	2,9848	1,1778	4,3421	1,1802	4,3644	1,6237
SCR (µS)	0,0589	0,0842	0,0515	0,0707	0,1125	0,1280	0,0965	0,0844
Number of peaks	47,8750	6,9166	53,0000	9,7688	52,3750	4,1726	48,1250	6,7493
Rise time (s)	0,7025	0,1678	0,6713	0,1520	0,8263	0,1621	0,8363	0,1868
Rec.t 50% (s)	0,5700	0,1374	0,5425	0,1270	0,6700	0,1328	0,6800	0,1518
Rec.t 63% (s)	0,7075	0,1696	0,6750	0,1550	0,8338	0,1649	0,8438	0,1878
Band 2 $(\mu S)^2$	1,8061	3,9967	6,4543	17,0362	6,9314	13,0131	6,4658	10,2412
Band 2 (nu)	0,1263	0,1901	0,2375	0,4776	0,2350	0,4143	0,9488	1,2376
Band 1 $(\mu S)^2$	85,0437	146,9753	214,2972	356,8060	148,0975	162,3756	110,2360	128,3767
Band 1 (nu)	7,2475	7,0882	9,2463	9,2874	7,7775	6,3433	16,8000	13,1851
VLF $(\mu S)^2$	893,4613	641,3577	1148,2186	1772,0061	2411,8345	2614,2274	454,5952	317,5892
Total Power $(\mu S)^2$	989,0162	725,3802	1429,7771	2169,3008	2578,7961	2663,9292	584,1263	432,7657

APPENDIX F - GROUP 2 EDA FEATURES

Table F.1: Group 2 - EDA Features Baseline 1

Variable	Mean	SE	Median	Min	Max	25th Percentile	50th Percentile	75th Percentile
SCL (µS)	3,1460	1,3679	3,2459	1,3990	5,2439	2,0825	3,2459	3,9843
SCR (µS)	0,0216	0,0119	0,0191	0,0089	0,0399	0,0117	0,0191	0,0299
Number of peaks	54,2857	6,6762	53,0000	46,0000	65,0000	49,5000	53,0000	58,5000
Rise time (s)	0,6314	0,0793	0,6300	0,5300	0,7300	0,5700	0,6300	0,6950
Rec.t 50% (s)	0,5114	0,0657	0,5100	0,4300	0,5900	0,4600	0,5100	0,5650
Rec.t 63% (s)	0,6371	0,0840	0,6400	0,5300	0,7400	0,5700	0,6400	0,7050
Band 2 $(\mu S)^2$	0,1935	0,1976	0,1288	0,0361	0,6177	0,0880	0,1288	0,1979
Band 2 (nu)	0,0386	0,0254	0,0300	0,0100	0,0800	0,0200	0,0300	0,0550
Band 1 $(\mu S)^2$	24,9496	25,3755	14,3019	5,0991	75,7597	7,3692	14,3019	32,3741
Band 1 (nu)	5,7014	4,9219	4,1800	1,0500	15,7500	2,7950	4,1800	6,6700
VLF $(\mu S)^2$	530,3035	513,8993	204,6912	148,0557	1424,1242	189,2500	204,6912	778,3769
Total Power $(\mu S)^2$	561,7810	532,7340	234,0846	154,4603	1454,3388	211,9408	234,0846	832,8510

Table F.2: Group 2 - EDA Features Baseline 2

Variable	Mean	SE	Median	Min	Max	25th Percentile	50th Percentile	75th Percentile
SCL (µS)	2,4544	1,1778	2,2590	1,1200	4,1457	1,5925	2,2590	3,2355
SCR (µS)	0,0139	0,0086	0,0134	0,0070	0,0309	0,0071	0,0134	0,0159
Number of peaks	58,7143	6,1837	60,0000	50,0000	67,0000	54,0000	60,0000	63,0000
Rise time (s)	0,5886	0,0696	0,5900	0,5200	0,7100	0,5300	0,5900	0,6200
Rec.t 50% (s)	0,4771	0,0579	0,4800	0,4200	0,5800	0,4300	0,4800	0,5000
Rec.t 63% (s)	0,5929	0,0697	0,5900	0,5300	0,7200	0,5350	0,5900	0,6200
Band 2 $(\mu S)^2$	0,1453	0,1577	0,1082	0,0115	0,4459	0,0249	0,1082	0,2009
Band 2 (nu)	0,0771	0,1072	0,0300	0,0100	0,3000	0,0100	0,0300	0,0900
Band 1 $(\mu S)^2$	27,0070	24,8423	29,0225	0,9294	59,6842	2,9091	29,0225	46,7974
Band 1 (nu)	10,9643	11,6783	5,0400	1,0500	31,3900	1,8300	5,0400	17,8050
VLF $(\mu S)^2$	267,2126	284,4171	126,1465	41,0887	851,1913	103,1183	126,1465	322,9126
Total Power $(\mu S)^2$	300,0222	294,6788	190,1358	42,2526	906,6900	125,1020	190,1358	355,4366

Table F.3: Group 2 - EDA Features Stress 1

Variable	Mean	SE	Median	Min	Max	25th Percentile	50th Percentile	75th Percentile
SCL (µS)	3,7687	1,5266	4,1615	1,8323	5,5238	2,4362	4,1615	4,9956
SCR (µS)	0,0666	0,0561	0,0416	0,0151	0,1503	0,0339	0,0416	0,0959
Number of peaks	55,0000	6,1644	56,0000	45,0000	63,0000	51,5000	56,0000	59,0000
Rise time (s)	0,7986	0,1529	0,8000	0,6000	1,0900	0,7200	0,8000	0,8300
Rec.t 50% (s)	0,6471	0,1241	0,6500	0,4800	0,8800	0,5850	0,6500	0,6750
Rec.t 63% (s)	0,8071	0,1551	0,8100	0,6000	1,1000	0,7300	0,8100	0,8400
Band 2 $(\mu S)^2$	2,3663	3,7677	0,5642	0,1315	10,2737	0,3606	0,5642	2,4369
Band 2 (nu)	0,1586	0,1958	0,0700	0,0100	0,5800	0,0650	0,0700	0,1600
Band 1 $(\mu S)^2$	81,3551	79,4476	48,6134	4,7355	217,9908	28,5554	48,6134	120,5176
Band 1 (nu)	10,3286	15,1559	3,2700	1,4400	42,7500	2,5750	3,2700	9,8450
VLF $(\mu S)^2$	1934,7960	2305,2131	900,1810	59,5796	5675,2445	300,0805	900,1810	3154,2030
Total Power $(\mu S)^2$	2040,6980	2415,6717	916,1279	113,7103	6026,4462	348,2005	916,1279	3266,1002

Table F.4: Group 2 - EDA Features Stress 2

Variable	Mean	SE	Median	Min	Max	25th Percentile	50th Percentile	75th Percentile
SCL (µS)	3,0249	1,5231	2,8570	1,1279	4,9896	1,8250	2,8570	4,2750
SCR (µS)	0,0788	0,0991	0,0346	0,0098	0,2908	0,0213	0,0346	0,0868
Number of peaks	58,7143	12,4461	53,0000	47,0000	80,0000	49,5000	53,0000	66,0000
Rise time (s)	0,7114	0,1676	0,6900	0,5500	0,9500	0,5600	0,6900	0,8350
Rec.t 50% (s)	0,5757	0,1362	0,5600	0,4400	0,7700	0,4550	0,5600	0,6750
Rec.t 63% (s)	0,7157	0,1682	0,7000	0,5500	0,9600	0,5650	0,7000	0,8350
Band 2 $(\mu S)^2$	15,2685	36,4489	0,4660	0,0554	97,7843	0,2859	0,4660	4,0011
Band 2 (nu)	0,5057	0,8129	0,1600	0,0600	2,3200	0,1050	0,1600	0,3950
Band 1 $(\mu S)^2$	945,5735	2313,1649	69,4227	3,9810	6189,3401	36,2037	69,4227	141,9318
Band 1 (nu)	19,7214	8,1362	22,8400	6,7800	29,1900	14,1350	22,8400	25,4850
VLF $(\mu S)^2$	2251,6095	5248,8256	209,0078	54,2928	14146,6983	146,3673	209,0078	529,2665
Total Power $(\mu S)^2$	3334,9408	7884,7586	264,8167	58,7455	21205,9638	207,8546	264,8167	699,6751

Table F.5: Group 2 - EDA Features Baseline-Stress

Variables	Baseline 1		Baseline 2		Stress 1		Stress 2	
	Mean	SE	Mean	SE	Mean	SE	Mean	SE
SCL (µS)	3,1460	1,3679	2,4544	1,1778	3,7687	1,5266	3,0249	1,5231
SCR (µS)	0,0216	0,0119	0,0139	0,0086	0,0666	0,0561	0,0788	0,0991
Number of peaks	54,2857	6,6762	58,7143	6,1837	55,0000	6,1644	58,7143	12,4461
Rise time (s)	0,6314	0,0793	0,5886	0,0696	0,7986	0,1529	0,7114	0,1676
Rec.t 50% (s)	0,5114	0,0657	0,4771	0,0579	0,6471	0,1241	0,5757	0,1362
Rec.t 63% (s)	0,6371	0,0840	0,5929	0,0697	0,8071	0,1551	0,7157	0,1682
Band 2 $(\mu S)^2$	0,1935	0,1976	0,1453	0,1577	2,3663	3,7677	15,2685	36,4489
Band 2 (nu)	0,0386	0,0254	0,0771	0,1072	0,1586	0,1958	0,5057	0,8129
Band 1 $(\mu S)^2$	24,9496	25,3755	27,0070	24,8423	81,3551	79,4476	945,5735	2313,1649
Band 1 (nu)	5,7014	4,9219	10,9643	11,6783	10,3286	15,1559	19,7214	8,1362
VLF $(\mu S)^2$	530,3035	513,8993	267,2126	284,4171	1934,7960	2305,2131	2251,6095	5248,8256
Total Power $(\mu S)^2$	561,7810	532,7340	300,0222	294,6788	2040,6980	2415,6717	3334,9408	7884,7586

APPENDIX G - EDA FEATURES KRUSKAL-WALLIS TEST

Table G.1: EDA Kruskal-Wallis test

Variable	B1-B2		B1-S1		B1-S2		B2-S1		B2-S2		S1-S2	
	H-value	p-value	H-value	p-value	H-value	p-value	H-value	p-value	H-value	p-value	H-value	p-value
SCL (µS)	1,4972	0,2211	2,9630	0,0852	0,6542	0,4186	6,5071	0,0107*	3,1075	0,0779	0,2275	0,6334
SCR (µS)	2,6849	0,1013	6,2972	0,0121*	2,5501	0,1103	8,7972	0,0030*	5,4933	0,0191*	0,0968	0,7557
Number of peaks	3,0436	0,0811	1,1245	0,2890	0,0277	0,8678	1,5042	0,2200	1,4537	0,2279	0,9168	0,3383
Rise time (s)	1,1270	0,2884	7,1686	0,0074*	2,6933	0,1008	10,4951	0,0012*	4,8510	0,0276*	0,4411	0,5066
Rec.t 50% (s)	1,3101	0,2524	6,9465	0,0084*	2,6220	0,1054	10,3587	0,0013*	4,9375	0,0263*	0,3876	0,5336
Rec.t 63% (s)	1,0371	0,3085	7,0579	0,0079*	2,6214	0,1054	10,6254	0,0011*	5,0313	0,0249*	0,4410	0,5066
Band 2 $(\mu S)^2$	0,5269	0,4679	6,4031	0,0114*	4,7419	0,0294*	6,7204	0,0095*	5,8877	0,0152*	0,0348	0,8519
Band 2 (nu)	0,0040	0,9498	2,5655	0,1092	8,4678	0,0036*	0,8788	0,3485	6,9948	0,0082*	3,7241	0,0536
Band 1 $(\mu S)^2$	0,0968	0,7557	4,9243	0,0265*	3,4069	0,0649	3,1075	0,0779	2,6843	0,1013	0,0968	0,7557
Band 1 (nu)	0,2908	0,5897	0,0521	0,8195	9,0430	0,0026*	0,0968	0,7557	3,7200	0,0538	5,4933	0,0191*
VLF $(\mu S)^2$	2,1682	0,1409	3,4069	0,0649	0,8710	0,3507	6,7204	0,0095*	0,7230	0,3952	5,1101	0,0238*
Total Power $(\mu S)^2$	1,7071	0,1914	3,4069	0,0649	0,2275	0,6334	6,9372	0,0084*	0,9501	0,3297	4,7419	0,0294*

* *p-value<0.05*

APPENDIX H - EDA GROUPS KRUSKAL-WALLIS TEST

Table H.1: EDA Group 1 Kruskal-Wallis test

Variable	B1-B2		B1-S1		B1-S2		B2-S1		B2-S2		S1-S2	
	H-value	p-value	H-value	p-value	H-value	p-value	H-value	p-value	H-value	p-value	H-value	p-value
SCL (µS)	0,3971	0,5286	2,8235	0,0929	2,4816	0,1152	3,9816	0,0460*	3,1875	0,0742	0,0110	0,9164
SCR (µS)	0,7059	0,4008	2,1618	0,1415	0,7059	0,4008	2,8235	0,0929	1,5882	0,2076	0,0441	0,8336
Number of peaks	1,4673	0,2258	1,4651	0,2261	0,0000	1,0000	0,3988	0,5277	1,1095	0,2922	2,6774	0,1018
Rise time (s)	0,1357	0,7126	2,1681	0,1409	1,8695	0,1715	4,6556	0,0310*	3,4078	0,0649	0,0028	0,9580
Rec.t 50% (s)	0,2243	0,6358	2,1649	0,1412	1,7259	0,1889	4,6488	0,0311*	3,3827	0,0659	0,0028	0,9580
Rec.t 63% (s)	0,1770	0,6740	2,0160	0,1556	1,7259	0,1889	4,6488	0,0311*	3,5841	0,0583	0,0028	0,9581
Band 2 (µS)²	0,0993	0,7527	2,4816	0,1152	1,1029	0,2936	2,1618	0,1415	1,3346	0,2480	0,0441	0,8336
Band 2 (nu)	0,0028	0,9577	0,1778	0,6733	2,6734	0,1020	0,0249	0,8746	3,0250	0,0820	2,0131	0,1559
Band 1 (µS)²	0,0110	0,9164	2,1618	0,1415	0,7059	0,4008	1,3346	0,2480	0,3971	0,5286	0,7059	0,4008
Band 1 (nu)	0,0110	0,9164	0,0442	0,8335	2,1618	0,1415	0,0442	0,8335	1,3346	0,2480	1,8667	0,1719
VLF (µS)²	0,3971	0,5286	2,8235	0,0929	1,3346	0,2480	3,1875	0,0742	0,1765	0,6744	5,8346	0,0157*
Total Power (µS)²	0,2757	0,5995	2,8235	0,0929	0,8934	0,3446	2,8235	0,0929	0,1765	0,6744	5,8346	0,0157*

*p-value<0.05

Table H.2: EDA Group 2 Kruskal-Wallis test

Variable	B1-B2		B1-S1		B1-S2		B2-S1		B2-S2		S1-S2	
	H-value	p-value	H-value	p-value	H-value	p-value	H-value	p-value	H-value	p-value	H-value	p-value
SCL (µS)	1,1796	0,2774	0,9184	0,3379	0,0367	0,8480	2,9755	0,0845	1,1796	0,2774	0,6898	0,4062
SCR (µS)	2,1639	0,1413	5,0000	0,0253*	2,5510	0,1102	7,5636	0,0060*	4,4547	0,0348*	0,2000	0,6547
Number of peaks	1,8119	0,1783	0,0657	0,7976	0,2624	0,6085	1,0612	0,3029	0,1489	0,6996	0,1027	0,7486
Rise time (s)	1,3371	0,2475	5,5878	0,0181*	0,6959	0,4042	7,2318	0,0072*	2,1687	0,1408	1,1822	0,2769
Rec.t 50% (s)	1,5032	0,2202	5,3132	0,0212*	0,8035	0,3700	6,9375	0,0084*	2,1687	0,1408	1,1796	0,2774
Rec.t 63% (s)	1,1954	0,2743	5,5878	0,0181*	0,8018	0,3706	7,2318	0,0072*	2,1639	0,1413	1,1796	0,2774
Band 2 $(\mu S)^2$	0,4939	0,4822	4,4449	0,0350*	4,4449	0,0350*	6,2082	0,0127*	5,0000	0,0253*	0,0041	0,9491
Band 2 (nu)	0,0168	0,8969	3,4631	0,0628	8,6749	0,0032*	1,6731	0,1958	5,0443	0,0247*	1,6399	0,2003
Band 1 $(\mu S)^2$	0,0367	0,8480	2,1592	0,1417	2,9755	0,0845	2,5510	0,1102	2,9755	0,0845	0,0041	0,9491
Band 1 (nu)	0,2618	0,6089	0,0367	0,8480	6,8612	0,0088*	0,0041	0,9491	2,1592	0,1417	3,4327	0,0639
VLF $(\mu S)^2$	2,1592	0,1417	0,6898	0,4062	0,2000	0,6547	3,4327	0,0639	0,6898	0,4062	0,9184	0,3379
Total Power $(\mu S)^2$	1,8000	0,1797	0,9184	0,3379	0,0041	0,9491	3,9224	0,0476*	0,6898	0,4062	0,6898	0,4062

*$p\text{-value}<0.05$

APPENDIX I - HRV RANDOM FOREST CLASSIFIER

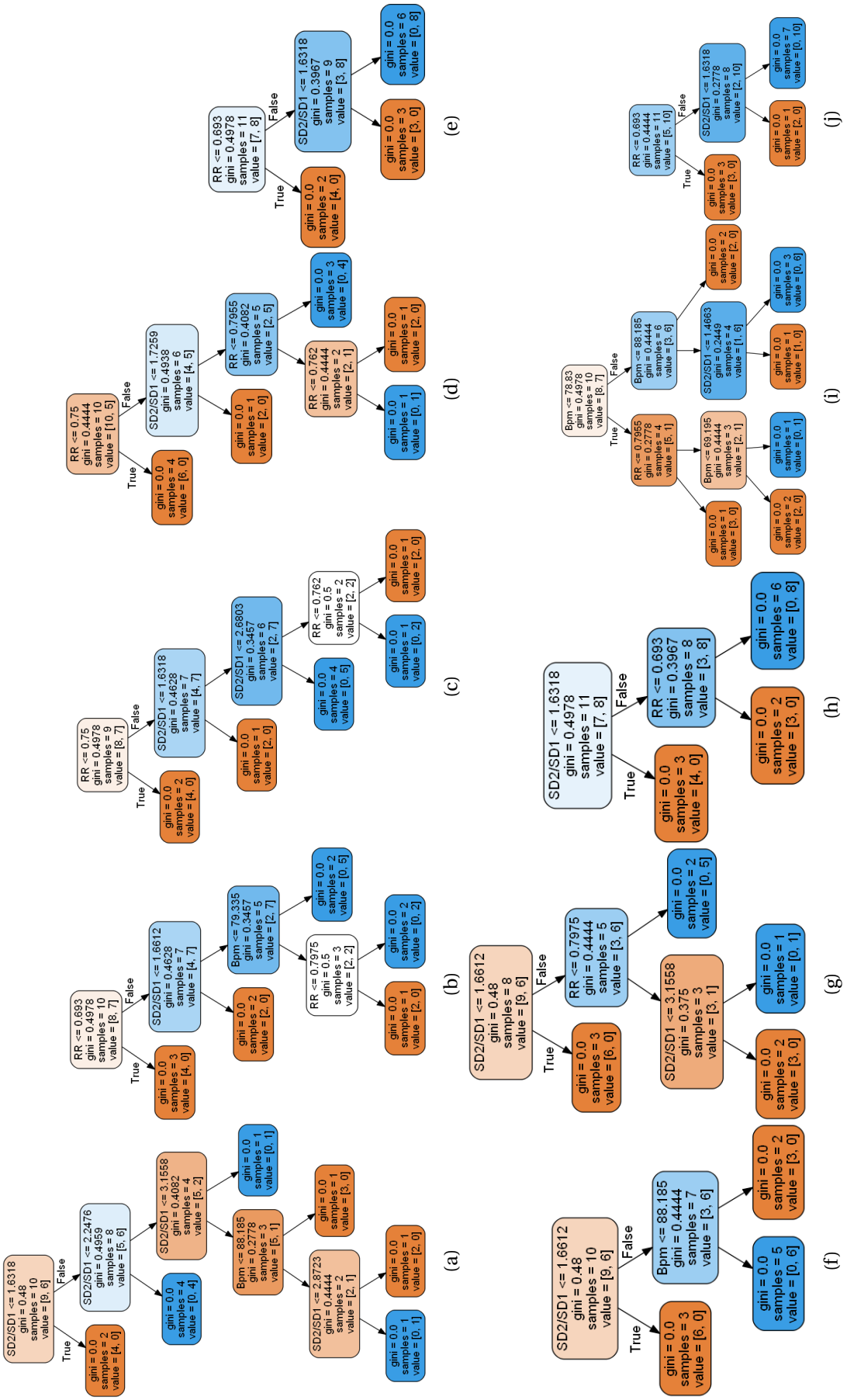
SD2/SD1 <= 1.6318
gini = 0.48
samples = 10
value = [9, 6]
True
False
gini = 0.0
samples = 2
value = [4, 0]
SD2/SD1 <= 2.2476
gini = 0.4959
samples = 8
value = [5, 6]
gini = 0.0
samples = 4
value = [0, 4]
SD2/SD1 <= 3.1558
gini = 0.4082
samples = 4
value = [5, 2]
Bpm <= 88.185
gini = 0.2778
samples = 3
value = [5, 1]
gini = 0.0
samples = 1
value = [0, 1]
SD2/SD1 <= 2.8723
gini = 0.4444
samples = 2
value = [2, 1]
gini = 0.0
samples = 1
value = [3, 0]
gini = 0.0
samples = 1
value = [0, 1]
gini = 0.0
samples = 1
value = [2, 0]
(a)
RR <= 0.693
gini = 0.4978
samples = 10
value = [8, 7]
True
False
gini = 0.0
samples = 3
value = [4, 0]
SD2/SD1 <= 1.6612
gini = 0.4628
samples = 7
value = [4, 7]
gini = 0.0
samples = 2
value = [2, 0]
Bpm <= 79.335
gini = 0.3457
samples = 5
value = [2, 7]
RR <= 0.7975
gini = 0.5
samples = 3
value = [2, 2]
gini = 0.0
samples = 2
value = [0, 5]
gini = 0.0
samples = 1
value = [2, 0]
gini = 0.0
samples = 2
value = [0, 2]
(b)
RR <= 0.75
gini = 0.4978
samples = 9
value = [8, 7]
True
False
gini = 0.0
samples = 2
value = [4, 0]
SD2/SD1 <= 1.6318
gini = 0.4628
samples = 7
value = [4, 7]
gini = 0.0
samples = 1
value = [2, 0]
SD2/SD1 <= 2.6803
gini = 0.3457
samples = 6
value = [2, 7]
gini = 0.0
samples = 4
value = [0, 5]
RR <= 0.762
gini = 0.5
samples = 2
value = [2, 2]
gini = 0.0
samples = 1
value = [0, 2]
gini = 0.0
samples = 1
value = [2, 0]
(c)
RR <= 0.75
gini = 0.4444
samples = 10
value = [10, 5]
True
False
gini = 0.0
samples = 4
value = [6, 0]
SD2/SD1 <= 1.7259
gini = 0.4938
samples = 6
value = [4, 5]
gini = 0.0
samples = 1
value = [2, 0]
RR <= 0.7955
gini = 0.4082
samples = 5
value = [2, 5]
RR <= 0.762
gini = 0.4444
samples = 2
value = [2, 1]
gini = 0.0
samples = 3
value = [0, 4]
gini = 0.0
samples = 1
value = [0, 1]
gini = 0.0
samples = 1
value = [2, 0]
(d)
RR <= 0.693
gini = 0.4978
samples = 11
value = [7, 8]
True
False
gini = 0.0
samples = 2
value = [4, 0]
SD2/SD1 <= 1.6318
gini = 0.3967
samples = 9
value = [3, 8]
gini = 0.0
samples = 3
value = [3, 0]
gini = 0.0
samples = 6
value = [0, 8]
(e)
SD2/SD1 <= 1.6612
gini = 0.48
samples = 10
value = [9, 6]
True
False
gini = 0.0
samples = 5
value = [0, 6]
Bpm <= 88.185
gini = 0.4444
samples = 7
value = [3, 6]
gini = 0.0
samples = 2
value = [3, 0]
gini = 0.0
samples = 5
value = [0, 6]
(f)
SD2/SD1 <= 1.6612
gini = 0.48
samples = 8
value = [9, 6]
True
False
gini = 0.0
samples = 3
value = [6, 0]
RR <= 0.7975
gini = 0.4444
samples = 5
value = [3, 6]
SD2/SD1 <= 3.1558
gini = 0.375
samples = 3
value = [3, 1]
gini = 0.0
samples = 2
value = [0, 5]
gini = 0.0
samples = 1
value = [0, 1]
gini = 0.0
samples = 2
value = [3, 0]
(g)
SD2/SD1 <= 1.6318
gini = 0.4978
samples = 11
value = [7, 8]
True
False
gini = 0.0
samples = 3
value = [4, 0]
RR <= 0.693
gini = 0.3967
samples = 8
value = [3, 8]
gini = 0.0
samples = 2
value = [3, 0]
gini = 0.0
samples = 6
value = [0, 8]
(h)
Bpm <= 78.83
gini = 0.4978
samples = 10
value = [8, 7]
True
False
RR <= 0.7955
gini = 0.2778
samples = 4
value = [5, 1]
Bpm <= 88.185
gini = 0.4444
samples = 6
value = [3, 6]
gini = 0.0
samples = 1
value = [3, 0]
Bpm <= 69.195
gini = 0.4444
samples = 3
value = [2, 1]
SD2/SD1 <= 1.4663
gini = 0.2449
samples = 4
value = [1, 6]
gini = 0.0
samples = 1
value = [0, 1]
gini = 0.0
samples = 2
value = [2, 0]
gini = 0.0
samples = 1
value = [0, 1]
gini = 0.0
samples = 3
value = [0, 6]
gini = 0.0
samples = 2
value = [2, 0]
(i)
RR <= 0.693
gini = 0.4444
samples = 11
value = [5, 10]
True
False
gini = 0.0
samples = 3
value = [3, 0]
SD2/SD1 <= 1.6318
gini = 0.2778
samples = 8
value = [2, 10]
gini = 0.0
samples = 1
value = [2, 0]
gini = 0.0
samples = 7
value = [0, 10]
(j)

APPENDIX J - HRV AND EDA RANDOM FOREST CLASSIFIER

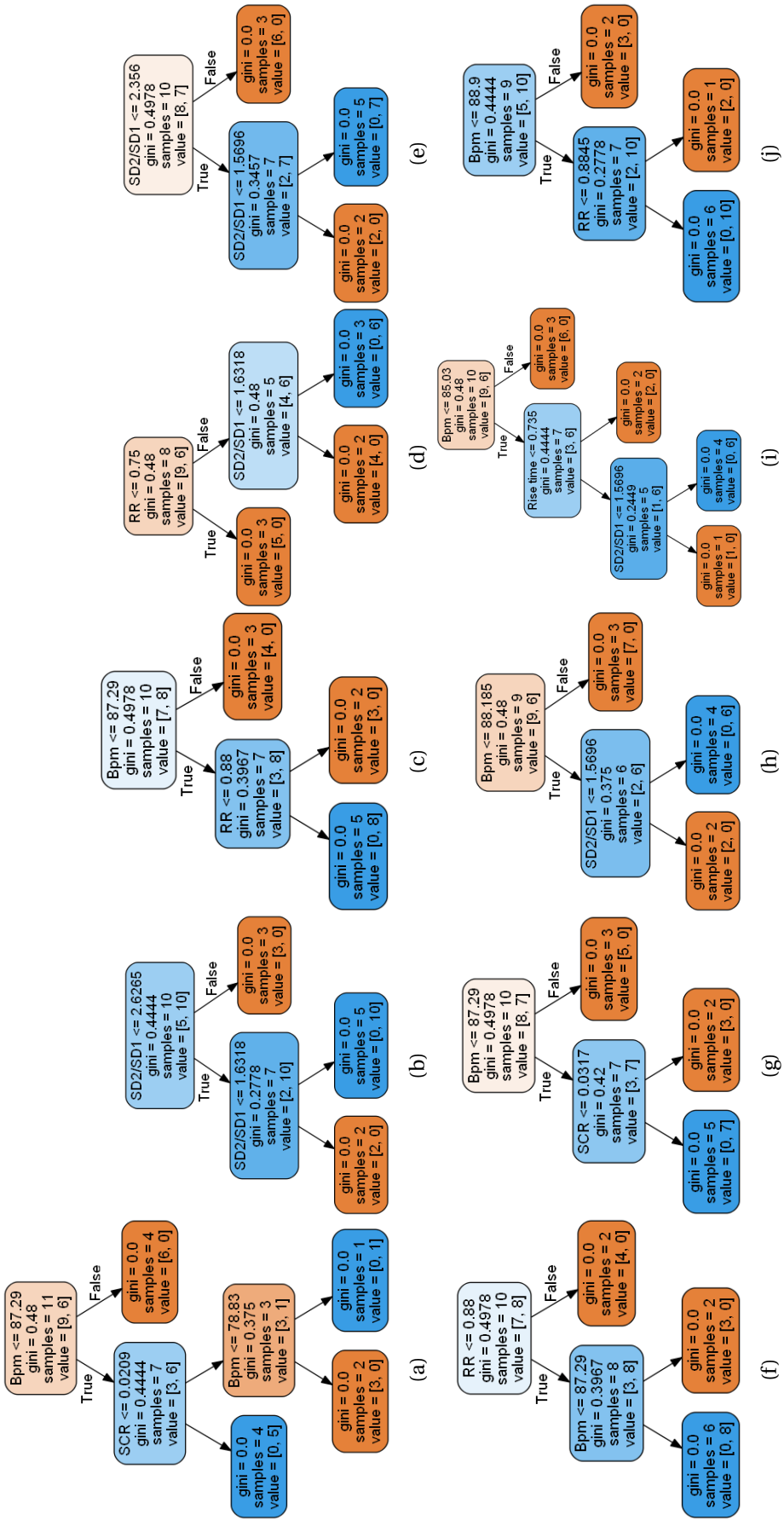
Bpm <= 87.29
gini = 0.48
samples = 11
value = [9, 6]
True
False
SCR <= 0.0209
gini = 0.4444
samples = 7
value = [3, 6]
gini = 0.0
samples = 4
value = [6, 0]
gini = 0.0
samples = 4
value = [0, 5]
Bpm <= 78.83
gini = 0.375
samples = 3
value = [3, 1]
gini = 0.0
samples = 1
value = [0, 1]
gini = 0.0
samples = 2
value = [3, 0]
(a)
SD2/SD1 <= 2.6265
gini = 0.4444
samples = 10
value = [5, 10]
gini = 0.0
samples = 3
value = [3, 0]
SD2/SD1 <= 1.6318
gini = 0.2778
samples = 7
value = [2, 10]
gini = 0.0
samples = 5
value = [0, 10]
gini = 0.0
samples = 2
value = [2, 0]
(b)
Bpm <= 87.29
gini = 0.4978
samples = 10
value = [7, 8]
gini = 0.0
samples = 3
value = [4, 0]
RR <= 0.88
gini = 0.3967
samples = 7
value = [3, 8]
gini = 0.0
samples = 2
value = [3, 0]
gini = 0.0
samples = 5
value = [0, 8]
(c)
RR <= 0.75
gini = 0.48
samples = 8
value = [9, 6]
gini = 0.0
samples = 3
value = [5, 0]
SD2/SD1 <= 1.6318
gini = 0.48
samples = 5
value = [4, 6]
gini = 0.0
samples = 3
value = [0, 6]
gini = 0.0
samples = 2
value = [4, 0]
(d)
SD2/SD1 <= 2.356
gini = 0.4978
samples = 10
value = [8, 7]
gini = 0.0
samples = 3
value = [6, 0]
SD2/SD1 <= 1.5696
gini = 0.3457
samples = 7
value = [2, 7]
gini = 0.0
samples = 5
value = [0, 7]
gini = 0.0
samples = 2
value = [2, 0]
(e)
RR <= 0.88
gini = 0.4978
samples = 10
value = [7, 8]
gini = 0.0
samples = 2
value = [4, 0]
Bpm <= 87.29
gini = 0.3967
samples = 8
value = [3, 8]
gini = 0.0
samples = 2
value = [3, 0]
gini = 0.0
samples = 6
value = [0, 8]
(f)
Bpm <= 87.29
gini = 0.4978
samples = 10
value = [8, 7]
gini = 0.0
samples = 3
value = [5, 0]
SCR <= 0.0317
gini = 0.42
samples = 7
value = [3, 7]
gini = 0.0
samples = 2
value = [3, 0]
gini = 0.0
samples = 5
value = [0, 7]
(g)
Bpm <= 88.185
gini = 0.48
samples = 9
value = [9, 6]
gini = 0.0
samples = 3
value = [7, 0]
SD2/SD1 <= 1.5696
gini = 0.375
samples = 6
value = [2, 6]
gini = 0.0
samples = 4
value = [0, 6]
gini = 0.0
samples = 2
value = [2, 0]
(h)
Bpm <= 85.03
gini = 0.48
samples = 10
value = [9, 6]
gini = 0.0
samples = 3
value = [6, 0]
Rise time <= 0.735
gini = 0.4444
samples = 7
value = [3, 6]
gini = 0.0
samples = 2
value = [2, 0]
SD2/SD1 <= 1.5696
gini = 0.2449
samples = 5
value = [1, 6]
gini = 0.0
samples = 4
value = [0, 6]
gini = 0.0
samples = 1
value = [1, 0]
(i)
Bpm <= 88.9
gini = 0.4444
samples = 9
value = [5, 10]
gini = 0.0
samples = 2
value = [3, 0]
RR <= 0.8845
gini = 0.2778
samples = 7
value = [2, 10]
gini = 0.0
samples = 1
value = [2, 0]
gini = 0.0
samples = 6
value = [0, 10]
(j)

ANNEX I

ANNEX 1 - PUBLICATION

Heart Rate Variability and Electrodermal Activity in Mental Stress Aloud: Predicting the Outcome

Rodrigo Lima[1,2], Daniel Osório[1,3] and Hugo Gamboa[1,2,3]

[1]*Plux-Wireless Biosignals S.A, Avenida 5 de Outubro 70, 1050-59, Lisboa, Portugal*

[2]*Department of Physics, Faculdade de Ciências e Tecnologia da Universidade Nova de Lisboa, Monte de Caparica, 2892-516, Caparica, Portugal*

[3] *Laboratório de Instrumentação, Engenharia Biomédica e Física da Radiação (LIBPhys-UNL), Faculdade de Ciências e Tecnologia da Universidade Nova de Lisboa, Monte de Caparica, 2892-516, Caparica, Portugal*

Keywords: Heart Rate Variability, Electrodermal Activity, Photoplethysmography, Autonomous Nervous System, Wearable Device, Biosignals, Machine-Learning, Classification.

Abstract: The assessment of changes in the autonomous nervous system (ANS), have important prognostic and diagnostic value, and can be used to assess stress levels. There are many approaches to directly measure the sympathetic and parasympathetic nervous system, although, most of them are invasive and unable to provide continuous monitoring. Heart rate variability (HRV) and Electrodermal activity (EDA) are noninvasive methods to assess the autonomous nervous system, by computing the spectral analysis of both HRV and EDA biosignals. In order to provide continuous monitoring, a wearable device is used, obtaining HRV features with photoplethysmography signals from the wrist and EDA from the fingers. The extraction of the HRV and EDA features, were obtained by submitting the subjects to a mental arithmetic stress test. The distinct response to stress was then classified using machine-learning techniques. The constructed models have the ability to predict how the subjects will respond, with an accuracy of approximately 80% in terms of HRV features in baseline and an accuracy of approximately 77% in terms of HRV and EDA simultaneous baseline features, when submitted to a situation of stress.

1 INTRODUCTION

The assessment of the changes in the autonomous nervous system (ANS) activity related with certain diseases and pathologies, such as myocardial infarction, cardiac transplantation, myocardial dysfunction, diabetic neuropathy and depression, has been demonstrated to have important prognostic and diagnostic value (Posada-Quintero et al., 2016a).

In recent times, cardiovascular research has played an important role in studying the activity of the ANS, so delineating the role of autonomous cardiac reactivity is important to prevent these serious health diseases (Posada-Quintero et al., 2016a).

The ANS is regulated by the central autonomous network in the brain, comprised of multiple neuroanatomical structures. These brain related structures influence heart activity, responding and adapting to environmental challenges, through the adjustment of physiological arousal by transmitting output to the sinoatrial node of the heart (Hamilton and Alloy, 2016).

The autonomous signals are transmitted to the body through two branches of the ANS: the sympathetic nervous system (SNS) and the parasympathetic nervous system (PNS). The sympathetic and parasympathetic nerve fibers secrete two synaptic transmitter substances: acetylcholine and epinephrine. The terminal nerve endings of the PNS secrete acetylcholine, also called cholinergic fibers, thus its influence on heart rate is mediated via release of acetylcholine by the vagus nerve, decreasing the strength of contraction and consequent heart rate (Hamilton and Alloy, 2016). The terminal endings of the SNS secrete epinephrine, also called adrenergic fibers, a term derived from adrenalin, thus its influence on the heart is mediated via release of epinephrine, increasing the force of contraction and consequent heart rate (Guyton and Hall, 2011). In a situation of stress, usually, vagal activity withdrawals, decreasing the control and influence on the heart by the vagus nerve, facilitating the activation of the SNS, with excitatory influences to the heart.

There are many approaches to directly measure the PNS and SNS activity, although, most of them are invasive and unable to provide continuous monitor-

ing, leading to an inaccurate assessment of the ANS dynamics (Posada-quintero and Hall, 2016). A non-invasive method to assess the ANS activity, is to compute the power spectral analysis of Heart Rate Variability (HRV) (Posada-Quintero et al., 2016a; Posada-Quintero et al., 2016b; Bansal et al., 2009).

HRV is a measure of the time series of beat-to-beat intervals from an electrocardiogram (ECG) between consecutive heart beats (Zoltan, 2013). HRV can also be computed by acquiring photoplethysmography (PPG) signals.

PPG is an optical measurement technique, used to detect blood volume changes in the microvascular bed of tissue, with widespread clinical application, such as ambulatory patient monitoring (Allen, 2007; Bolanos et al., 2006). PPG signals are a source of HRV information due to the synchronization between heart beats in the ECG and the systolic peak in the PPG waveform.

In order to monitor the effects of neural mechanisms to the heart, the spectral analysis of HRV has been performed to asses the level of unbalance of the ANS. The PNS is a major contributor to the high frequency (HF) component (0.15-0.4 Hz), while the low frequency (LF) component (0.04-0.15 Hz) is considered to be a marker of the sympathetic modulation, despite being influenced by both the PNS and the SNS (Zoltan, 2013; Bussmann, 1998; Miranda Dantas et al., 2012). The ratio LF/HF reflects the balance between the sympathetic and parasympathetic activity, so it has not been fully accepted as an accurate measure of the ANS, since the LF component is also influenced by the parasympathetic system (Posada-Quintero et al., 2016a).

Electrodermal Activity (EDA) is an alternative method to directly assess the SNS (Kleckner et al., 2017). The human skin is innervated by numerous efferent fibers, including sympathetic fibers, such as eccrine sweat glands, which produce sweat when the acetylcholine transmitter passes from sudomotor fibers to these glands, changing the skin's electrical characteristics (Boucsein, 2012). Eccrine glands are mostly involved in emotional responses to external stimulus and reflect only activity from the SNS, because there is no innervation of the PNS in these glands (Posada-quintero et al., 2016).

EDA signals can be divided into two different components: phasic component (SCR - Skin Conductance Response) and the tonic component (SCL - Skin Conductance Level) (Gamboa and Fred, 2008). The phasic component is the result of the activation of the SNS, after a stimuli presentation, being usually overlapped by the tonic component, which is not directly related to an external stimuli, because it is a slow changing signal (Benedek and Kaernbach, 2010).

To establish a connection between both techniques, each subject was submitted to a mental arithmetic stress test, the Paced Visual Serial Addition Test (PVSAT). The PVSAT is the visual version of the PASAT, a test where the participants are presented with a series of digits that must be summed in a narrow time interval. The participants must respond aloud the correct answer, prior to the presentation of the next digit (Tombaugh, 2006; Royan et al., 2004; Parsons and Courtney, 2014), triggering a state of anxiety and stress among the participants, increasing heart rate and electrodermal activity, making it easier to detect changes in the SNS and PNS, during the situation of stress compared to baseline.

This paper is divided in 4 sessions. In the next session the materials and methods are presented, with the description of the population, materials and protocol of the stress test performed. The methods used to analyze the data are also described in this session, with details of the algorithms used to compute HRV and EDA features. Additionally, a statistical analysis and machine-learning algorithms are also presented. Then, the results obtained are presented in session 3, with the classification and construction of the models to predict the outcome. Finally, the results obtained are discussed in session 4.

2 MATERIALS AND METHODS

2.1 Study Population

Data was acquired from a group of volunteer subjects. Fifteen participants (9 females and 6 males) of ages from 21 to 55 years old (31 $\pm$ 11), height from 1.57 to 1.85 meters (1.73 $\pm$ 0.09) and weight from 52 to 94 kilograms (72 $\pm$ 13) signed an informed consent. Table 1 gives the statistics for the study population.

Table 1: Study population statistics.

	Mean	SE	Min	Max
Age (years)	31	11	21	55
Height (m)	1.72	0.09	1.57	1.85
Weight (kg)	72	13	52	94

SE - Standard Error

2.2 Materials

The acquisition of the biosignals was made with a BITalino wearable wrist device prototype composed of six different sensors: EDA wrist, PPG, Spare sensor, Total Volatile Organic Compounds (TVOC), Car-

bon Dioxide (CO2) and Temperature (TEMP), developed by Plux Wireless Biosignals (see Table 2). For this experiment only the PPG (Channel 2) and the EDA spare sensor (Channel 3) were used. Both the PPG and EDA signals were acquired, simultaneously, with a sampling rate of 1000 Hz and 10-bit resolution. The PPG sensor is a green LED with a photodetector in reflection mode while the EDA sensor uses gelled electrodes.

Table 2: Wearable Wrist Device Specifications.

Sensor	Channel	Resolution (bits)	Sampling Rate
EDA wrist	1	10	
PPG	2	10	10 Hz
Spare	3	10	100 Hz
TVOC	4	10	1000 Hz
CO2	5	6	
TEMP	6	6	

2.3 Protocol

The experiment was performed in a quiet room, in order to avoid interference that would distract the participants, due to the fact that, in order to perform the PVSAT several cognitive functions are required, such as attention and working memory. The duration of the experiment was 12 minutes (6-min baseline + 6-min stress). The stress status is defined by the changes in physiological parameters derived by the complexity and difficulty of the PVSAT, in comparison with the baseline status. The subjects were asked to sit in a comfortable chair and avoid any movement during the entire experiment, specially in the left arm. PPG and EDA signals were recorded simultaneously using the wearable device described in section 2.2. The EDA signals were recorded attaching the electrodes to the anterior middle phalanges of the 2nd finger (Position 1 in Fig.1(a)) and 3rd finger (Position 2 in Fig.1(a)) of the left hand. The PPG signal was recorded on the posterior distal left wrist, as shown in Fig.1(b).

After placing the wearable device and the EDA spare sensor, the PVSAT test was explained to the subjects. The PVSAT was presented to induce stress in the last 6-min, in a 12.2" tablet with white single numbers from 1 to 9, on a black screen. The digits were presented with a 3s rate for the first 2min, decreasing half a second every two minutes (2.5s and 2s). The subjects had to respond prior to the presentation of the next digit, and speak aloud each response. A warning 30s before the beginning of the PVSAT was given to all participants (Blue line in Fig.2). In baseline status, the subjects were asked not to speak.

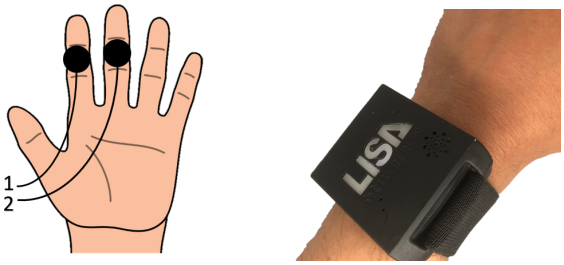

(a) EDA. (b) PPG.

Figure 1: Recording sites for the biosignals.

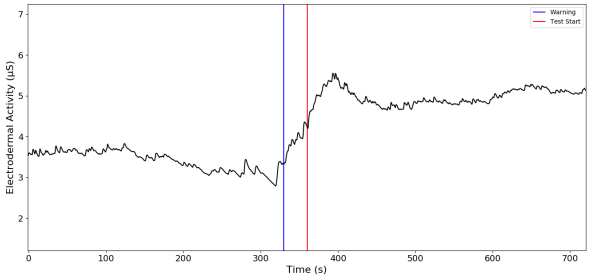

Figure 2: Representation of the warning and start of the PVSAT. EDA signal increases at the warning 30s before the PVSAT starts (Blue line). The start of the PVSAT is represented by the Red line.(Brennan et al., 2001)

2.4 Data Processing

2.4.1 PPG Peak Detection

HRV features were acquired with PPG signals. In order to detect the systolic peaks in the PPG, the algorithm implemented is based on the work perfomed by (Kuntamalla et al., 2014). This algorithm applies a 2nd order lowpass Butterworth filter at 2 Hz, followed by a 2nd order highpass Butterworth filter at 0.1 Hz. Then it detects the peaks and valleys of the PPG wave, and computes the difference in amplitude between the peaks and the valleys. After calculating this difference, the algorithm will search for the differences that are greater than 50% of a 5-point window moving average, discarding the peaks that do not satisfy this criteria. This process is then repeated until the number of peaks between two consecutive iterations is the same. The systolic peaks detected are shown in Fig.3.

2.4.2 Heart Rate Computation

Heart rate is obtained by calculating the interval between two consecutive systolic peaks, detected with the algorithm in section 2.4.1. In order to remove artifacts influence or errors in the detection of the peaks, RR intervals lower than 380 ms were removed due to physiological conditioning, as a normal heart cycle lasts at least 380 ms. The instantaneous heart rate

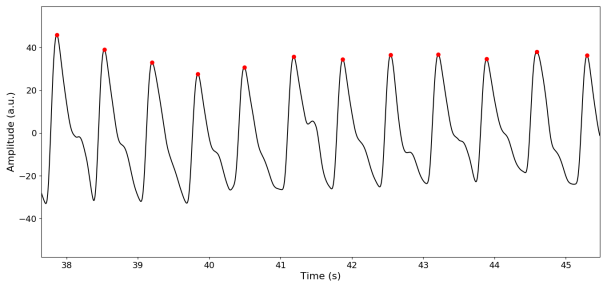

Figure 3: Peaks Detected (Red dots) with the algorithm implemented.

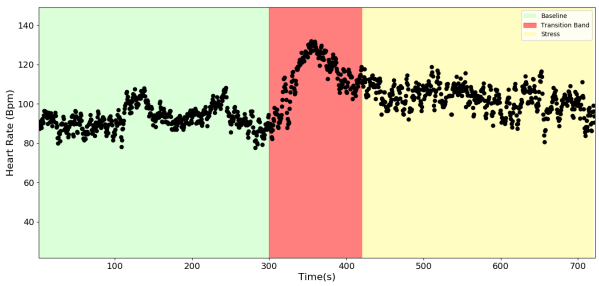

Figure 4: HRV data division in 5-min segments. Baseline status - 0-min to 5-min (Green band), Stress status - 7-min to 12-min (Yellow band). The Red band corresponds to the excluded Transition band.

(IHR) in beats per minute (Bpm) is given by equation 1.

$$\text{IHR (Bpm)} = \frac{60}{\Delta RR}; \quad \Delta RR = RR_i - RR_{i-1}; \qquad (1)$$

2.4.3 RR-interval Series Filtering

RR-interval series recorded from a wearable device PPG sensor are subject to different kinds of artifacts (Jang et al., 2014), as the most common are motion artifact, breathing artifact and ectopic beats, leading to a wrong detection of the R-peak (Logier et al., 2004).

To correct the miscalculated peak, a 7-point moving average window was computed. If a RR-interval differs more than 20% of the moving average, or if the RR_{i+1} is smaller than 75% of the value RR_{i-1}, those points are considered as a wrong detection (Logier et al., 2004). Then, a linear interpolation is computed to replace each interval considered as a wrong detection.

2.4.4 HRV Features

Time-domain features and frequency-domain were calculated to quantify HRV, in 5-min segments for baseline and stress. The time between the 5th and 7th minute, was considered to be the transition band, where heart rate changes significantly from baseline to stress (Fig.4).

Statistical features related to the variance of RR-intervals, such as SDNN, RMSSD, NN50 and pNN50, were computed for 5-min recordings (Vollmer, 2015; Guidelines, 1996).

The 5-min Poincaré plot represents the diagram in which each RR interval is plotted against the previous RR interval. From the Poincaré plot it is possible to extract non-linear variables, such as SD1, SD2 and SD2/SD1 ratio, that reflects the balance between the SNS and PNS (Hsu et al., 2012).

Frequency-domain features were also computed. The RR-interval series are an irregularly time-sampled series, though it is necessary to resample the series, to avoid the appearance of additional harmonic components in the power spectrum. Resampling was performed at a frequency of 10 Hz.

The power spectrum for baseline status (at rest) and stress status (perfoming the PVSAT) (Fig.5), was computed using a periodogram, applying to each segment, a Hanning window. Then, the Fast Fourier Transform (FFT) was calculated for each windowed segment. Very-low (VLF), low (LF), high (HF) frequency components and total power were obtained by integrating the power in each frequency band. The normalized frequency components were calculated by dividing the LF and HF power, by the total power minus the power of the VLF band (Guidelines, 1996).

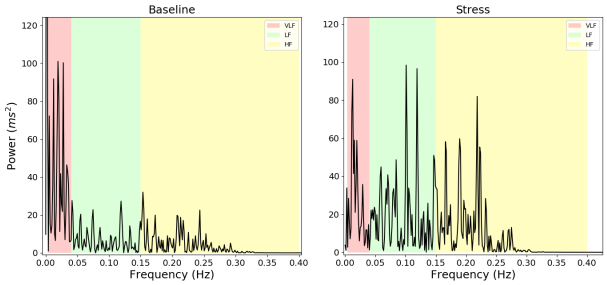

Figure 5: HRV power spectrum. The left spectrum corresponds to a Baseline status and the rigth spectrum corresponds to the Stress status. VLF (0.0033-0.04 Hz) - Red band, LF (0.04-0.15 Hz) - Green band, HF (0.15-0.4 Hz) - Yellow band.

2.4.5 EDA Features

In terms of EDA recordings, time-domain features were computed, by dividing the data into four segments: two bands of 2-min each in baseline (Baseline 1, Baseline 2) and in stress (Stress 1, Stress 2). The Red band in Fig.6, 4th to 6th minute, was considered the transition band, where EDA level changes significantly, due to the warning of the start of the PVSAT test, 30s before the start.

Time-domain features were extracted by applying

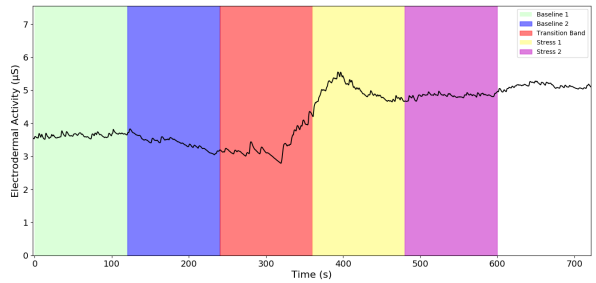

Figure 6: EDA data division in 2-min segments. Baseline 1 - 0-min to 2-min (Green Band), Baseline 2 - 2-min to 4-min (Blue band), Stress 1 - 6-min to 8min (Yellow band), Stress 2 - 8-min to 10-min (Purple band). The Red band corresponds to the Transition band.

a 4th order lowpass Butterworth filter at 1 Hz. Then the model proposed by (Gamboa and Fred, 2008), computed the SCR component. From the SCR waveform, time domain features such as SCR amplitude, Rise time, Recovery Time 50% (Rec.t 50%) and Recovery Time 63% (Rec.t 63%), were obtained as shown in Fig.7. A threshold of 0.005 μS was applied. The SCL component was obtained by subtracting the total EDA signal by the SCR component.

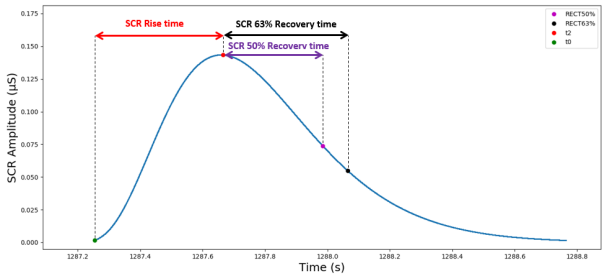

Figure 7: SCR features. The green mark corresponds to 1% of the maximum value (t0), the red mark corresponds to the maximum value of the peak (t2), the purple and the black mark correspond to the values in which the amplitude decreases, respectively, 50% and 63%.

Frequency-domain analysis was also performed (Posada-Quintero et al., 2018). After filtering the EDA signal, the signals was downsampled. Downsampling from 1000 Hz to 1 Hz was performed in three steps using consecutive factors of 1/10. Then the signals was highpass filtered with a 8th order Butterworth filter at 0.01 Hz, to remove any trend.

The power spectrum was computed using a periodogram, applying to each segment, a Blackman window. Then, the FFT was calculated for each windowed segment. The frequency band to assess the activity of the SNS through EDA used by Posada-Quintero et al., was modified to the frequency band of 0.04-0.35 Hz. Finally, the power for Band 1 (0.04-0.35 Hz) and Band 2 (0.35-0.50 Hz). The normalized frequency components were calculated by dividing Band 1 and Band 2 power, by the total power, to verify if there was an increase in power on Band 1 during the stress situation, in order to confirm the stimulation of the SNS (Fig.8).

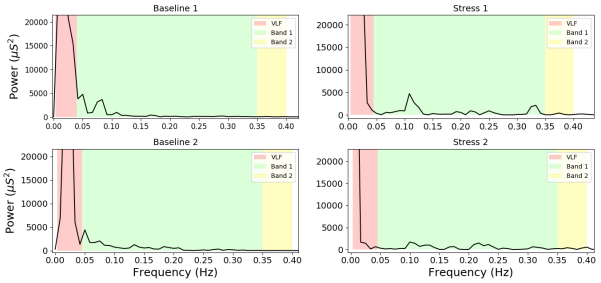

Figure 8: EDA power spectrum. VLF (0-0.045 Hz) - Red band, Band 1 (0.045-0.35 Hz) - Green band, Band 2 (0.35-0.5 Hz) - Yellow band.

2.5 Statistical Analysis

Statistical tests analysis were performed in order to assess the significance of the results obtained, between the baseline and stress features.

Kruskal-Wallis test is a non-parametric test, so it means that is does not assume the normality of data nor the homoscedaticity (standard deviation are equal). The H-test uses ranked values, so the values observed are converted to their ranks. The Kruskal-Wallis null-hypothesis is that the mean ranks of the different groups are the same (McDonald, 2014). Probabilities lower than the significance level of 5% ($p\text{-}value < 0.05$) were considered significant, concluding that the null hypothesis may not adequately explain the observation - there is in fact variation between the ranked means of the groups.

Chi-square test χ^2 was also applied to test the goodness of fit in section 3.2. This test is applied to determine whether a categorical variable from a single population is consistent with a hypothesized distribution. The null hypothesis is that the categorical data has the given frequencies (Cochran, 2013). In the context of this paper, the χ^2 test will be applied to determine the goodness of the fit of the linear regression line performed, by comparing the values observed calculated using the regression line obtained, with the expected values. Probabilities higher than the significance level of 5% ($p\text{-}value < 0.05$) lets us conclude that the difference between the observed values and the expected values is minimized, so the linear regression is a good fit.

2.6 Machine-Learning

Machine-learning algorithms were applied in order to classify the data.

Support Vector Machines (SVM) algorithms for learning two-class discriminant functions from a set of training examples were applied, in order to find a suitable boundary (hyperplane), in data space to separate two classes. The basis of this boundary is the concept of margin, which is the minimal distance between the hyperplane separating the two classes and the closest points to it, defined as the support vectors. In linearly separable data, the kernel of SVM used is the maximal margin classifier or hard margin SVM (Vapnik, 1999).

Random Forest classifiers are based on the Decision Tree algorithm. Decision Trees are a supervised method of classification in machine learning, using pre-classified data. The division of the data is based on the values of features of the given data, by deciding which features, best divide ir, creating a set of rules for the values of each feature. The Random Forest classifier is a combination of multiple decision trees, where each decision tree is made by randomly selecting portions of the data, reducing the correlation between trees, improving the prediction power and results with a higher efficiency (Breiman, 2001; Donges, 2018).

3 RESULTS

The results obtained showed that the PVSAT induced stress to the subjects, reflected by the increase in heart rate and in EDA features, such as SCR and SCL, during stress.

Frequency analysis of EDA, also confirmed the activation of the sympathetic nervous system with an increase in Band 1 power in stress.

For HRV, the results obtained for spectral measures were opposite to the expected. It was expected to verify an increase in LF(nu) and LF/HF ratio during stress, but no significant result was found for frequency-domain features.

Despite no significance was obtained in frequency-domain features for HRV, a thorough analysis of these spectral characteristics, revealed that in some subjects the LF(nu) decreased in stress, while in other subjects there was an increase in stress. Actually, within the 15 subjects that were analyzed, there was a division of 8 subjects in which LF(nu) decreased during stress, and 7 subjects that LF(nu) increased during stress. So, when analyzing the group as a whole, it is possible that the opposite responses cancels out the LF(nu) results. Therefore, two distinct groups were formed: group 1 consisted of subjects which LF(nu) decreased during stress, and group 2 consisted of subjects which LF(nu) increased during stress. Then, all features for HRV were analyzed for each group.

For group 1, the results showed a significant increase in HF(nu) power, LF(nu) power and LF/HF ratio. For group 2, the results showed significant effect only for Bpm and RR interval .

3.1 Support Vector Machines

In this section, SVM were applied to try separate by a hyperplane the two different responses of the subjects to stress: decrease in LF(nu) and increase in LF(nu) (see Fig.9). This separation is based on the work of Vuksanovic et al. (Vuksanović and Gal, 2007), that verified this distinct response to stress, but in respect to HF power.

First, a binary classification of each group was applied: Group 1 - Decrease in LF(nu) was classified as $Y = -1$ and Group 2 - Increase in LF(nu) was classified as $Y = 1$. The decision function obtained to separate the two groups is given by equation 2, where w_1 and w_2 represents, respectively, the weights for groups 1 and 2, $\vec{x_1}$ and $\vec{x_2}$ represents, respectively, a point for group 1 (Blue circles in Fig.9) and group 2 (Red circles in Fig.9).

$$w_1.\vec{x_1} + w_2.\vec{x_2} + b = 0 \tag{2}$$

The results obtained for the weights and the b parameter were: $w_1 = -0.31$, $w_2 = 0.25$ and $b = 4.85$. The number of support vectors for each group were: Group 1 - 1 support vector, Group 2 - 2 support vectors. The coordinates ([LF(nu) Baseline, LF(nu) Stress]) of the support vectors (Black not filled circles in Fig.9) for each group were: Group 1 - [78.48,74.64] and in Group 2 - [77.35,81.25];[63.08,63.41].

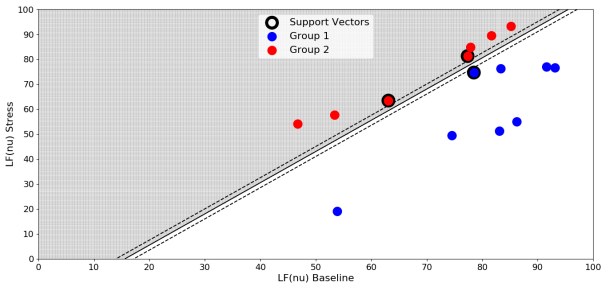

Figure 9: SVM Group Separation by the hyperplane: $-0.31.\vec{x_1} + 0.25.\vec{x_2} + 4.85 = 0$. Blue circles - Group 1. Red circles - Group 2. The support vectors are the points with black border.

3.2 Linear Regression

In session 3.1, the results showed that the responses of the groups were parallel, so it was possible to predict the LF (nu) values during stress based on the baseline values for each group separately. A linear regression was then computed for each group (Fig.10). For Group 1 regression (Red line in Fig.10), the following regression line was obtained: LF(nu) Stress $= 1.40 \times$ LF(nu) Baseline $- 53.15, r^2 = 0.728$. For Group 2 regression (Blue line in Fig.10), the regression line obtained was LF(nu) Stress $= 1.06 \times$ LF(nu) Baseline $+$ $1.48, r^2 = 0.972$.

Finally, a chi-squared test for goodness of fit was applied to the regression lines, comparing the expected values with the observed values using the regression line obtained. For group 1 the chi-square result was $\chi^2(6) = 12.785; p = 0.047$ and for group 2 was $\chi^2(5) = 0.674; p = 0.984$. With the results obtained for the χ^2 statistic, it is possible to reject at a significance level of 5%, the null hypothesis for group 1, concluding that the fit of the regression line is not adequate, while for group 2, with a *p-value*=0.984 it is possible to accept the null hypothesis, concluding that the fit of the regression line is suitable.

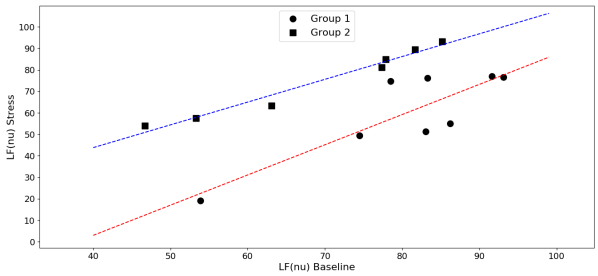

Figure 10: Linear Regression for each group. Group 1 regression line (Red line): LF(nu) Stress $= 1.40 \times$ LF(nu) Baseline $- 53.15, r^2 = 0.728$; Group 2 regression line (Blue line): LF(nu) Stress $= 1.06 \times$ LF(nu) Baseline $+$ $1.48, r^2 = 0.972$.

3.3 Random Forest Classifier

In section 3.1, it was possible to separate the subjects into two groups, by evaluating their response to stress, with an increase or a decrease in LF(nu) during stress. As this separation is based on a frequency-domain feature, requiring the recording of the data for at least 10 minutes (5-min in baseline, 5-min in stress), in order to predict the subject's response to a situation of stress in a shorter recording time, a classification of the subjects using only time-domain features for both HRV and EDA, was performed, to classify the subjects into the two different groups obtained in the previous section.

This classification was performed with a random forest classifier, with 10 decision trees, and a Gini criteria to assess the impurity and the quality of the split. Training of the classifier was performed with a cross validation method, using 6 different random splits and a test sample of 30% of the subjects. This process was repeated 100 times, so that it was possible to choose the model that best classifies the data, that is, the model with a higher accuracy score for the cross validation training method.

First, a random forest classifier using only the following time-domain features for HRV was performed: Bpm, RR-interval and SD2/SD1 ratio. Then, the importance of each feature is plotted in figure 11. From this figure, we verify that RR-interval is the most important feature in this model, followed by the SD2/SD1 ratio and the Bpm. The accuracy score for this model to classify correctly each subject to the corresponding group was approximately 80%.

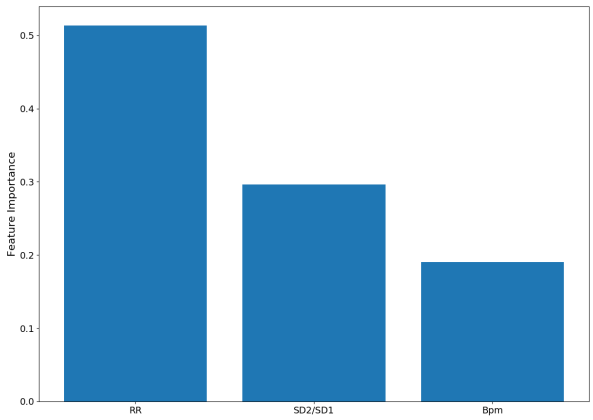

Figure 11: Feature Importance for HRV features obtained with the random forest classifier.

In order to obtain a better visualization of the regions defined by the random forest classifier, the features boundaries are shown in a 3D graph (Fig. 12). A subject with features coordinates that belong to the blue region will be assigned to group 1 - decrease in LF(nu), and subjects that belong to the red region will be assigned to group 2 - Increase in LF(nu).

Information related to EDA was added to the classifier. Similarly to the previous classifier, in order to reduce the recording time, only time-domain features for EDA were added to the classifier. The following features for EDA were selected: SCR, SCL and Rise Time. The more accurate estimators were selected, with the corresponding decision trees. The importance of each feature in plotted in figure 13. The accuracy score for this model was approximately 77%.

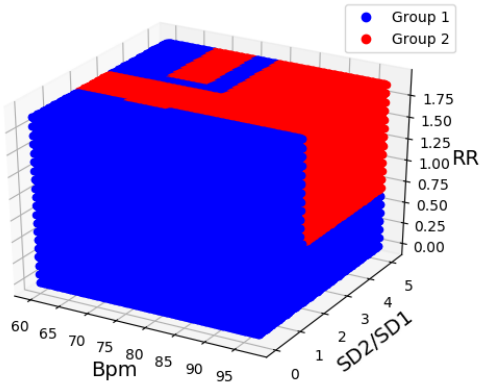

Figure 12: 3D Decision Surface for the Random Forest Classifier. Features selected: Bpm, SD2/SD1 and RR-interval (s). Blue region - Group 1 and Red region - Group 2.

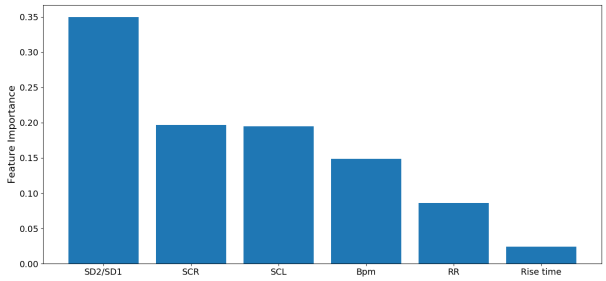

Figure 13: Feature Importance for HRV and EDA features obtained with the random forest classifier.

4 DISCUSSION

This was a pilot study to see the influence of stress induction on the autonomous nervous system, by processing HRV and EDA from a wearable device.

The results obtained in section 3, showed that the arithmetic test (PVSAT) induced stress to the subjects, reflected by the increase in heart rate (Bpm) and in EDA features, such as, SCR and SCL, during stress.

For EDA features, SCR, SCL, Rise time, Rec.t 50% and Rec.t 63%, revealed to be good markers of stress, with the increase of values during all the segments studied during stress compared to the baseline segments. In section 2.4.5, the frequency analysis of EDA signals was performed to confirm the activation of the sympathetic nervous system with an increase in power for low frequency bands. The results obtained showed that there was a significant increase in Band 1 power. This confirms that the dynamics of the sympathetic nervous system are confined to low frequencies, in agreement with the work performed by Posada et al., although in this paper the frequency band studied was extended more 0.10 Hz, the increase in power was also verified, making frequency analysis of EDA a potential marker of quantitative assessment of the level of stress and sympathetic nervous system impairments (Posada-Quintero et al., 2016a).

For HRV, the results obtained for spectral measures were opposite to the expected. The inducement of stress in subjects was expected to increase LF(nu) and LF/HF ratio (Visnovcova et al., 2013; Hjortskov et al., 2004; Vuksanović and Gal, 2007). Contrarily to the expectation, the results obtained showed that there was a decrease in LF(nu) and LF/HF ratio during stress, results also reported by (Tharion et al., 2009; Vuksanović and Gal, 2007; Hjortskov et al., 2004). Vuksanovic et al. reported that vocalization of the answers, assigned to parasympathetic activity, during the PVSAT interfered with the spectral analysis and concealed out the changes in spectral measures of HRV (Vuksanović and Gal, 2007). Langewitz et al. showed that the breathing pattern for some subjects during vocalization affects the low frequency band power, as the breathing frequency falls in the 0.1 Hz frequency band, the resonance phenomenon will not increase the power in the LF band (Langewitz and Ruddel, 1989), concluding that the fact subjects answered the PVSAT aloud might have influenced the spectral measures of HRV. These facts also show that the LF band does not reflect purely the cardiac response to the activation of the sympathetic nervous system, but a mixture of the sympathetic and parasympathetic systems, with counteracting effects of activation of the sympathetic system and withdrawal of the parasympathetic system (Sloan et al., 1991). From the point of view of humoral mechanisms, these results can be explained, as, during a situation of stress, the sympathetic nervous system affects the heart through release of catecholamines (Terkelsen et al., 2005), such as epinephrine, leading to an increase in heart rate without changing heart rate variability measures, as the release of epinephrine does not affect spectral measures (Ahmed et al., 1994).

In section 3.1, despite the results for HRV were concealed out when analyzing the subjects as a whole, it was possible to verify significant changes in spectral measures for HRV after separating the subjects into the two different groups, based on the work performed by Vuksanovic et al., and as an exploratory method in order to find a pattern, taking into account that subjects can exhibit distinct response when submitted to stress. From figure 10, it is possible to see that the slopes for each group do not intercept with one another, so the two responses are parallel. For group 2, the results obtained were in agreement with

the expectations that during stress, the LF(nu) and the LF/HF ratio increased with a small decrease in HF(nu) power with no significance. This group responds to stress with the withdrawal of the parasympathetic nervous system and the activation of the sympathetic nervous system. For group 1, the results showed significant decrease in LF(nu) and LF/HF ratio during stress and significant increase in HF(nu) power. The simultaneous increase in HF(nu) and heart rate is more difficult to explain, although it could be an influence of complex respiratory pattern (Vuksanović and Gal, 2007), or it could be the effect of different co-activation humoral mechanims, caused by compensatory sympatho-adrenal activation with catecholamine release into the circulation (Terkelsen et al., 2005).

In terms of EDA, both groups showed an increase in Band 1 power, although significance was only found in group 2 between baseline 2 and stress 1 segments. It is possible to conclude that even if there is a distinct response to stress in terms of HRV, there is activation of the sympathetic nervous system during the stress situation, due to the fact that the sympathetic nervous system influences the heart and sweat through distinct hormones, respectively, epinephrine and acetylcholine.

Finally, the classification model implemented in section 3.3, showed that it was possible to predict the type of response for each subject during stress, using only their baseline features for both HRV and EDA features, making it possible to classify the subjects into the two different groups, with an accuracy of approximately 80% for HRV features in baseline and an accuracy of approximately 77% for HRV and EDA simultaneous features. This model assumes to be a good asset for future assessment of the type of response when the subjects are under a stress situation.

REFERENCES

Ahmed, M. W., Kadish, A. H., Parker, M. A., and Goldberger, J. J. (1994). Effect of physiologic and pharmacologic adrenergic stimulation on heart rate variability. *Journal of the American College of Cardiology*, 24(4):1082–1090.

Allen, J. (2007). Photoplethysmography and its application in clinical physiological measurement. *Physiological Measurement*, 28(3).

Bansal, D., Khan, M., and Salhan, A. (2009). A Review of Measurement and Analysis of Heart Rate Variability. In *2009 International Conference on Computer and Automation Engineering*, pages 243–246.

Benedek, M. and Kaernbach, C. (2010). A continuous measure of phasic electrodermal activity. *Journal of Neuroscience Methods*, 190(1):80–91.

Bolanos, M., Nazeran, H., and Haltiwanger, E. (2006). Comparison of heart rate variability signal features derived from electrocardiography and photoplethysmography in healthy individuals. In *Annual International Conference of the IEEE Engineering in Medicine and Biology - Proceedings*, pages 4289–4294.

Boucsein, W. (2012). *Electodermal Activity*. Second edi edition.

Breiman, L. (2001). Random forests. *Machine Learning*, 45(1):5–32.

Brennan, M., Palaniswami, M., and Kamen, P. (2001). Do existing measures of Poincareé plot geometry reflect nonlinear features of heart rate variability? *IEEE Transactions on Biomedical Engineering*, 48(11):1342–1347.

Bussmann, B. (1998). Differentiation of autonomic nervous activity in different stages of coma displayed by power spectrum analysis of heart rate variability. pages 46–52.

Cochran, W. G. (2013). The $\chi 2$ Test of Goodness of Fit. *The Annals of Mathematical Statistics*, 23(3):315–345.

Donges, N. (2018). The Random Forest Algorithm.

Gamboa, H. and Fred, A. (2008). Electrodermal Activity Model. *Psychophysiology*, (April):30.

Guidelines (1996). Guidelines Heart rate variability. *European Heart Journal*, 17:354–381.

Guyton, A. C. and Hall, J. E. (2011). *Textbook of Medical Physiology*.

Hamilton, J. L. and Alloy, L. B. (2016). Atypical reactivity of heart rate variability to stress and depression across development: Systematic review of the literature and directions for future research.

Hjortskov, N., Rissén, D., Blangsted, A. K., Fallentin, N., Lundberg, U., and Søgaard, K. (2004). The effect of mental stress on heart rate variability and blood pressure during computer work. *European Journal of Applied Physiology*, 92(1-2):84–89.

Hsu, C. H., Tsai, M. Y., Huang, G. S., Lin, T. C., Chen, K. P., Ho, S. T., Shyu, L. Y., and Li, C. Y. (2012). Poincaré plot indexes of heart rate variability detect dynamic autonomic modulation during general anesthesia induction. *Acta Anaesthesiologica Taiwanica*, 50(1):12–18.

Jang, D.-G., Park, S., Hahn, M., and Park, S.-H. (2014). A Real-Time Pulse Peak Detection Algorithm for the Photoplethysmogram. *International Journal of Electronics and Electrical Engineering*, 2(1):45–49.

Kleckner, I. R., Jones, R. M., Wilder-Smith, O., Wormwood, J. B., Akcakaya, M., Quigley, K. S., Lord, C., and Goodwin, M. S. (2017). Simple, Transparent, and Flexible Automated Quality Assessment Procedures for Ambulatory Electrodermal Activity Data.

Kuntamalla, S., Ram, L., and Reddy, G. (2014). An Efficient and Automatic Systolic Peak Detection Algorithm for Photoplethysmographic Signals. *International Journal of Computer Applications*, 97(19):975–8887.

Langewitz, W. and Ruddel, H. (1989). Spectral analysis of heart rate variability under mental stress. *J Hypertens Suppl*, 7(6):S32—-3.

Logier, R., De Jonckheere, J., and Dassonneville, A. (2004). An efficient algorithm for R-R intervals series filtering. *Conference proceedings : ... Annual International Conference of the IEEE Engineering in Medicine and Biology Society. IEEE Engineering in Medicine and Biology Society. Conference*, 6:3937–3940.

McDonald, J. H. (2014). KruskalWallis test - Handbook of Biological Statistics.

Miranda Dantas, E., Lima Sant'Anna, M., Varejão Andreão, R., Pereira Gonçalves, C., Aguiar Morra, E., Perim Baldo, M., Lamêgo Rodrigues, S., and Geraldo Mill, J. (2012). Spectral analysis of heart rate variability with the autoregressive method: What model order to choose? *Computers in Biology and Medicine*, 42(2):164–170.

Parsons, T. D. and Courtney, C. G. (2014). An initial validation of the Virtual Reality Paced Auditory Serial Addition Test in a college sample. *Journal of Neuroscience Methods*, 222:15–23.

Posada-Quintero, H., Florian, J., Orjuela-Cañón, A., and Chon, K. (2018). Electrodermal activity is sensitive to cognitive stress under water. *Frontiers in Physiology*, 8(JAN):1–8.

Posada-Quintero, H. F., Florian, J. P., Orjuela-Cañón, A. D., Aljama-Corrales, T., Charleston-Villalobos, S., and Chon, K. H. (2016a). Power Spectral Density Analysis of Electrodermal Activity for Sympathetic Function Assessment. *Annals of Biomedical Engineering*, 44(10):3124–3135.

Posada-Quintero, H. F., Florian, J. P., Orjuela-Cañón, Á. D., and Chon, K. H. (2016b). Highly sensitive index of sympathetic activity based on time-frequency spectral analysis of electrodermal activity. *American Journal of Physiology - Regulatory, Integrative and Comparative Physiology*, 311(3):R582–R591.

Posada-quintero, H. F. and Hall, S. (2016). Electrodermal Activity : What it can contribute to the Assessment of the Autonomic Nervous System. page 24.

Posada-quintero, H. F., Member, S., Chon, K. H., and Member, S. (2016). Frequency - Domain Electrodermal Activity Index of Sympathetic Function. pages 497–500.

Royan, J., Tombaugh, T. N., Rees, L., and Francis, M. (2004). The Adjusting-Paced Serial Addition Test (Adjusting-PSAT): Thresholds for speed of information processing as a function of stimulus modality and problem complexity. *Archives of Clinical Neuropsychology*, 19(1):131–143.

Sloan, R. P., Korten, J. B., and Myers, M. M. (1991). Components of heart rate reactivity during mental arithmetic with and without speaking. *Physiology and Behavior*, 50(5):1039–1045.

Terkelsen, A. J., Mølgaard, H., Hansen, J., Andersen, O. K., and Jensen, T. S. (2005). Acute pain increases heart rate: Differential mechanisms during rest and mental stress. *Autonomic Neuroscience: Basic and Clinical*, 121(1-2):101–109.

Tharion, E., Parthasarathy, S., and Neelakantan, N. (2009). Short-term heart rate variability measures in students during examinations. *National Medical Journal of India*, 22(2):63–66.

Tombaugh, T. N. (2006). A comprehensive review of the Paced Auditory Serial Addition Test (PASAT). *Archives of Clinical Neuropsychology*, 21(1):53–76.

Vapnik, V. N. (1999). An overview of statistical learning theory. *IEEE transactions on neural networks / a publication of the IEEE Neural Networks Council*, 10(5):988–99.

Visnovcova, Z., Calkovska, A., and Tonhajzerova, I. (2013). Heart Rate Variability and Electrodermal Activity As Noninvasive Indices of Sympathovagal Balance in Response To Stress. *Acta Medica Martiniana*, 13(1):5–13.

Vollmer, M. (2015). A robust, simple and reliable measure of heart rate variability using relative RR intervals. *Computing in Cardiology*, 42(6):609–612.

Vuksanović, V. and Gal, V. (2007). Heart rate variability in mental stress aloud. *Medical Engineering and Physics*, 29(3):344–349.

Zoltan, G.-S. (2013). Wavelet transform based HRV analysis. *The 7th International Conference Interdisciplinarity in Engineering (INTER-ENG 2013)*, 12:105–111.